INFORMATION TO USERS

This manuscript has been reproduced from the microfilm master. UMI films the text directly from the original or copy submitted. Thus, some thesis and dissertation copies are in typewriter face, while others may be from any type of computer printer.

The quality of this reproduction is dependent upon the quality of the copy submitted. Broken or indistinct print, colored or poor quality illustrations and photographs, print bleedthrough, substandard margins, and improper alignment can adversely affect reproduction.

In the unlikely event that the author did not send UMI a complete manuscript and there are missing pages, these will be noted. Also, if unauthorized copyright material had to be removed, a note will indicate the deletion.

Oversize materials (e.g., maps, drawings, charts) are reproduced by sectioning the original, beginning at the upper left-hand corner and continuing from left to right in equal sections with small overlaps.

Photographs included in the original manuscript have been reproduced xerographically in this copy. Higher quality 6" x 9" black and white photographic prints are available for any photographs or illustrations appearing in this copy for an additional charge. Contact UMI directly to order.

Bell & Howell Information and Learning
300 North Zeeb Road, Ann Arbor, MI 48106-1346 USA

UMI®
800-521-0600

The Osseous Response to Corundum Blasted Implant Surfaces in a Canine Total Hip Arthroplasty Model

Steven Adam Hacking
Department of Biomedical Engineering
McGILL UNIVERSITY
Montreal, Quebec, Canada

September 1997

A Thesis submitted to the
Faculty of Graduate Studies and Research
in partial fulfillment of the requirements
of the degree of
Master of Engineering (MEng)

The osseous response to corundum blasted implants in a canine total hip arthroplasty model

Adam Hacking

The purpose of this study was to examine the radiographic and histologic response to corundum blasted implant surfaces of varying roughness in a canine total hip arthroplasty model. Three types of tapered femoral implants were made from titanium alloy and were identical in every respect except surface finish. The entire surface of the femoral implant possessed either a 2.9, 4.2 or 6.7 micrometer average surface roughness (R_a) from blasting with 60, 24, or 16 grit corundum particles, respectively. Staged bilateral total hip arthroplasties were performed such that each dog received a 60 grit on one side and a 24 grit or 16 grit implant on the contralateral side. Twenty-two stems in 11 dogs were evaluated at 6 months. The appearance of the bone implant interface was qualitatively characterized by both high resolution radiography of the implant *in situ* and radiographs obtained from 2 mm thick transverse serial sections. Further qualitative and quantitative analysis of the bone-implant interface was performed by backscattered scanning electron microscopy. Bone apposition and average bone-implant contact length were determined. Twenty-one of the stems demonstrated osseointegration while one stem developed a stable fibrous interface. All three types of corundum blasted implants demonstrated consistently high amounts of bone apposition, averaging 30.5%. Abundant new peri-implant bone consistently formed, particularly within the intramedullary canal where trabeculae spanned implant-cortical gaps up to 5 mm and established osseointegration. There was no statistical difference amongst bone apposition with the 60, 24, and 16 grit stems which averaged 31.7%, 32.0% and 27.9% respectively. However, the pattern of new bone formation was different in that the average length of each region of bone apposition for the 60 and 24 grit surfaces was 50% greater than that for the coarser 16 grit surface ($p<0.02$). Through detailed qualitative and quantitative radiographic and histologic elucidation of the osseous response to corundum blasted hip implant surfaces, this study provided new understanding of their potential for biologic fixation. The observations of this study clearly indicate that because of their highly osteophillic nature, corundum blasted surfaces represent an important and valuable technology for the design of noncemented implants.

Résultat osseux de l'implant de la hanche au sablage de corindon de l'arthroplastie totale chez un modèle canin

Adam Hacking

Le but de cette étude était d'examiner le résultat radiographique et histologique des surfaces d'implants sablées au corindon des variantes rugueuses de l'arthroplastie total de la hanche chez un modèle canin. Trois types d'implants du fémur fuselés ont été fabriqués d'alliage de titane et sont identiques sur tous les niveaux sauf pour la surface de finition. La surface entière de l'implant du fémur possède soit: 2.9, 4.2, ou 6.7 de surface rugueuse au micromètre (R_a) avec un grain respectif de 60, 24, ou 16 de particules de corindon . Vingt-deux tiges chez onze chiens ont été évaluées à six mois. L'apposition des os et la durée de contact ont été déterminées. Vingt-une des tiges ont démontré une osséointégration tandis qu'une tige a développé une interface stable rugueuse. Les trois types d'implants sablés au corindon ont démontré avec consistance un niveau élevé d'apposition des os, moyennant 30.5%. Il n"y a pas de difference statistique parmi l'apposition des os avec les tiges 60, 24, et 16 de particules qui en moyenne sont de 31.7%, 32.0% et 27.9% respectivement. Des détails qualitatifs et quantitatifs des résultats radiographiques et histologiques sur les surfaces de l'implant de la hanche sablé au corindon fournit une approche du potentiel de fixation biologique.

ACKNOWLEDGEMENTS

This thesis is a result of the generous efforts of many talented people. My deepest thanks to Dr. Michael Tanzer for his instruction, guidance and patience both inside and out of the OR. Many thanks to Jan Krygier, whose technical skills and insight played a role in facilitating the completion of each step of this thesis. I wish to thank my good friend and colleague Frank Chan, whose advice is always valued and whose example has been a source of inspiration. I would also like to thank Mrs. Diane Murray and Mr. Danny Yee whose diligent and compassionate conduct resulted in excellent care for the animals used in this study. Thanks to Jamie McGowan and Amy McGinn who patiently assisted the preparation and processing of many of the histological specimens and assisted with some of the surgeries. To Helen Campbell, thank you for your instruction and tireless patience developing my skills with the scanning electron microscope. My warmest thanks to Paria Radmard who spent countless hours organizing photos, arranging sections and maintaining my spirits. A special thanks to MJ Milloy who prepared some of the graphics in this thesis. I would also like to thank the Medical Research Council of Canada that provided the necessary funding that made this study possible. and Zimmer Inc., for the generous supply of the implants.

Adam Hacking
Montreal, 1997

Table of Contents

Table of Contents

Table of Contents

Table of Contents

LIST OF FIGURES

Legend

AP - Anterior-Posterior

Lat. - Medio-Lateral

TSS - Transverse serial section

SEI - Secondary electron microscopy

BSEM - Backscattered electron microscopy

LIST OF FIGURES

LIST OF TABLES

1.0 INTRODUCTION

1.1 INTRODUCTION

The scope of orthopaedics is broad, encompassing many areas from fracture fixation to joint arthroplasty. Low friction cartilaginous surfaces are characteristic of synovial joints and provide a durable articulation essential for pain free mobility. Not surprisingly, joint surfaces excessively compromised by disease, injury, congenital defects or inadequate blood supply result in chronic pain and deterioration of joint function. Arthroplasty, or replacement of the articulating surfaces of a joint, has represented a revolutionary leap forward in the treatment of joint diseases and disorders. Replacement of one or both articulating surfaces in THA alleviates pain and allows restoration of joint mobility.

Prior to the development of hip arthroplasty, therapeutic options for management of the pathological hip joint were simple analgesia, femoral osteotomy, hip arthodesis (fusion of the joint) or hip joint amputation (removal). Since Charnley's introduction of joint replacement in the early 1960's[1], joint replacement has been recognized as one of the most successful surgical procedures of our time. It is estimated that 2.5 million people world wide have hip joint replacements and that about 800,000 new operations are performed annually.[2] About 40% of all hip replacements are of the cementless type. The elderly account for the majority of hip replacement surgeries, but younger patients (less than 50 years of age) with traumatic or adolescent hip disorders represent an increasing proportion. Thus, hip replacement surgery is a prevalent and growing form of treatment. An ongoing research effort to improve implant function and longevity is essential as patients live longer, healthier and more active lives. Crucial to the maximization of implant function and longevity is the establishment and maintenance of mechanical fixation of implants with host bone.

1.2 TYPES OF IMPLANT FIXATION

Joint replacements must be mechanically functional and biologically compatible over an extended time period, ideally for the life of the patient. Implant stability is one mechanical parameter that directly affects implant longevity. Implant fixation refers to the generation of a

stable interface between the implant material(s) and surrounding bone. Over the last three decades, a variety of approaches have been developed for implant fixation. Implant fixation can be broadly classified as mechanical attachment with and without bone cement.

1.2.1 Bone cement

Charnley initiated the use of bone cement, polymethylmethacrylate (PMMA) in the early 1960's, which remains the most studied and most widespread method of implant fixation in joint replacement. PMMA is the combination of a liquid monomer and a powder polymer that cure within several minutes of mixing. Advances in the mixing and application of PMMA have given rise to cementing techniques that provide excellent clinical results. The pressurized application of PMMA in conjunction with scrupulous cleaning and drying of bone surfaces have, in large part, contributed to this success. Bone cement has relatively weak adhesive properties. Fixation is achieved by grouting an area 2-5 mm between the implant and the endosteal walls of the femoral canal. The roughened surface of the implant and the irregular surface of the endosteal cortex facilitate cement microinterlock. Implant geometry and surface texture influence the characteristics of the transfer of the applied implant load. Unlike biological fixation, implants fixed with bone cement acquire immediate and maximal stability once the curing process is complete.

1.2.2 Biologic fixation

Biologic fixation is achieved by the direct incorporation of an implant by osseous tissue. This can be attained by bone *in*growth in the case of a porous coated implant or bone *on*growth (apposition) in the case of a solid or microtextured implant. Osseointegration is another term frequently used to describe biologic fixation, defined at the light microscope level as the direct apposition of bone to an implant surface without intervening fibrous tissue. The process of osseointegration is often compared to the process of fracture healing and considered a process by which the implant is "healed" into the surrounding tissue.

The process of osseointegration

In a normal healthy animal, the process of bone repair can be divided into three phases: the inflammatory phase, the reparative phase and the remodeling phase. [2,3]

Day 1-3 The first few days of implantation are the *inflammatory phase.* Hematoma and fluid accumulate in the space near the implant and an acute inflammatory response occurs stimulating vasodilatation and cellular infiltration.

Day 4-18 The *reparative phase* begins when osteoprogenitor mesenchyme cells from the periosteum and endosteum (depending upon the implant location) surround the implant. These osteoblast stem cells are supported by fibrovascular tissue that replaces the hematoma of the inflammatory phase. Osteoclast cells resorb devitalized necrotic bone while osteoblast stem cells multiply, spread and differentiate along the implant surface. The process of bone formation begins.

After implantation, the conditions of the micro-environment at the bone-implant interface dictate the ensuing tissue formation. Tissue formation at the implant interface is either fibrous or osseous or a combination of both. Repetitive motion at the healing interface, in excess of about 40 μm increases the likelihood of fibrous tissue encapsulation at the implant interface.[4] Additionally, the nature of the implant surface also affects tissue formation. Smooth surfaces are most often encapsulated by fibrous tissue whereas porous and roughened surfaces are more likely to be apposed by bone.[5] Finally, closeness of fit also dictates tissue response. Intimate apposition of implant and bone results in the direct formation of woven bone at the implant surface.[6] Large gaps between implant and bone may be bridged by either cartilaginous or fibrous tissue. Cartilaginous tissue may remodel into woven bone however it is highly unlikely that fibrous tissue will transform into osseous tissue.

Osseointegration is not necessary for implant fixation since an implant may be effectievly stabilized by fibrous tissue. If the relative motion at the implant interface is not too excessive, fibrous tissue will align itself much like Sharpey's fibers into the porous spaces of sintered implants. The resultant fibrous tissue will support some degree of fixation. However, if the

relative motion at the implant interface is too great, the fibers will align along the axis of motion and the effect on providing implant stability will be reduced.

Day 19-200 The reparative phase lasts approximately two weeks after which the *remodeling phase* begins. The remodeling phase transforms woven bone formed during initial implant healing into a functional and potentially load bearing structure. Structural normalization, or adaptation of adjacent bone to the new loading environment resulting from the implant, may occur within 6-8 months.

1.2.3 Porous and plasma spray coatings

Many approaches to achieving implant stability without bone cement have been developed and biologic fixation can be achieved by a variety of methods. In the mid 1970's, investigation began to optimize implant fixation by tissue growth into porous materials.[7] Porous coatings on implants are typically fabricated by surface bonding a few layers of tiny cobalt chromium or titanium beads (Fig. 1.1) or crushed titanium fiber wires using high temperature heat treatments in vacuum furnaces. The resulting implant surface provides open (porous) spaces for tissue ingrowth (Fig 1.2). Bone growth into porous coated implants develops significant interface shear strengths, on the order of several hundred to several thousand kilograms per square cm.[8] Thus, even a limited area of bone ingrowth provides an effective mechanical attachment between the implant and bone.

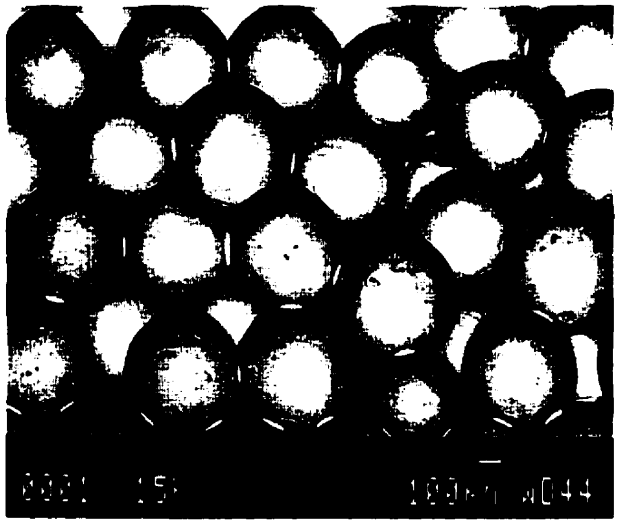

Figure 1-1 (above) Porous sintered bead coating.

Figure 1-2 (left) Bone growth as deep as three layers into porous coating. Bone (grey) metal (black) Bone Courtesy of Dr. JD Bobyn.

Porous or coarsely textured surfaces can also be obtained by plasma spray techniques. Implant surfaces with porosity of 45% and high surface roughness up to 625 μm have been created by injecting titanium particles into a plasma flame (15,000°C) while spraying them at the implant surface. Upon impact, molten particles cool and solidify yielding a surface resembling coarse sandpaper (fig 1.3). Plasma spray surfaces have been used successfully in clinical practice for a number of years. [9]

Figure 1-3 Bone apposition to plasma spray surface.

Depending on the quality of the manufacturing process, with both sintered porous coatings and plasma spray coatings, there is a risk of particle debonding form the substrate. This risk increases if the implant is unstable within the implant site. Particle debonding can further reduce implant stability and cause osteolysis or problems with third body wear at the articulating surfaces of the artificial joint.

1.2.4 Other textured implant surfaces

Implant surfaces can be prepared that have either random or predetermined textures. Textured implant surfaces have been produced by plasma spray, microknurling, casting, chemical etching, grit blasting and laser etching.

1.2.4.1 Surface description and classification

Surface texture can be defined as the repetitive or random deviations form the nominal surface which form a three dimensional surface topography. Surface texture consists of four elements: roughness, waviness, lay and flaws. ***Roughness*** is a quantitative surface characteristic described by the parameters in table 1.1. ***Waviness*** is all irregularities whose spacing is greater than the roughness sampling length. Waviness is a description of the underlying surface on which a rough surface is superimposed. Waviness can be accounted for and eliminated as a source of error in most surface analysis systems. ***Lay*** is the direction of the predominant surface pattern. ***Flaws*** are unintentional irregularities in the surface pattern that occur at one or few intervals on the surface.[10]

Table 1.1. Parameters describing surface roughness

Parameter	Description
R_a	Arithmetic mean of the departures from the mean profile line (Fig. 1.4)
R_z	Ten-point height is the average distance between the five highest peaks and five deepest valleys (Fig. 1.5)
R_{max}	Maximum peak to valley height within a sampling length
S	Mean spacing between adjacent peaks. (Fig. 1.6)

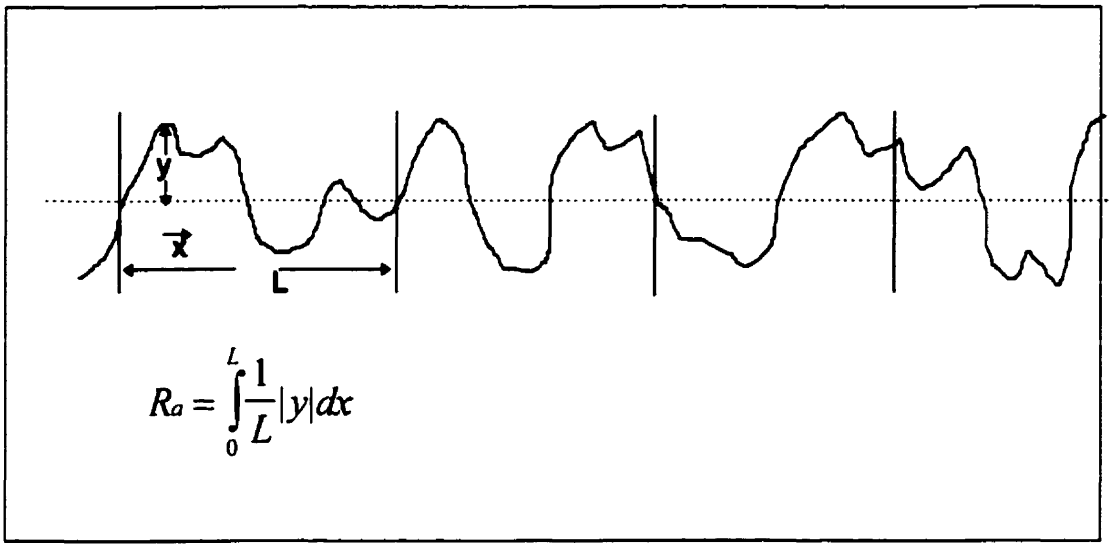

Figure 1-4 Derivation of mean centerline average roughness (R_a) the arithmetic mean of the departures in the y direction from the mean profile line.

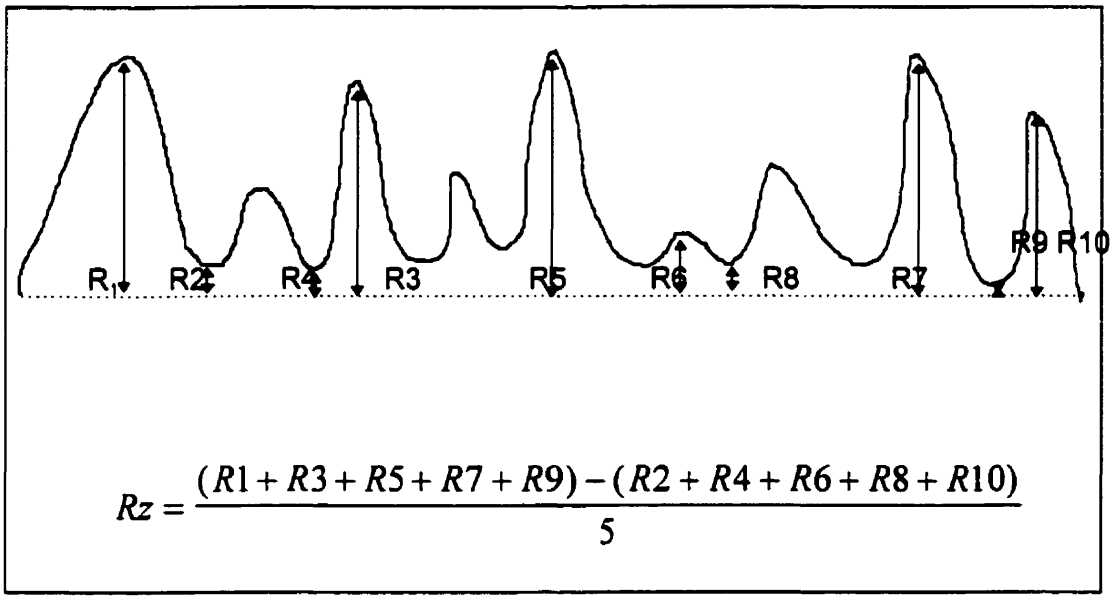

Figure 1-5 Derivation of average peak to valley height (R_z)the average distance between the five highest peaks and five deepest valleys

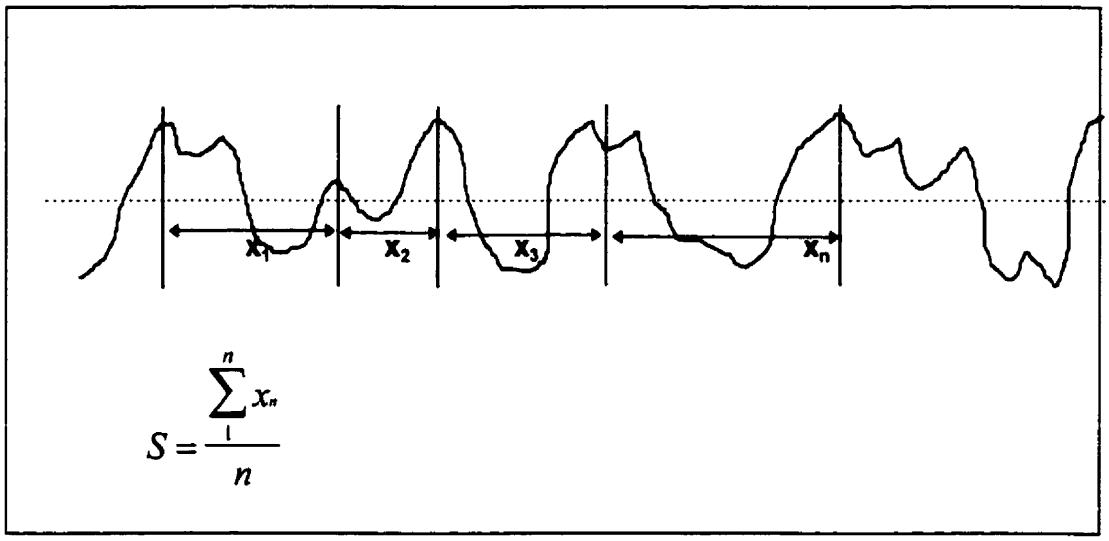

Figure 1-6 Derivation of average peak spacing (S), the average distance between adjacent peaks.

1.2.4.2 Microknurled surface

Bobyn et al.[11], by numerically controlled machining, prepared patterned and controlled macrotextured surfaces for osseointegration. Microknurling plastically deforms the underlying substrate to produce an undercut surface capable of resisting shear and capable of transmitting tension to the surrounding bone (Fig. 1.7). Although developed as an alternative to sintered coatings, microknurled implants suffer a reduction in fatigue strength resulting from the notch sensitivity of titanium.[12]

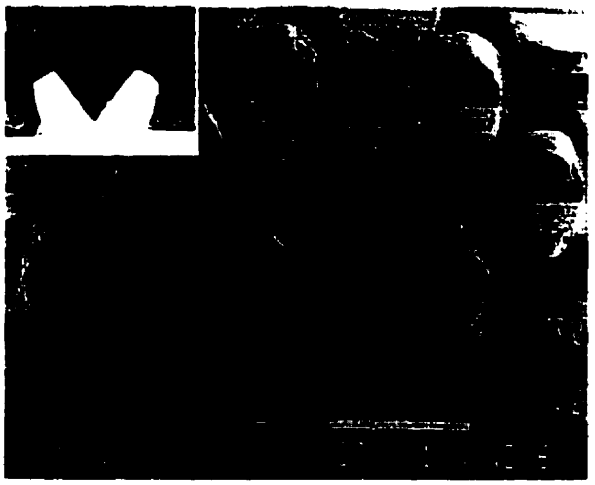

Figure 1-7 Microknurled surface (inset: cross section of bone ingrown microknurled surface) From L Bourassa, Masters thesis.[12]

1.2.4.3 Laser etching

Specific microtextured surfaces have been produced with a laser. Although not evaluated for orthopedic applications, Matsuda et al.[13] precisely fabricated a variety of pore sizes and spacings in polyurethane tubing. Laser etching is commonplace in the orthopedic industry as a means of implant marking.[14] This technology may hold immediate promise for precise

fabrication of implant surfaces in future investigations to determine the roles of various roughness parameters (Table 1.1) in tissue response. Laser etching technology would enable investigators to manipulate and investigate the causative effects of specific parameters independently. Achieving such specific control is difficult with conventional blasting or etching techniques. For example, an investigation to explore the effects of subtle changes in surface texture on cell activity may evaluate a variety of surfaces with different peak spacing but identical R_a. (this assumes that laser etching would not appreciably alter the surface chemistry of titanium)

1.2.4.4 Porous textured surfaces created by casting

Two of the original porous hip prostheses, the Judet and Lord stems, were created by casting techniques, but these femoral stems are no longer used. Recently, however, advances in casting materials and manufacturing techniques, namely computer assisted design and manufacturing, have spurred new interest in developing surfaces with predetermined three dimensional geometry and controlled porosity. Referred to by Melican et al.[15] as three dimensional printing, canine trials with this new surface have demonstrated bone ingrowth and interface shear strength comparable to porous surfaces.

1.2.4.5 Calcium phosphate coatings

Hydroxyapatite (HA) and tricalcium phosphate are well tolerated, biologically active materials used as coatings (50-170 μm thick) on the bone contacting surfaces of cementless implants to enhance initial bone formation. HA is a ceramic of calcium and phosphorous having a molecular ratio of 1.67. In canines, HA coatings have demonstrated the ability to induce bone formation over large (2-3 mm) gaps between implant and bone[2]. HA coatings applied to femoral implants are believed to decrease the likelihood of fibrous tissue formation by promoting rapid bone development onto the implant surface.[16] However, the long term benefit of HA coated implants has yet to be characterized.[17,18]

Hydroxyapatite is also commonly applied by the plasma spray method.[19] To increase the bonding strength between coating and substrate, HA is usually sprayed onto grit blasted (GB) surfaces. The resulting surface has an irregular structure and an R_a of 3-8 μm.[20,21]

Alternatively, sintering techniques have been employed to produce finely textured HA surfaces with average roughnesses less than 1 μm.

1.2.5 Microtextured surfaces without HA coating.

1.2.5.1 Acid etched (AE)

Microtextured surfaces can be created by subjecting the implant surface to corrosive conditions (fig 1.8). Acid etching (AE) of implants is usually carried out with sulfuric (H_2SO_4) and hydrochloric (HCl) acid at elevated temperatures of 125°C for a short (five minute) duration. Additionally, hydroflouric (HF) and nitric acid (HNO_3) have also been used as etching agents. A roughened surface topography is created by removing a portion of the metallic grains whose boundaries are not continuous at the implant surface. In animal models, acid etched surfaces have demonstrated a substantial amount of bone apposition.

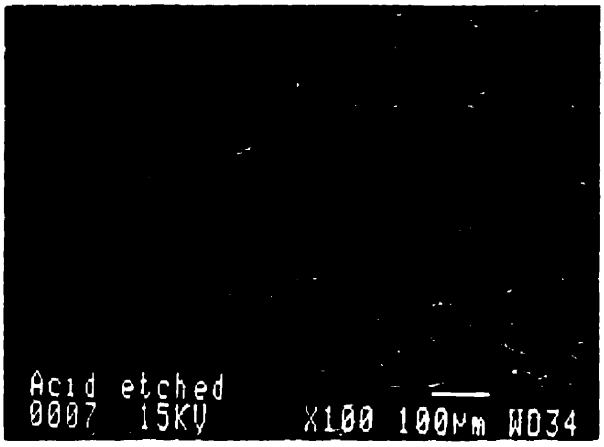

Figure 1-8 Grit blasted and acid etched Ti6Al4V surface.

Unfortunately, little work has been done to characterize the effects of reagent, temperature and etch time on the resulting surface topography of the Ti6Al4V alloy. However, Wong et al.,[22] described acid etched surfaces for osseointegration with fine R_a values averaging 1-2 μm. Acid etched surfaces present a different morphology than those surfaces obtained by grit blasting. Upon inspection, acid etched surfaces present closer peak spacing and sharper peaks than grit blasted specimens of similar R_a values. Acid etching has been used in conjunction with grit blasting to create surfaces that possess a fine texture resulting from etching superimposed on a coarser texture arising from grit blasting. Enhanced fixation of a dual textured surface may benefit from an increased surface area for bone attachment, an idealized surface topography for cellular response, and an increase in the interface shear strength arising from an increase in the number of undercuts or surface irregularities for bone integration.

1.2.5.2 Grit blasted (GB)

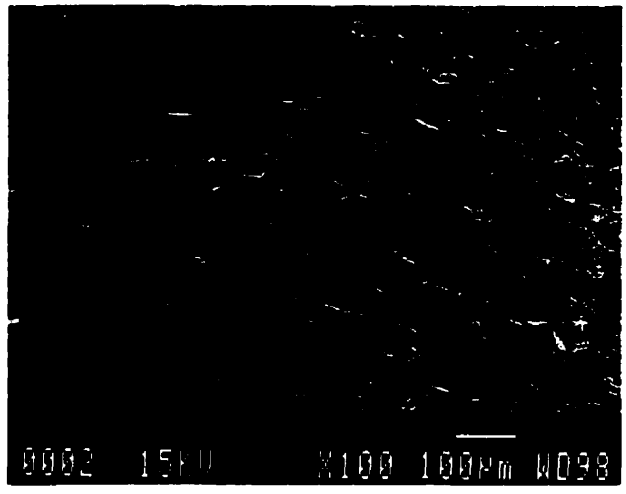

Figure 1-9 Grit blasted Ti6Al4V surface.

Bombarding metallic surfaces with small hard particles traveling in a high velocity stream of either air or water produces surfaces with an irregular texture (Fig. 1.9). Grit blasting is a process commonly known as sandblasting. Many agents, alumina oxide (Al_2O_3), silica, steel shot and hard organics (nut shells and corn kernels) have been used as the blast particle; however, in biomedical applications alumina oxide prevails. In orthopaedic and dental applications, titanium is the substrate of choice due to its ease of texturization (corundumization) and proven biocompatibility. Osseointegration of GB surfaces has been reported in both animal studies and human retrievals.[20,21,22,56,57,60,61,62,64,65,66,70,71,72,74,75,75] The low production cost, lack of deleterious heat treatments, minimal risk of substrate debonding and ease of manufacture are some advantages of producing cementless implants with grit blasted surfaces. Surface texture is a result of both plastic deformation and material removal. Topography can be controlled by varying the energy or size of the incident particle. Typically, particle size is varied and ranges from millimeter (coarse) to micrometer (fine) sized particles. Blast pressure and substrate have significant effects on the overall surface characteristics. Particle size is often referred to by grit number, the number of particles covering a known area. For the sake of clarity, particle size (and hence surface roughness) increases as the corresponding grit number decreases. The grit blasting process typically produces surfaces with an average roughness (R_a) of 0.5 to 10 µm.

1.3 SUMMARY

Joint replacement surgery is a successful and widespread form of treatment for joint disorders involving loss or degradation of articular cartilage. The longevity of any joint replacement is due in large part to the maintenance of implant stability *in situ*. Cement and biologic fixation are two options for implant fixation. There are several means to achieve stable biologic fixation. Fixation may be achieved through the use of porous coated implants (bone ingrowth) or surface textured implants (bone ongrowth). The concept of bone ongrowth using grit blasted surfaces is relatively new in the field of total joint implants. It forms the subject of the experimental work described in this thesis.

2.1 OSSEOINTGRATION AT THE CELLULAR LEVEL

2.1.1 The cellular perspective

From a cellular perspective, many porous and plasma spray implant coatings possess surface structures 10-30 times the size of an osteoblast. In contrast, acid etched or grit blasted surfaces present surface structures comparable in magnitude to the size of an osteoblast. [Within the scope of this thesis it is helpful to define surfaces based on the 20-30 μm diameter of an osteoblast cell.] A classification system is presented to differentiate between surfaces with macro and micro structures (Fig. 2.1) based upon the relative size of the cell and the surface features. Since surface structures will be designed for different tissue cells, the absolute criteria for classification as micro or macrotexture will change slightly. For osseointegrated devices, the osteoblast cell will establish the benchmark for surface classification. The **primary surface structure** is the topographical characteristics of any surface with the greatest magnitude and can be classified as possessing either a micro or macro texture. Any surface with a **macrotexture** possesses an average peak to valley height, (R_z), greater than the cell diameter. Any surface with a **microtexture** possesses an average peak to valley height less than the cell diameter. The **secondary surface structure** is the surface roughness, that, if present, is much smaller than and hence superimposed upon the primary surface texture.

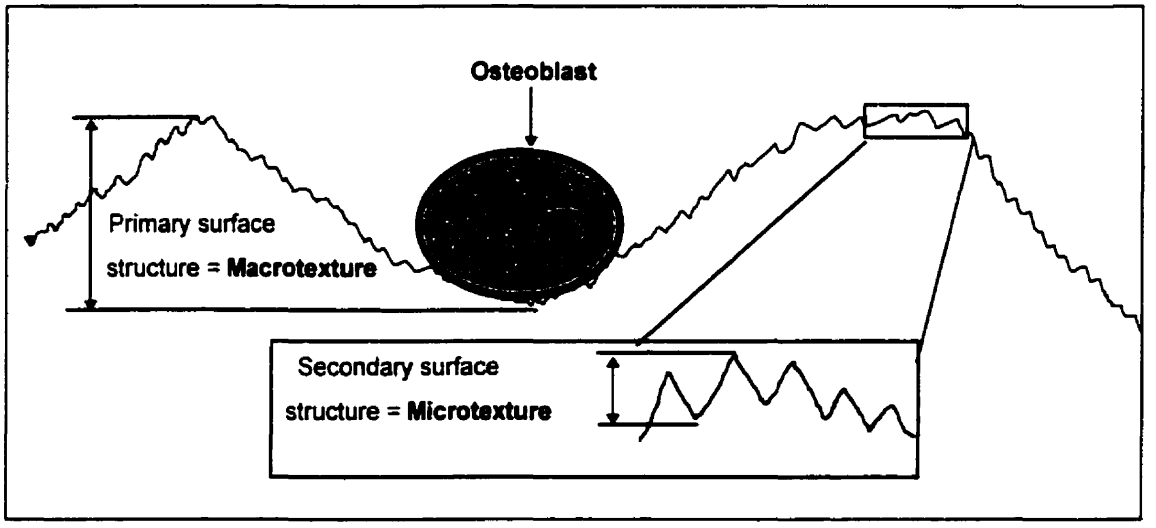

Fig.ure 2.1 Surface possessing both primary and secondary surface structures Primary surfaces and secondary surface structures possess macrotexture and microtexture respectively. (Inset) Depiction of secondary surface

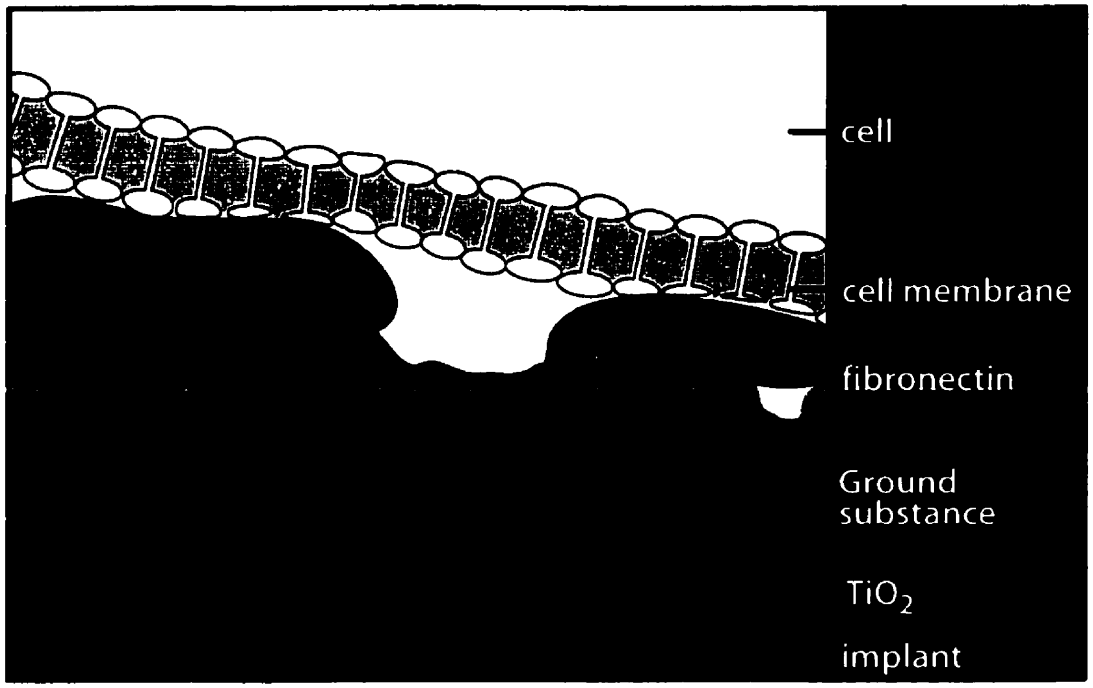

Fig.ure 2-2 Possible mechanism of cell adhesion to rough titanium alloy surfaces.

structure superimposed on primary surface. Surface structure is defined in reference to cell size, dimensions are not stated.

Process of cellular adhesion to titanium alloy surfaces

It is generally accepted that the biocompatibility of titanium arises from its continuous oxide layer.[23] Once exposed to air, titanium oxidizes rapidly and forms a thick, consistent and stable oxide layer comprised of Ti_2O_4, TiO_3 and TiO_2, the latter, TiO_2, being most prevalent. As a result, no biologically active molecule is ever in direct contact with the titanium alloy. Cells do not adhere directly to the oxide but instead bond to intermediaries: protein, proteoglycans, adsorbed water and fibronectin. The formation of the intermediate layer bound to the corrosive resistant oxide layer is responsible for the initial attachment and growth of osteoblast-like cells. [24]

The specific mechanisms of cell adhesion to a titanium implant are not well understood[25], but may be described as follows (Fig. 2.2). Macro-molecules (proteoglycans) and water molecules form a 20 nm thick[26] layer referred to as the ground substance. The ground substance is bound by hydrogen bonds to the titanium oxide layer which is 3-5 nm thick.[27] Osteoblasts are bound by integrins to the ground substance.

Integrins, specifically fibronectin, join the cell to the hydrophilic implant surface.[28,29] Osteoblast cells recognize fibronectin as an adhesion site, attach and begin growth on the media enhanced surface.[30] Thus, any preferential differences in cell attachment may be largely determined by the binding characteristics of the conditioned protein layer at the implant surface.

2.1.3 Osteoblast response at titanium interface

As previously shown, the titanium interface is conditioned with protein and water from tissue fluids that bind to the oxide layer and influence the behavior of both cell-adhesive molecules and cells at the implant surface. Following a series of cell-material interactions, growth factors, hormones and chemotactic factors are released stimulating the activity of surrounding cells. Osteoblast stem cells divide and increase the number of osteoblast cells that seed the implant surface. Osteoblast cells that adhere to the implant surface form the constituents of new bone. Collagen is first produced and then mineralized by calcium and phosphate from vesicles within the osteoblast cell.

The oxide surface on the implant surface is conditioned by Ca^{2+}, P^{5+} and OH^- which form a complex layer within the TiO_2 layer.[31] This effect may be due in part to the high surface energy of TiO_2 which is thermodynamically favorable for Ca^{+2}, P^{+5} and OH^- ions. It is this complex oxide - ion layer that interacts with the apatite of bone tissue and forms the bone-titanium interface.[32]

2.1.4 Cellular response to surface texture

All cells are exposed to some type of topographical environment. Cell-cell interactions, the extracellular matrix and biomaterials all present a surface to the cell that is definable and quantifiable. Extracellular surface topography affects the morphology, proliferation, migration, adhesion and metabolic activity of osteoblast cells,[33,34,35,36,37,38] however, the mechanism responsible for this effect is not well understood. Furthermore, the cellular response to surface structure is dependent upon cell type. Different cell lines respond uniquely to the same topographical surface. For example, epithelial cells and fibroblasts are differentially affected by micromachined grooves.[39,40] Epithelial cells will not migrate

across grooved substrata of depths greater than 2 μm whereas fibroblasts will. Fibroblast cells demonstrate greater adhesion and activity when cultured on smooth surfaces whereas the opposite is true for osteoblast cells. Osteoblasts adhere preferentially and seem to be activated by roughened surfaces but demonstrate faster growth and spreading on smooth surfaces. Early studies revealed that surfaces with an R_a greater than 0.5 μm are necessary for bone and not fibrous tissue apposition to occur.[41] In vitro studies have confirmed that osteoblast bone formation and adherence are positively stimulated on surfaces with R_a's ranging from 0.38 to approximately 6 μm.

As can be inferred, osteoblast cells cultured on both rough and smooth surfaces demonstrate markedly different morphology. On flat surfaces, osteoblasts spread out and conform to the implant surface and present few extracellular processes (Fig. 2.3b). This "flattened" morphological response is associated with cell spreading, proliferation and poor substrate adhesion. On rough surfaces osteoblasts present an irregular cell body with many processes extending radially from the cell (Fig. 2.3a). The "irregular" morphology is associated with increased cellular activity (production of constituents of bone), decreased proliferation and increased attachment strength. It must be noted that these images present cells in isolation on the culture surface and may not be representative of actual *in vivo* conditions when large cell numbers are present.

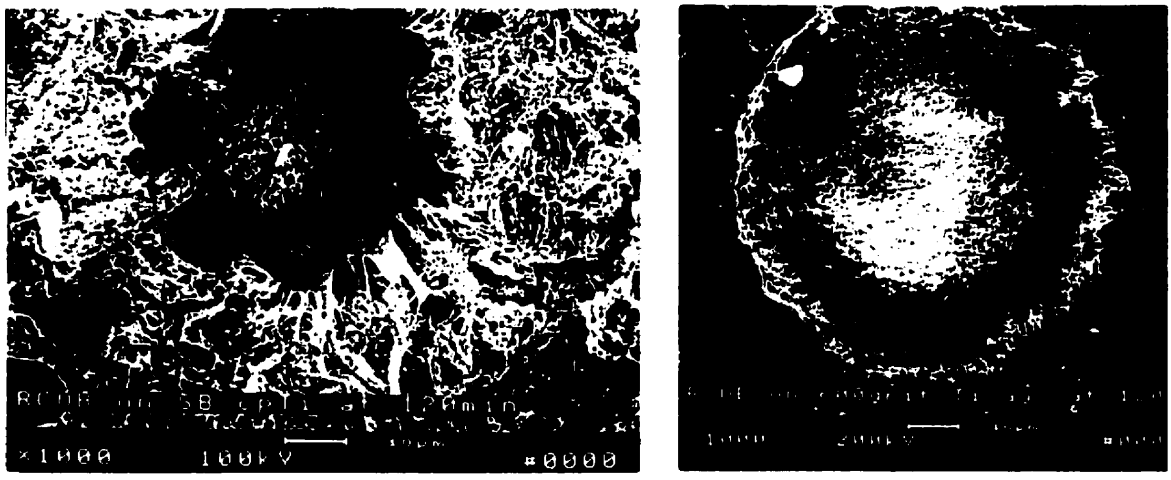

*Fig.ure 2-3a **Left**, osteoblast cells cultured on grit blasted (Ra=0.87 μm) surface. Cell appears to be non conforming and tented over surface. 2.3b **Right**, osteoblast on 600 grit sanded surface (Ra= 1.12 μm). Cell possess regular shape and close conformity to substrate (From Keller et al[38]., JBMR 1994)*

The effect of surface roughness on cellular response may result from a direct stimulatory effect on the cell, much like the lock and key model of cellular signaling. Alteration in the shape of the cell membrane may spatially activate or inactivate proteins that are part of the signaling cascade responsible for bone formation. Similarly, it has also been suggested that alteration in cell shape may have profound effects on cellular signaling. Morphological configuration can affect the function of ion channels modulating one pathway of cellular signaling. Tensile changes in the cell cytoskeleton are associated with cell guidance. Similarly, tension in the osteoblast cytoskeleton may provide a suitable stimulus for new bone formation. The morphology of the tented osteoblast in Figure 2.3 is visually suggestive of some tensile strain in the osteoblast membrane.

The cellular response to surface topography may also result from a preferential adhesion of water and serum media to the roughened surface. An enhanced protein layer may present an increased number of cell binding sites resulting in an increased number of bound cells.

Investigations concerning the relationship between cell behavior and oxide layer thickness have determined that cellular activity is affected by oxide layer thickness and composition. Coarse GB surfaces also have thicker oxide layers than polished or smoother surfaces[42] however, the relative contribution of oxide layer thickness to cell behavior on roughened surfaces is unknown. Additionally, the thickness of the oxide layer may be an important aspect of cell-implant adhesion and bone ongrowth as it may enhance the homogeneity and integrity of the adsorbed protein layer .

Alternatively, roughened surfaces may simply present more surface area and more sites for the hydrogen bonding of protein at the titanium oxide interface. A roughened surface may also provide unique three dimensional conFig.urations of the oxide layer that greatly enhance hydrogen and protein bonding. In support of this, Kasemo has suggested that "surface roughness will modify the interaction (van der Waals) since it influences the local electromagnetic fields at the (implant) surface."

2.2 STUDIES INVOLVING CORUNDUM BLASTED SURFACES *In Vitro*

2.2.1 Cell culture models

The potential for osseointegration of a biomaterial can be determined by culturing osteoblast or osteoblast stem cells on the surface of a representative sample. The nature of the biochemical processes occurring can be determined from assays of supernatant collected from the cell culture or electron beam analysis of material deposited onto the substrata. Benchmarks such as protein, mRNA, cytokines and growth factors are involved in the development of new bone and as such are used to characterize cell activity. Transmission electron microscopy is often used to characterize crystalline structures of mineralized deposits. Scanning electron microscopy and light microscopy elucidate the morphological characteristics of the cell and extracellular matrix. Infrared spectroscopy provides information about the chemical composition of organic phases and their respective molecular bonds. Finally, x-ray photoemission spectroscopy provides information pertaining to the chemical constitution of inorganic phases.

The wide-reaching genetic control over cell lines and rapid experimental results are strong advantages of cell culture studies with biomaterials. While some proponents question the accuracy and relevance of cell culture studies to *in vivo* conditions, numerous studies have shown a strong correlation between the performance of biomaterials *in vitro* and *in vivo*. Recent work by Lind et al.[43] has confirmed that transforming growth factor ß-1 (TGF ß-1) increases bone healing around gap defects providing a direct correspondence between *in vitro* and *in vivo* studies of osseointegration. Bone morphogenetic protein (BMP) [44], isolated from *in vitro* studies, has been similarly linked to new bone formation.

Thus, cell culture studies provide an effective means of evaluating the initial potential of a new biomaterial under very controlled conditions.

Various studies have reported that osteoblast or osteoblast-like cells show different morphology, proliferation, differentiation and protein synthesis when cultured on implant surfaces that are not smooth. Surface roughness affects the rate of cell growth, cell activity and the adhesive properties of cells cultured *in vitro*.

2.2.2 In vitro studies of corundum blasted surfaces

Surface topography determines cell morphology and function.

Based on their findings, Bowers et al.[45] concluded that "implants in contact with bone should be prepared with roughened surfaces". Substrates with surface roughness ranging from 0.14 - 1.15 μm were evaluated. The following R_a (μm) values for rough surfaces were created by: sandblasting, 0.87, etching, 0.25 and polishing with sandpaper, 0.14, 0.47 and 1.15. It should be noted that grit blasting produces an irregular surface while polishing with sandpaper produces a "rilled" or striated surface. Numerous authors have described differences in the response of various cell types to regularly patterned surfaces like those created by sanding. Surfaces with rilled or parallel lined structures do not enhance osteoblast adhesion or bone formation. Bowers et al. concluded that the sandblasted surface had the highest rate of cell attachment and presented osteoblast cells with a unique morphology, characterized by an irregular cell body with filopodial processes extending outward in all directions from the central body. Smooth and lightly acid etched surfaces presented cells with a flattened cell body and few radiating filopodial processes. Furthermore, it has been shown that specific cell shape can affect the phenotypic expression of cultured cells which led Bowers to postulate that "implant topography may affect the long term cell function as well".

Osteoblast-like cell proliferation and growth rate are greater on smooth surfaces while cell attachment and protein production are greater on rough surfaces.

Martin et al.[46] studied Osteoblast-like (MG63) cells cultured on electropolished surfaces (R_a= 2.5 μm), electropolished and acid etched surfaces (R_a= 5.15 μm), fine (R_a= 4.77 μm) and coarse (R_a= 5.76 μm) sandblasted surfaces and plasma spray (R_a= 9.14 μm)

surfaces. The greatest number of cells were present on the smooth surfaces and cell differentiation was suppressed by rough surfaces. However, as surface roughness increased, RNA, protein and collagen production increased. This increase in cell activity may be a result of cells actively producing the constituents of new bone. The authors concluded that on titanium surfaces, roughness affects osteoblast differentiation, proliferation and matrix production *in vitro.*

Martin et al. also suggest that differences in surface roughness may affect the thickness of the oxide layer increasing the amount of bound fibronectin which in turn affects cell adhesion. The authors found that the oxide layer ranged between 10 nm on the smooth samples up to 30 nm on rough samples. Potentially, differences in oxide layer thickness may affect the rate of ion loss from the substrate, known as ion leeching, which has also been shown to affect cell behavior, even with the use of titanium alloy [47] .

On titanium surfaces, surface topography directly affects osteoblast attachment strength whereas oxide thickness appears to have little influence.

In contrast to the theory of Martin et al., Keller et al.[38] determined that the osteoblast response to titanium is not dependent upon oxide layer thickness. A thorough surface analysis of commercially pure titanium (c.p. Ti) and titanium alloy disks with matched surface topography revealed no difference amongst wetting angles and carbon, oxygen and nitrogen adsorption. There was, however, nearly a three fold difference in oxide layer thickness between c.p. Ti (3.2 ±0.8 nm) and titanium alloy (8.3 ±1.2 nm).

Osteoblasts were cultured on grit blasted (R_a=0.7/0.9 μm), sanded (R_a=0.1/0.2 μm) and Al_2O_3 polished (0.04/0.03) Ti-6Al-4V/c.p. Ti. There were no significant differences in cell attachment at time periods of 15, 30, 60 and 120 minutes between Ti-6Al-4V or c.p. Ti. However, percent cell attachment correlated with increasing surface roughness.

In addition, Keller et al. cultured osteoblasts at all time periods on a control of tissue culture plastic (TCP). TCP has a highly hydroxlyated surface[48] and demonstrated greater osteoblast attachment than the rough titanium surfaces at 15 and 30 minutes

which was not significantly different at 60 and 120 minutes. It would appear that a certain surface energy or state is necessary for cell attachment and in such cases, surface topography does influence cell response. As demonstrated by the response to TCP, osteoblasts may also respond to a variety of surface modifications like hydroxylation that demonstrate a comparable ability to influence cell attachment.

Surface roughness modulates paracrine signaling[1] of osteoblast cells.

Kieswetter et. al.[49] reported that surface roughness affects production of the cytokine prostaglandin E_2 (PGE_2)[2] and the growth factor transforming growth factor β_1 (TGF-β_1). PGE_2 and TGF-β_1 are two potent mediators of bone growth. Cell number decreased with increasing surface roughness, however, PGE_2 obtained from the culture media was 1.5-4.0 times greater in the rough surface samples when compared to the smooth surfaces. This represented a six to eight fold increase in PGE_2 production when normalized for cell number. PGE_2 production correlated to an increase in surface roughness being 2 times greater on rough blasted samples than fine blasted samples. TGF-β_1 was 3-5 times higher for rough surfaces (coarse grit blasted) compared with smooth (plastic) surfaces and also when normalized for cell number.

Maximum [PGE_2] was low and would not affect osteoblast cells, however at these concentrations PGE_2 may act as a secondary messenger thus modulating cell activity. Conversely, [TGF-β_1] was sufficient to have a positive effect on osteoblast activity. These results suggest that surface morphology affects the bone stimulating activity of osteoblast - like cells *in vitro*. It was also shown that cell morphology was affected by the substrate surface. These studies have been corroborated by Stanford et. al.[50] who showed that surface protein deposition increased as surface roughness increased.

Ninomiya et al.[51], with a smooth and 24 grit blasted titanium alloy surface and a smooth plastic surface, reported that fibroblast cell proliferation decreases with increasing

[1] Paracrine signaling - chemical mediators that act on local cells only

surface roughness. Ninomiya also demonstrated increased levels of bone resorbing cytokines, interleukin-1β and interleukin-6 as well as increased levels of collagenase and stromelysin (enzymes that break down collagen). It is interesting to note that of the four bone resorbing mediators, the GB samples showed higher levels of collagenase and Interleukin-1β while both GB and smooth showed moderate increases in Interleukin-6 and stromelysin activity. This suggests that some mediators of bone resorption are enhanced by grit blasted surfaces. However, the increase in mediators by smooth surfaces as well suggests that this effect may be a part of the bone remodeling process. Furthermore, the authors failed to record the level of any bone inducing proteins or mediators. Biological processes do not function in simple linear relationships, rather a feedback loop of opposing processes determines the resulting cell activity. It is quite possible that the levels of TGF-β_1 and PGE_2 greatly outweighed the resorptive effects of Interleukin-1β, Interleukin-6, collagenase and stromelysin.

Cell response to roughened surfaces is dependent upon the state of cell differentiation.

Schwartz et al. [52] using the same surface preparations as Martin et al., investigated the effects of surface roughness on chondrocytes from the resting zone, (less mature, RC) and growth zone (more mature, GC) of rat osteochondral cartilage. This study determined the effects of surface structure on endochondral bone formation, a precursor to lamellar bone often found at immature bone-implant interfaces. Cell proliferation was reduced for the RC cells by roughened surfaces when compared to smooth surfaces, however the opposite was true for GC cells.

Cell activity on surfaces differed. While mRNA activity (indicative of protein production) increased for both RC and GC cells, protein produced by RC and GC cells differed. GC cells demonstrated decreased levels of collagen production and increased levels of alkaline phosphatase-specific activity which is linked to calcification of the collagen

[2] In low concentrations, PGE_2 has a positive effect on osteoblast activity but at higher concentrations inhibits osteoblasts and stimulates osteoclasts.

matrix. RC cells produced more collagen while demonstrating decreased alkaline phosphatase-specific activity.

Osteoblast cells form new bone directly on corundum blasted surfaces.

Groessner-Schreiber at al.[99] reported that the surface topography created by blasting with corundum particles stimulates osteoblastic bone formation directly on the implant surface. Osteoblasts were cultured on Ti6Al4V discs with a smooth, corundum blasted, titanium plasma sprayed surface or on a smooth plastic surface control. Assays of alkaline phosphatase activity (ALP), Ca incorporation and collagen synthesis were significantly elevated on both plasma sprayed and corundum blasted titanium samples. Extracellular matrix calcification, quantified by alizarin red bound absorbance was greatest ($p=0.001$) on the corundum blasted surface. SEM analysis verified ossification on the implant surface.

2.2.3 Summary

In summary, rough (R_a's >0.40 μm) irregular surfaces:

1. Decrease osteoblast cell proliferation.
2. Increase osteoblast cell adhesion.
3. Increase the production of proteins required for collagen formation.
4. Increase the activity of enzymes responsible for matrix mineralization.
5. Increase paracrine factors responsible for osteoblast stimulation and bone formation.
6. Produce cells of differing morphology when compared to cultures on smooth substrates.
7. Elicit osteoblastic bone formation and direct deposition on the implant surface.

Furthermore, the surface roughness (R_a) of the substrate is not the sole characteristic that determines the cellular response *in vitro*. It has been shown that irregular surfaces, like those created by sandblasting, have significantly different effects on the morphological appearance and cellular activity of osteoblast and epithelial cells when

compared to regularly (polished by sandpaper) or pitted (etched by acid) surface structured samples. It can be concluded that roughened surfaces created by grit blasting affect the activity of osteoblast cells *in vitro*. Amongst titanium implants with stable oxide layers, surface roughness, not oxide thickness, influences osteoblast adhesion. Based on these data, it is hypothesized that GB surfaces may induce the formation of new bone and promote osseointegration of such a surface structured implant *in vivo*.

2.3 STUDIES INVOLVING CORUNDUM BLASTED SUFACES *In Vivo*

2.3.1 Non-functional implant models

In vitro studies offer an excellent means of isolating and controlling the overwhelming number of confounding variables that exist *in vivo*. However, information acquired *in vitro* is done so in isolation outside of the physiological milieu. Due to the complexity of the *in vivo* environment and the simplistic nature of *in vitro* studies, only inferences to the biological performance of a biomaterial can be made. Although invasive, animal studies provide valuable information that *in vitro*, or computer models cannot predict with certainty. Factors such as the radiographic and scanning electron micrographic appearance of the implant-bone interface, bone growth or resorption rates, degree of calcification, soft tissue response, and an array of mechanical parameters can only be evaluated *in vivo*. [53]

However, there are widespread ethical concerns regarding the use of animal models which limits their use in experiments where other scientific avenues will not provide suitable or accurate information. Animal models are costly, require longer study durations and have inherently greater genetic variability than cell culture models.

Non-load bearing animal models are used as an initial attempt to evaluate the performance of orthopedic implant materials *in vivo*. The rabbit model is frequently used but the canine is the preferred model due to its prevalence in published work[2], similarity in bone structure to humans and rapid rate of bone development.[54] Implants are typically placed in either cancellous or cortical bone. Commonly, transcortical cylindrical implants placed in the diaphysis of the femur are used to evaluate the shear strength of fixation of and relative amount of bone apposition to the biomaterial in question. Cylindrical implants placed in the femoral canal have also been studied in an attempt to better simulate the biologic interface of a femoral hip stem *in vivo*.

Interface shear strength (MN/m^2 or MPa) is evaluated by measuring the force required to push or pull an implant out (0.5-1.0 mm/min) of host bone. Bone apposition can be

determined from light microscopy but is more accurately determined from backscattered electron microscopy (BSEM).[55] Thin sections are cut from the implant, analyzed by BSEM and the proportion of bone in contact with the implant perimeter is determined.

2.3.2 *In vivo* studies of non-functional corundum blasted implants

Non-load bearing studies, in either cortical or cancellous bone, evaluate the fixation strength or amount of bone apposition to a new material or surface treatment for osseointegration.

A rough and irregular surface structure increases the likelihood of implant osseointegration.

Thomas and Cook[56] evaluated the histological characteristics and mechanical fixation strengths of a variety of transcortical implants in canine femora. In this 8 month study, commercially pure titanium and alumina oxide (Al_2O_3). Implants were prepared with either smooth (polished) or rough (grit blasted) surfaces. The titanium implants had R_a's of 0.25μm (smooth) and 0.38 μm (rough). The alumina oxide implants presented rougher surfaces after treatment with R_a's of 1.6 μm (smooth) and 2.1 μm (rough). The vast majority of smooth surfaces for both the titanium and alumina oxide plugs were encapsulated by fibrous tissue in spite of the fact that the smooth alumina oxide plugs had a greater R_a (1.6 μm vs 0.38 μm) than the rough titanium plugs. This may be attributed to the surface structure presented to the cell. Surfaces of similar R_a can range from wavy to rough and present very different morphologies. Therefore, scanning electron micrographs of the surface under investigation are a necessary adjunct to any surface measurement to understand the topography existing at the cellular level. The smooth implants, both titanium and alumina oxide, used in this study did not present the same irregular surface as the blast treated implants. The blast treated implants in both groups had greater amounts of bone apposition and a 20-30% greater interface shear strength, however the difference was not statistically significant.

Osseous response to various implant substrates is highly dependent upon surface topography not surface chemistry.

Carlsson et al.[57] compared bone apposition to HA coated (R_a= 5.1 ± 0.66 μm), smooth (R_a = 0.9 ± 0.01 μm) and GB (R_a = 3.1 ± 0.53μm) cylindrical Ti implants in the tibia of arthritic human knees. Histological analysis revealed a fibrous interface around the smooth implants and bone apposition around the GB and HA coated implants. No statistical difference in bone response could be determined between the GB or HA coated implants. Carlsson suggested that the lack of differences may have been due to the similar surface roughness.

Chappard et al.[58] compared the tissue response to grit blasted titanium (Ti6Al4V) cylinders implanted in the distal metaphysis of the rabbit to grit blasted titanium cylinders coated with xenogeneic bone particles. At study periods of one, two and three months there was no significant difference in bone apposition between groups. In this study, tissue response was not dependent upon the different implant materials, suggesting that tissue response may indeed depend primarily upon implant surface structure. Other factors may have masked a difference in response. For example, the rapid resorption of bone particles or biochemical differences between the bovine and rabbit physiology may have negated any effects of the bovine bone particles in this model.

Larsson et al.[59] investigated the effect of titanium oxide layer thickness on the amount of bone apposition to threaded implants placed in cortical bone. Machined and electropolished surfaces differing in oxide layer thickness and oxide topography (not chemical composition) were evaluated. Topographical differences were determined by atomic force microscopy and were slight in nature. Smooth electropolished implants, regardless of the amount of surface oxidation, were apposed by less bone than the machined implants at both 1 and 6 weeks. If the cell-oxide interaction is limited to the first few atomic layers, little effect would result from differences in oxide layer thickness. Surface topography, smooth (electropolished) vs. rough (machined), was the sole factor influencing bone apposition at the bone-implant interface.

Bone apposition is a function of surface roughness (R_a).

Buser et al.[60] studied the effect of surface roughness on bone apposition to different titanium implants in pig cancellous bone. Three implants were inserted into the epicondyles of each femur. Of the six surfaces studied, electropolished and medium sandblasted with acid etch had the lowest amount of bone apposition, 20-25%. Titanium plasma sprayed implants and coarse sandblasted had 30-40% bone apposition and coarse sandblasted with acid etch had 50-60% bone apposition. Implants coated with HA had bone apposition of 60-70%, but the HA showed consistent signs of resorption. The authors concluded that as surface roughness increased, so did the extent of the bone-implant interface apposed by bone.

Goldberg et al.[20] compared the amount of bone apposition and the strength of the bone-implant interface of smooth, fibermetal (400 μm pore size) and grit blasted Ti-6Al-4V implants (Ra = 3.0 μm), at 3, 6 and 12 weeks. In contrast to the study by Friedman et al, the investigators concluded the GB implants had significantly more bone apposition (31%), than the fibermetal (17%) or polished (15%) implants. Furthermore, the investigators discovered that there was no significant difference between the fixation strength of the GB implants and fibermetal implants. Goldberg et al. concluded that GB surfaces were "an excellent surface for bone-implant integration".

Surface roughnesses greater than 0.61 μm enhance initial bone development and strength of fixation.

Gotfredsen et al.[61] investigated the osseous response to GB (Ra = 0.61 ± 0.03 μm), smooth (Ra = 0.31 ± 0.12 μm), and HA (Ra = 1.89 ± 0.15 μm), coated transcortical implants in the proximal tibial metaphysis of the rabbit. Torque removal tests were significantly dependent on surface texture ($p<0.0001$). Most interestingly, removal torques for the HA coated and GB implants did not increase significantly between 3 and 12 weeks, however, the smooth implants demonstrated an increase in removal torque between 3 and 12 weeks. This suggests that surface roughness is an important factor in enhancing the initial strength of fixation. Since fixation strength is a function of surface roughness and bone apposition, it may be inferred that surface roughness enhances

bone response. In support of this, the authors noted bone growing along the surface of the GB implants away from the endosteal cortex, concluding that GB surfaces have osteoconductive properties.

At 12 weeks, interface shear strength is directly proportional to surface roughness whereas bone apposition to implants (R_a 1.2 - 6.4μm) is not.

Wong et al.[22] studied the effect of surface roughness on the extent of bone apposition to titanium implants in the distal metaphysis of the miniature pig knee. Morphometric studies determined the extent of bone apposition to each surface and mechanical push out tests determined the bone-implant interface shear strength. Wong also evaluated the effect of different materials, commercially pure titanium (CP-Ti), and titanium alloys, Ti-6Al-7Nb and Ti-6Al-4V for their effect on bone apposition. All three materials were surface finished as either fine blasted, rough blasted or rough blasted and etched. As well a group of Ti-6Al-7Nb implants that were rough blasted, etched and coated with HA were evaluated. The R_a surface values ranged from 1.2 μm for the fine blasted sample to 6.4 μm for the coarse blasted sample etched and coated with HA. The investigators found an excellent correlation (r^2 = 0.90) between the surface roughness and the strength of mechanical fixation. Furthermore, no significant difference in fixation strength due to implant material, excluding the HA coated implant was reported. Of importance, the authors also concluded that surface coverage did not differ significantly between the different surface treatment groups or alloys. These findings suggest that quantification of bone apposition alone is not sufficient to predict implant stability in load bearing systems.

Friedman et al.[62] also studied the fixation strength and histological characteristics of a variety of surfaces on titanium implants in the cancellous bone of the distal rabbit femur. The investigators compared plasma sprayed (500 μm coating), sintered bead (450 μm diameter), arc deposited (50-350 μm) and grit blasted (R_a = 1.97 μm) titanium implants after 6 and 12 weeks of implantation time. The authors concluded that the bone-implant interface strength and amount of bone apposition of the GB implants was the lowest in

the study group. Bone apposition and interface shear strength did not increase significantly between 6 and 12 weeks.

Luckey et al.[63] evaluated the fixation strength and histological interface of transcortical plugs in both cancellous and cortical sites in the hind limb of the goat. Plugs had either sintered bead, (250-300 μm pore size) plasma spray (R_a = 625 μm) or a fine GB surface (R_a = 2 - 4 μm). At eight weeks the GB plugs had an average interface shear strength of 1.05 ± 0.52 MPa in cancellous bone and 2.20 ± 1.90 MPa in cortical bone, notably less than either the porous coated, [5.96 ± 2.36 MPa (cancellous) and 6.86 ± 3.76 MPa (cortical)], or plasma spray implants [5.50 ± 1.26 MPa (cancellous) and cortical 4.31 ± 3.26 (cortical)]. Bone was apposed to approximately 33% of the GB plug surface, however, bone apposition was limited only to the bony spot welds in the porous coated and plasma spray implants.

Saha et al.[64] compared plasma spray, (R_a > 500 μm), grit blasted, (R_a = 3.81 μm) and grit blasted implants (R_a = 1.40 μm) in a transcortical canine model. All implants demonstrated bone apposition. Similar to the findings of Wong et al., interface shear strength increased as implant R_a increased as shown in the following table:

Table 2.2 Interface shear strength of corundum blasted and plasma spray implants

IMPLANT R_a (μM)	INTERFACE SHEAR STRENGTH (MPa)
1.40	1.042 ± 0.317
3.81	3.170 ± 0.806
500 +	11.536 ± 2.959

Prior to 4 weeks, the rate of bone apposition is greater for implants with R_a's less than 4.2 μm.

Feighan et al.[65] evaluated the effect of a range of surface textures on bone-implant apposition and bone-implant interface strength using a smooth surface (R_a= 0.5μm), two GB surfaces (R_a = 4.2 & 5.9 μm) and one surface created by blasting with steel shot (Ra = 5.8 μm). The investigators determined that the formation of new bone on the implant increased when compared to the smooth surface and increased with implantation time. At three weeks the 4.2 μm surface possessed the greatest amount of bone apposition which at 6 and 12 weeks was not significantly different from the 5.9 μm surface. Both the 4.2 and 5.9 μm surfaces had greater bone apposition than the surfaces blasted with steel shot. In addition, the pull out strengths of the three roughened surfaces were 6 times stronger than the fixation strength of the smooth surfaced implants and comparable to the pull out strengths of HA and fibermetal coatings in previous studies. The investigators also noted that the total amount of bone was affected by the proximity of the implant to the endosteal cortex and the location of the implant within the femur of the rabbit.

Is an R_a of 1.45 μm an optimal surface roughness ?

In contrast to these studies, Wennerberg et al.[66] determined that titanium surfaces of R_a = 1.11 μm developed greater amounts of bone apposition at four weeks than implants with an R_a = 2.52 μm. The authors concluded that "a highly increased surface roughness compared to a moderately increased one is a short term disadvantage for bone tissue."

In another study, Wennerberg et al. investigated the tissue response to textured screws in the cortex of the rabbit femur. Three surfaces were evaluated with R_a's of 1.11 μm, 1.45 μm and 2.52 μm. At 12 weeks the 1.11 μm and 1.45 μm implants had significantly greater bone apposition and removal torques than the 2.52 μm implants.

Amongst the 1.11 μm & 1.45 μm implants, the 1.45 μm implants demonstrated the highest values of bone apposition (p=0.04, Wilcoxon signed rank test). However, the removal torque which was significantly different in cortical bone (p=0.006) was not

significantly different in cancellous bone. These findings suggested that the optimal surface roughness for bone apposition may lie in the 1.5 μm range.

2.3.3 Summary

In summary, *in vivo*:

1. Osseointegration is dependent upon surface structure and surface roughness.
2. Textured irregular titanium surfaces support extensive bone ongrowth.
3. Amongst comparably biocompatible surfaces, osseous response is dependent more upon surface texture than surface chemistry. Whether or not this has implications regarding the current understanding of the affects of HA on bone development remains unanswered.
4. At four weeks, bone apposition is greater for implants with R_a's less than 4.2μm and may be optimal at 1.45 μm.
5. At 12 weeks there is no difference in bone apposition between R_a's 1.2 - 6.4 μm.
6. Interface shear strength is directly proportional to surface roughness.
7. There are similarities between HA and GB implants with respect to initial osseous response, osseoconduction and strength of fixation.
8. Mechanical testing has proven that GB interface strengths are comparable to fibermetal and HA coatings in the rabbit intermedulary model at short time periods, however the interface shear strength in cortical bone appears to be considerably less.

2.4 *In Vivo* STUDIES OF FUNCTIONAL CORUNDUM BLASTED IMPLANTS

Load bearing models permit the assessment of implant function under simulated *in vivo* conditions. This provides information of clinical importance, such as implant stability, bone remodeling and quantification of the bone-implant interface.

2.4.1 Functional implant models

Load bearing or functional implant models are the final stage of interface testing. Once cell culture and non load bearing studies have demonstrated the potential efficacy of a new biomaterial, the next phase is to evaluate its performance in a clinical scenario prior to clinical trials. When evaluating the tissue response and initial performance of orthopaedic implants the effect of implant design, experimental model, site of implantation, surgical technique, post operative conditions and implant position must be considered. Furthermore, one must realize that a laboratory animal does not accurately represent the pathological conditions under which the device is required to perform. Therefore, information gathered from laboratory studies and inferences made to the clinical scenario must be made with caution. Nevertheless, careful experimental design can simulate implant performance under a "worst case scenario", yielding relevant information from a healthy test subject.

Radiographic and histological parameters are most often assessed. Implant performance is scrutinized for radiographic evidence of loosening, migration or subsidence. Soft tissue samples harvested for histological assessment elucidate any adverse reaction. High resolution radiographs enable a gross overview of the implant in situ. However, backscattered electron microscopy provides the most accurate assessment of the bone- implant interface. Mechanical data can be gathered if the implant and experimental design permits.

From a survey of the literature, minimal periods of implantation can be established for observing bone related changes around load bearing implants in the canine model. Six

months is a suitable period for the assessment of bone ingrowth into porous coated devices. Between eighteen months and two years is the recommended study length for the observation of density related bone changes around load bearing implants[67,68]. Bone apposition reaches a steady state at a much faster rate than bone ingrowth as shown in Table 2.2. Longer study periods enable comparison with other studies and permit the observation of the bone-implant interface after a suitable period of remodeling. A six month period may be the minimal period to observe the bone-implant interface in a remodeled state, comparable to longer term human retrievals.

Table 2.2 Osseous tissue reaction to different surface treatments at different time periods [67,68]

MONTHS OF IMPLANTATION	% LINEAR APPOSITION	FIBER METAL - % BONE INGROWTH	SINTERED BEAD - % BONE INGROWTH
1	31.8	16.6	25.2
6	38.5	37.3	23.3
24	38.9	32.7	24.1

The load bearing environment of the canine model is suitable for implant studies. Although the dog weighs considerably less than a human the forces generated across the hip are greater. During jumping or running most of the force is derived from the hind limbs. As such, the relative hip joint loading force appears to be two to three times greater in the canine model than for human beings (Table 2.3).[69] As a result, the canine presents a favorable environment which includes an inherent safety factor for evaluating the potential of new surfaces for biologic fixation.

Table 2.3 Comparison of human and canine hip loading forces (from Geesink, 1987)[69]

	CANINE	HUMAN
Average body weight (kg)	30	70
Peak activity	jumping	stair climbing
Load factor (x body weight)	x 12	x 8
Surface area of prosthesis (cm^2)	20	90
Relative hip loading (kg/cm^2) body wt x load factor/surface area	18	6.2

2.4.2 Studies of functional corundum blasted implants in animal models

Only one study has apparently been published on the tissue response to CB surfaces in a load bearing model. Maistrelli et al [70] evaluated HA coated and grit blasted implants both with an Ra of 6-8 μm in a load bearing canine model. The femoral implants used in this study were not a canal filling design. A large and statistically significant difference in bone apposition was found between the HA coated (72%) and grit blasted (16%) implants. This large difference is not comparable to the findings of other authors in non load bearing applications and may arise from the ability of HA to stimulate bone formation across large gaps between the implant and the endosteal cortex.

2.5 CLINICAL RESULTS WITH CORUNDUM BLASTED IMPLANTS

Initially, corundum blasted press fit stems were not intended for fixation by osseointegration. However, retrievals at autopsy have demonstrated bony attachment, significant fixation strength and bone-implant interfaces characteristic of osseointegration. McCutchen et al.,[71] reported excellent results with a series of press fit titanium implants; extensive bone apposition and direct bone contact without intervening fibrous tissue was observed. Both European and American centers have demonstrated interest in the potential clinical application of these non porous surfaces for osseointegration.[72]

There are several common design features amongst stems with grit blasted surfaces: the surface roughness, as reported by the manufacturer, ranges from 3-5 μm (methodology and measured surface parameter unreported in the literature), the stem has a tapered geometry in the anterior-posterior and medio-lateral aspects, specific components of the stem, such as fins, are incorporated to achieve immediate fixation and the stem is fabricated from titanium alloy. Design philosophy varies amongst stems but immediate primary fixation by mechanical interlock followed by secondary fixation by bone apposition are common to each concept.

2.4.1 Corundum blasted press fit femoral stems in clinical use

Four press fit femoral components in clinical use have been described in the literature, however two are prevalent, the Zweymuller (Allopro, Switzerland) and CLS (Protek, Switzerland) stems. The Zweymuller and CLS stems are reported to possess an average surface roughness of 3-5 μm. Both stems possess a tapered geometry, however, there is a difference in the philosophy of implant design between these two systems. The CLS stem is more tapered and smaller than the Zweymuller stem. The CLS stem is also proximal filling, designed primarily for fixation in the cancellous bone of the proximal femur. In contrast, the Zweymuller stem is designed for fixation in the region of the femoral isthmus.

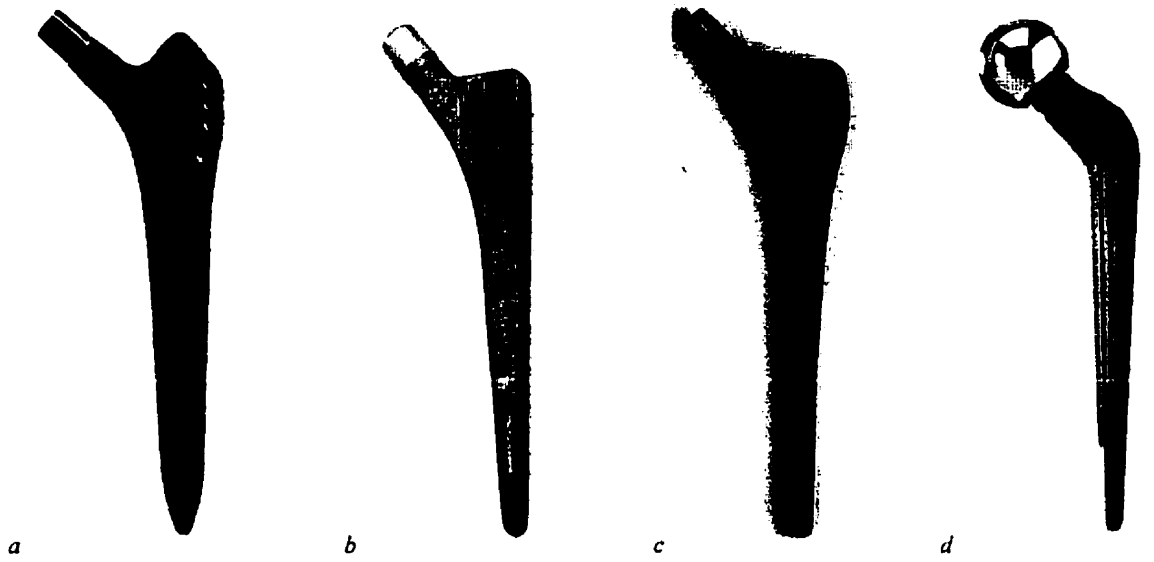

Fig.ure 0-1 Four corundum blast femoral implants for biological fixation by bone apposition: a.) Zweymuller , b.) CLS, c.) CLW , d.) Conical Stem (a, Allopro, Switzerland), (b -d, Protek, Switzerland)

Two other femoral implant designs with grit blasted surfaces have been reported in the literature, the CLW[73] and the Conical Stem[74] (Protek, Switzerland). The CLW stem is similar in design to the CLS stem. To enhance primary fixation, this slender collarless stem has a number of small parallel fins running the length of the implant surface in the direction of the long axis and one large fin at the proximal posterior implant end. The implant is slotted distally to reduce stem stiffness and has an average surface roughness of 3-5 μm. The Conical Stem is a cone shape stem with a 5° taper angle and eight radial longitudinal sharp ribs around the circumference. The ribs increase primary stabilization and surface area for secondary fixation by bone apposition.

2.4.2 Zweymuller stem

From retrievals at autopsy, Zweymuller et al.[75] have reported bone-implant contact covering up to 40% of the Zweymuller prosthesis surface. Thin section histology revealed direct apposition of bone along the irregular contours of the implant surface. Circumferential apposition of bone was evident around the proximal portion of the implant.[76,77] No fibrous tissue interfaces were observed between the trabecular bone and stem surface. Similarly, Lester et al.[100] reported extensive osseointegration of Zweymuller femoral implants retrieved at autopsy. Transverse serial radiographs and

light microscopy demonstrated periimplant ossification and circumferential bone apposition without intervening fibrous tissue. Backscattered electron microscopy revealed intimate bone-prosthesis contact. Together these retrieval studies provide evidence strongly indicative that stable, reproducible and long term implant fixation can be achieved with corundum blasted surfaces. Furthermore these studies have demonstrated that corundum blasted surfaces develop intimate bone-implant interfaces characteristic of osseointegration.

A 5-9 year retrospective clinical study of 72 hips by C. Delaunay et al.,[78] using the Zweymuller stem described above, reported a 98.5 % survival rate defined as loosening and/or revision at the six to seven year interval. Clinical results were graded as excellent in 90% of cases, fair in 5% and poor in 5%. The authors reported an absence of distal radiolucencies in Gruen Zones 2-3 and 5-6, but a consistent appearance of radiolucencies in zones 1 and 7. The investigators concluded that 71 stems were stable and the proximal radiolucency was "not a concern as the Zweymuller stem was not designed to fill the proximal femoral component".

Huo et al.[79] in a minimum three year prospective clinical study of the Zweymuller femoral component in 46 patients reported good or excellent results in 96% of the hips (HHS) in Dorr B or C type femurs. No stem was classified as probably loose (radiolucencies in greater than 50% of the zones) or definitely loose (subsidence > 5mm and change in position > 5°). Three stems displayed radiolucencies or reactive sclerotic lines in no more than three of 14 zones. Ninety-five percent of the stems were considered stable at final follow-up examination. Furthermore, there was no incidence of femoral osteolysis up to six years. The investigators concluded that the results with the Zweymuller stem were excellent.

2.4.3 CLS stem

Robinson et al.[80] in a six year prospective study of 57 hips determined that the "corundum blast finish was associated with reliable implant stability". At six years, 92% of the hips were rated good or excellent with a mean HHS of 92. The investigators

attributed proximal bone erosion to polyethylene debris. No erosion was noted in the distal portion of the stem. The investigators concluded that "bone apposition to the GB surface resulted in a barrier to migration of wear debris".

Blaha et al.[81] in a prospective study of three hundred hips undergoing THA with the CLS femoral stem reported that 83% of patients had no pain, 11% had slight pain and 4% had localized pain in the thigh. A total of 258 hips with a minimum five year follow-up had a 0.8% incidence of loosening and a 1.6 % incidence of subsidence. The authors concluded that bone ingrowth and distal fit and fill are not requisites for successful joint replacement.

Spotorno et al.[82] in a study of 258 hips with a minimum five year follow up reported three aseptic femoral loosenings, two of which were related to undersized implants and the remainder related to fracture of the proximal femur. Radiographic analysis showed demarcation in 108 hips, but in only 9 was the maximum width more than two mm. In 82.4 % of the cases this demarcation was limited to one or two Gruen zones.

In summary, femoral implants with a grit blasted surface of roughness of 3-5 μm have demonstrated favorable short and long term clinical results. In the vast majority of patients, stable stem fixation without thigh pain has been reported. Implant retrievals have demonstrated significant amounts of bone apposition although retrieval information is limited. Quantification of the relative amounts of bone apposition over extended time periods and a variety of clinical and pathological conditions will help to characterize the suitability of this surface design for osseointegration.

2.6 Summary

Despite the clinical success with grit blasted implants there appears to be little scientific evidence to support the clinical use of implants with a surface roughness of 3-5 μm. While the literature suggests strongly that an optimal surface roughness for osseointegration exists, no functional implant studies in animals have determined this parameter to be 3-5 μm. Cell culture studies have demonstrated a clear relationship between osteoblast function, proliferation and surface roughness; bone formation at the implant interface is highly dependent upon a rough surface. Evidence from non-functional studies suggests that the strength of implant fixation is a direct function of surface roughness, however, the extent of bone apposition is not a function of R_a. In contrast, short term studies report that smoother surfaces develop higher percentages of bone apposition and interface shear strengths. The apparent lack of cohesion in the literature requires clarification and comprehension concerning the effects of surface roughness on bone apposition, stem stability and overall implant function. Experimental investigation concerning the effects of a variety of surface roughness on implant stability and bone apposition may provide relevant information for the improved clinical performance of corundum blasted implants.

3.0 THESIS OBJECTIVE

Grit blasted surfaces have been used extensively on clinical hip prosthesis for the past decade in Europe. Compared with cemented and porous coated implants, little experimental data exists. The methodology used to determine the surface characteristics of grit blasted implants in clinical use has not been extensively quantified or thoroughly described. Furthermore, there appears to be little scientific literature supporting the utilization of the currently employed surface roughness. To the best of our knowledge, there are no other studies that have quantified the effects of implant topography on the extent bone apposition in a load bearing model. The purpose of this investigation was to determine the effect of surface roughness on the tissue response to tapered femoral implants. Implants were evaluated in a load bearing canine model under conditions of poor fit yielding information on implant performance in a worst case scenario. A study period of six months was selected to evaluate the bone-implant interfaces under long term (remodeled) conditions.

4.0 MATERIALS AND METHODS

4.1 IMPLANTS

4.1.1 Acetabular implant (Fig. 4.1)

A 28 mm diameter noncemented acetabular component was used for all arthroplasties (Fig 4.1). It was a nonmodular design with a porous tantalum metal backing and injection molded polyethylene articulating surface (Implex corp., Allendale, New Jersey). Data from the acetabular implants were reserved for a separate study and are thus beyond the scope of this thesis.

Figure 4-1 Acetabular implant.

4.2.1 Femoral implant (Fig. 4.2)

A grit blasted canine femoral stem was designed based on measurements made from radiographs of the canine femora. Three groups of canine femoral implants (Fig 4.2) were fabricated (Zimmer, Warsaw, Indiana) from medical grade titanium alloy (Ti 6%Al - 4%V) and were identical in every respect except surface finish. Surface finish was produced by blasting the entire bone contacting surface with 16, 24 or 60 grit particles of alumina oxide (Table 4.1) traveling in a high velocity air stream. The gun nozzle was fixed at a distance of 15 cm from the implant surface. Blast pressure was 200 KPa. Implant surface texture is further described in section 4.2.2

Table 4.1 Grit number and particle size

GRIT NUMBER[1]	PARTICLE DIAMETER (μm)
16	1080
24	750
60	250

The collarless stem was 9.0 cm long from shoulder to tip and possessed a double taper configuration in both the medio-lateral and anterior-posterior aspect (Fig. 4.3). A 17 mm modular cobalt-chrome alloy head was impacted onto the femoral neck Morse taper to

[1] Grit number describes particle size. An increase in grit number corresponds to a decrease in particle size and a decrease in blasted implant surface roughness.

articulate against the cementless acetabular (Fig. 4.1) implant. A larger lateral fin and a smaller central fin on both the anterior and posterior aspects of the implant (Fig. 4.2) were incorporated to engage the cancellous bone of the proximal femur and thereby increase initial rotational stability.

Figure 4-2 The femoral implant used in study. Parallel fins, two on each of the anterior and posterior aspects of the stem are visible.

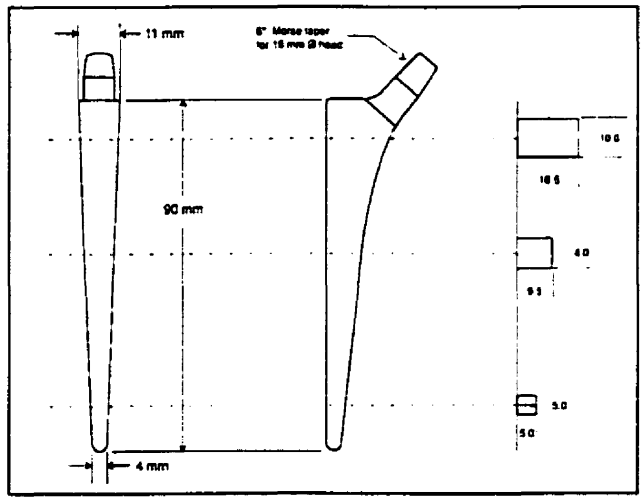

Figure 4-3 Design of the grit blasted canine femoral implant.

4.2 Surface analysis

4.2.1 Femoral implant surface analysis

Scanning electron microscopy (SEM), x-ray dispersive analysis (EDAX) and stylus profilometry were used to qualitatively and quantitatively depict the three implant surface textures.

Surface roughness was characterized by profilimetry measurements (DEKTAK 3030ST, Veeco Instruments Inc., Santa Barbara, CA) using a diamond stylus. One implant from each of the three surface texture groups was randomly selected and analyzed in a strictly controlled class 2000 HEPA filtered clean room with laminar air flow. A trace

length of 5 mm was selected at low scan speed, high resolution and a force setting of 5mg.

Figure 4-4 Profilimetry region of analysis

Measurements from each of the three implants were obtained from the anterior, medial and lateral regions outlined in Figure 4.4. Two traces were obtained from each of the medial, lateral and anterior aspects of the implant. Results were obtained in both paper and electronic file format. An overview of the general characteristics of each surface was obtained from scanning electron microscopy.

All stems demonstrated irregular surface textures with varying degrees of surface roughness. The results of the profilimetry testing are summarized in table 4.2. Nearly a three-fold increase in R_a and a two-fold increase in R_z existed between the 60 and 16 grit stems.

Table 4.2 Mean Peak to valley height(R_z) and Centerline average roughness (R_a) and peak spacing of implant surfaces

Stem surface	R_z (μm)	Std. Dev (±μm)	R_a (μm)	Std. Dev (±μm)	S (μm)	Std. Dev (±μm)
60 grit	19.7	1.80	2.85	0.26	28.5	4.1
24 grit	25.3	2.51	4.16	0.25	40.3	5.3
16 grit	37.9	1.94	6.7	0.56	64.8	5.9

Profilimetry traces of the surface textures demonstrated an irregular profile and produced a two dimensional visual image of the surface structure. Figures 4.5, 4.7 & 4.9 are profiles obtained from 60, 24 and 16 grit surfaces and plotted on the same scale. Figures were constructed from 2000 points acquired along a 2mm trace. Accompanying the images are low power scanning electron micrographs (SEM) of the implant surfaces (figs. 4.6, 4.8 & 4.10). Upon SEM analysis, each of the three implant surfaces presented a homogeneous and irregular microtexture.

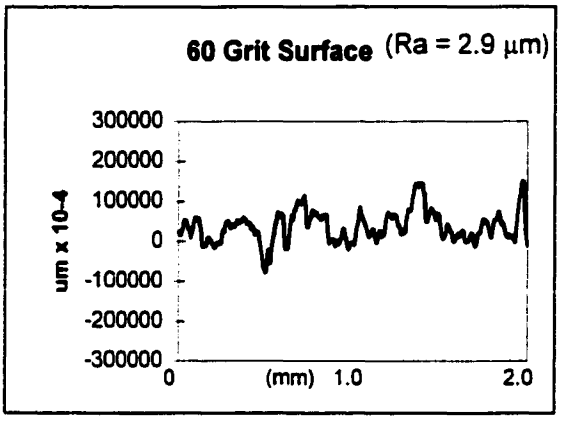

Figure 4-5 Line profile scan 60 grit blasted stem surface

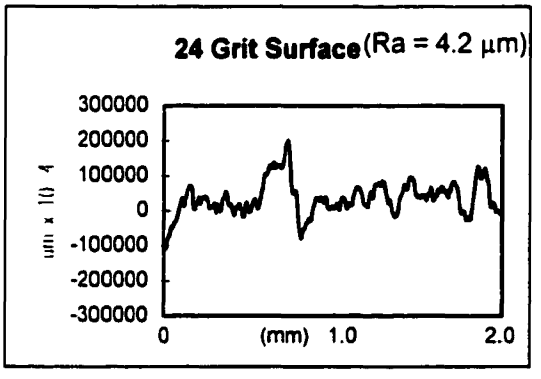

Figure 4-7 Line profile scan 24 grit blasted stem surface.

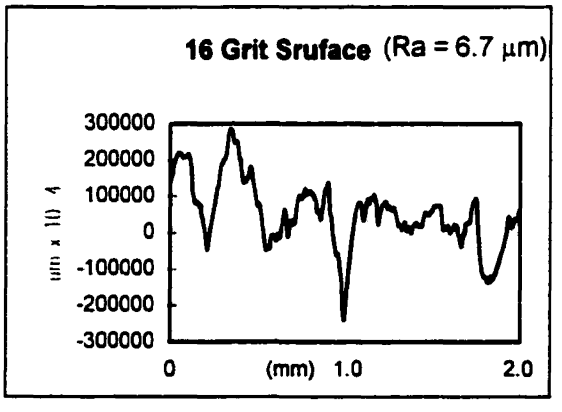

Figure 4-9 Line profile scan 16 grit blasted stem surface.

Smooth areas were often present within the rough implant surface. Dimensions of these smooth areas increased with abrasive particle size. Smooth areas are visible throughout Figures 4.6, 4.8 & 4.10 but are particularly well demonstrated in Figures 4.11, 4.12 & 4.13 of 16, 24 & 60 grit stems respectively. Ridges are a result of plastic deformation of the underlying substrate in Figures 4.11 & 4.13. The very smooth surface in Figure, 4.12 , is a likely result of substrate fracture and flaking.

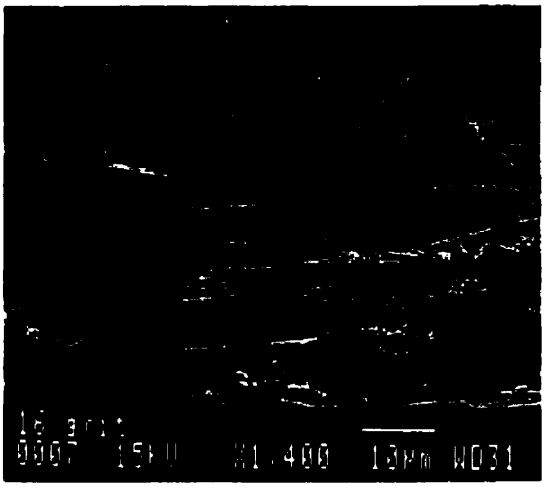

Figure 4-11 40 x 25 μm^2 flat spot on 16 grit surface.

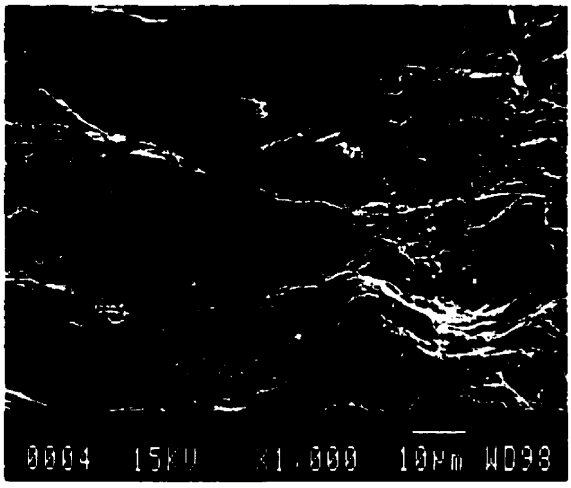

Figure 4-12 70 x 30 μm^2 flat spot on 24 grit surface.

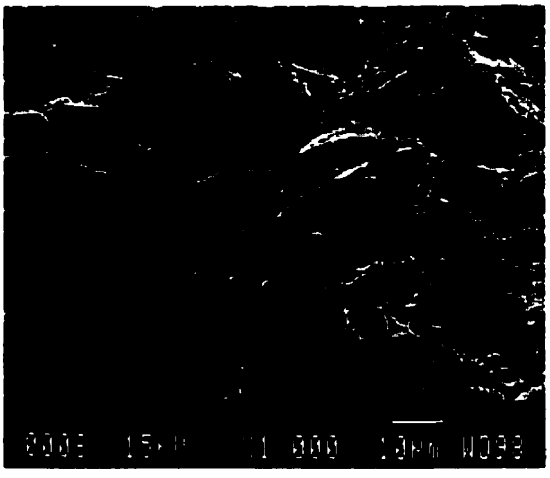

Figure 4-13 25 x 15 μm^2 flat spot on 60 grit surface.

The surface structure of each sample was resolved at high power using secondary electron imaging. Included in the analysis were the fracture surfaces of a canine ulna. All

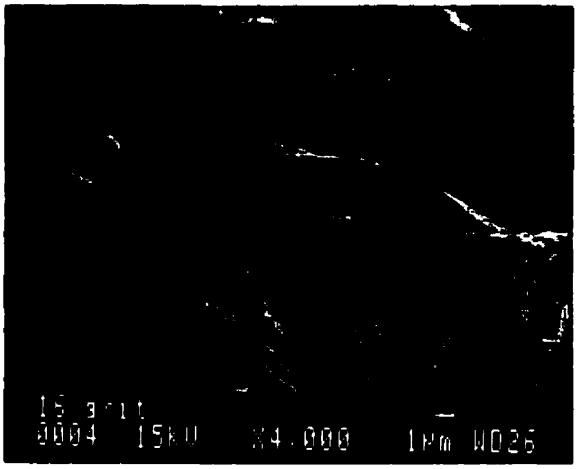

Figure 4-14 High power image microtexture of microtexture of 16 grit surface.

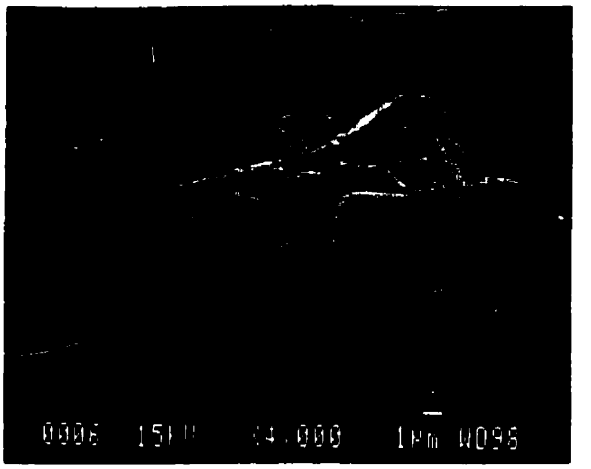

Figure 4.15- High power image of microtexture of 24 grit 24 grit surface

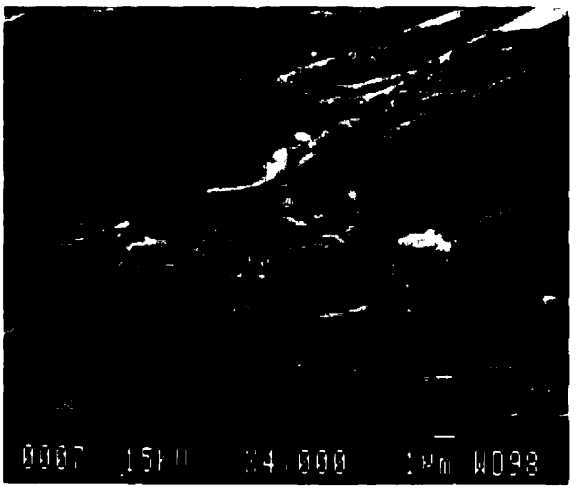

Figure 4-16 High power image microtexture of microtexture of 60 grit surface.

Figure 4-17 High power image of microtexture of low energy canine fracture surface .

grit blasted surfaces (4.14-4.16) possessed an irregular surface topography with numerous sharp edges and changes in surface structure. The irregular microtexture of the bone (4.17) was significantly smaller and more uniform than the 24 or 60 grit surfaces. The topographical changes in the fracture specimen were less abrupt and slightly rounder in appearance. The topographical quantification of the fracture surface is presented in Table 4.3

In some transverse serial sections of 16 grit samples, surface failure was observed under secondary electron imaging. Discontinuities of the substrate with the implant surface were observed (Fig 4.20). Cracks at the implant surface were also noted (4.21). It was presumed that these surface defects were created at the time of processing by the grit blasting procedure.

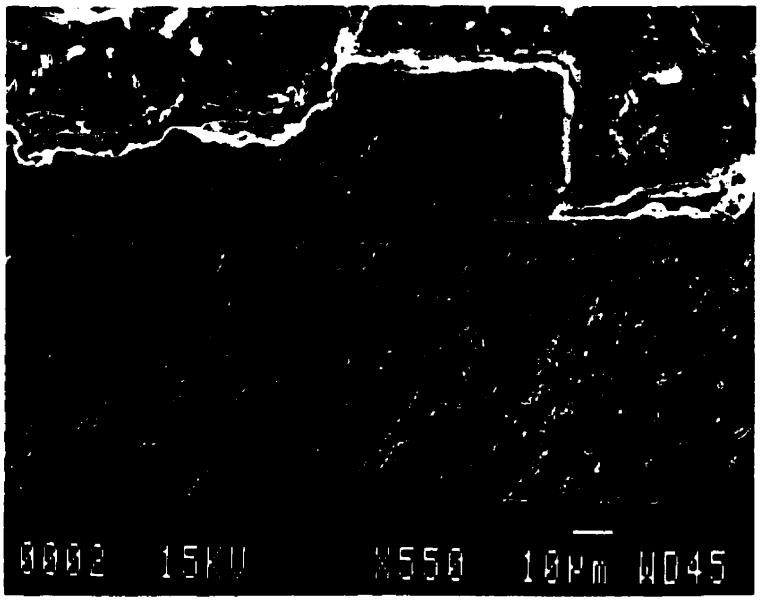

Figure 4-20 Surface damage in 16 grit specimen. Arrows indicate damaged regions.

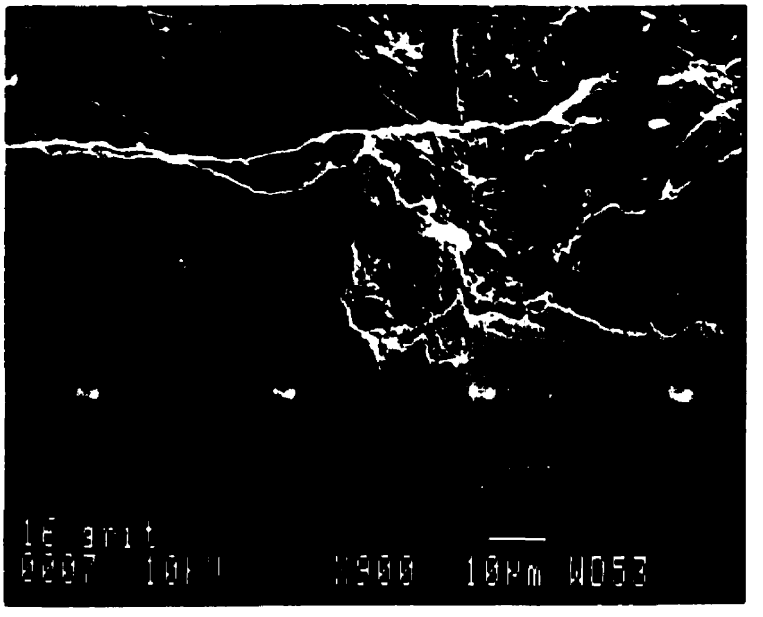

Figure 4-21 Surface damage in 16 grit specimen. Arrows indicate damaged regions.

In some samples numerous contaminant particles were noted (Fig. 4.22). These particles were identified by x-ray dispersive analysis to consist largely of alumina, and were most likely alumina oxide particles form the texturing process (Fig 4.23).

Figure 4-22 Surface of 16 grit stem. Bright particles in dark regions are most likely remnants from grit blasting.

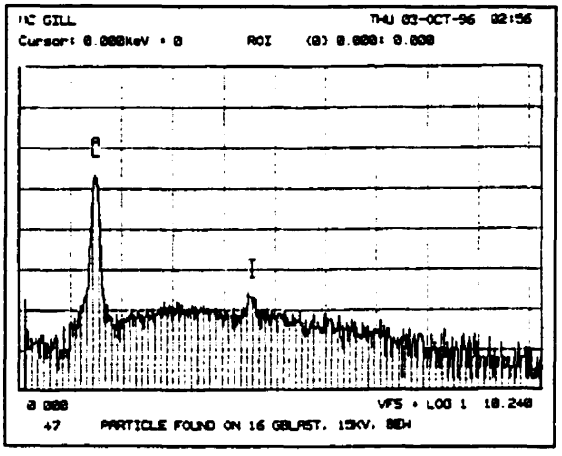

Figure 4-23 EDAX analysis of contaminant particle. Particle is composed of alumina, and is most likely alumina oxide.

4.2.2 Canine cortical fracture surface analysis

Osseous formation reported with non functional grit blasted titanium implants is greatly affected by differences in surface texture and minimally affected by differences in surface oxide chemistry and composition. Therefore, it is likely that surface texture is an important cue in the regulation of osetoblastic bone forming activity. In mature bone, the usual stimulus for rapid new bone formation occurs after fracture. In engineering materials, fracture surfaces are generally rough and irregular in nature, much like the grit blasted surface. The fracture surfaces of two canine ulna were characterized to determine if there was a biological semblance to the grit blasted surface and a possible topographical connection between new bone formation at the fracture site and new bone formation on the implant surface.

Two canine ulna were harvested and fractured immediately after explantation. One end of each bone was secured in a vise while a force was applied at the free end until failure. Although not specifically quantified, the two bones were fractured at slow and high rates. The bones were sectioned one inch from the fracture site, cleaned of any remaining soft tissue, dried in 95% ethanol for 96 hours and then air dried. The cut end of each bone segment was embedded in PMMA with the fracture surface facing upward. One fracture surface was sputter coated for SEM analysis while the opposing surface was retained for surface analysis.

Table 4.3 Quantification of canine fracture surface

Surface	Mean peak to valley height (R_z)	Centerline average roughness (R_a)	Peak Spacing (S)
Canine fracture	17.3 ± 1.92	1.9 ± .38	21.2 ± 3.7

Figures 4.18 and 4.19 are lower power images of the canine cortical fracture surface. The smooth surface of the endosteal cortex terminates at the fracture site (Fig. 4.18). The rough irregular surface of the cortex is visible in Figure 4.19.

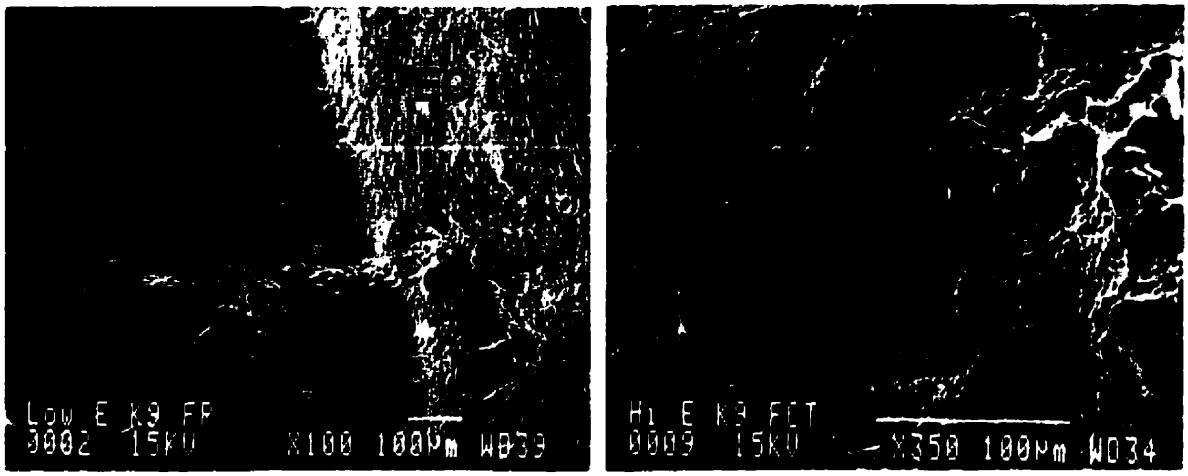

Figure 4-18 (left) Low power image of cortical canine fracture. The endosteal cortex (EC) possesses a smooth surface.

Figure 4-19 (right) Higher power image of canine fracture demonstrating a rough irregular surface.

4.3 STUDY PROTOCOL

Fourteen dogs of mixed breed with an average weight of 35.2 kg ± 5.8 kg underwent bilateral total hip arthroplasty. In each dog a 60 grit femoral component (control) was implanted while the contralateral femur had either a 24 or 16 grit implant. This yielded two study groups: group 1, 60 grit vs. 16 grit stem and group 2, 60 grit vs. 24 grit stem. The right side of each animal was implanted first, the contralateral side was implanted four to six weeks later. The control implant was randomly assigned to either the right or left side. The study period was six months from the mid-point date between operated sides. Bilateral surgeries greatly reduced the number of subjects required and eliminated intra-subject variability as a potential source of error.

4.3.1 Selection of Animal model

The canine was selected as the animal model because it has commonly been used for total hip research in numerous prior studies (see section 2.4.1). Dogs were selected for the study on the basis of body mass and femoral canal size to accommodate the implant size. No dog was rejected as a result of excessively large femora.

4.4 SURGICAL PROCEDURE

4.4.1 Anesthesia and surgical preparation

In preparation for surgery each dog was anesthetized with intravenous Nembutal (MTC Pharmaceuticals, Cambridge, On.), [33 mg/kg]. One gram of Cefazolin (Ancef; Kefzol) was administered intravenously for infection prophylaxis. The animal was intubated and placed on gaseous anesthetic, Halothane [0.5-1.5%] (MTC Pharmaceuticals, Cambridge, On.). Pre-operatively the hind quarter of the animal was shaved and then cleaned with Proviodine (Rouger inc., Chambly, QC). To prevent tissue necrosis, an inflatable support was placed under the contralateral side both during and after surgery. Using standard aseptic technique, the pre-operative region was recleaned thoroughly with Proviodine and then draped.

4.4.2 Instrument and implant sterilization

Femoral implants and surgical instruments were steam sterilized (Wilmot Castle Co., Rochester NY) at 225°C for 20 minutes. All heat sensitive tools (drills & saws) were sterilized by ethylene oxide gas. Acetabular implants were supplied in double sterile packaging. Care was taken to ensure all femoral implants were sterilized under the same conditions.[1]

4.4.3 Operative techniques

A lateral (modified Hardinge) approach was used to access the hip joint. This approach permitted excellent exposure of the hip joint and facilitated early subject mobilization. A lateral incision, approximately 12 centimeters long, was made in the mid-line of the femur and centered over the greater trochanter. The tensor fascia lata was incised and the anterior joint capsule was exposed. One half of the gluteus minimus muscle and one third of vastus lateralis muscle were split one cm beyond the proximal and distal aspect of the trochanter respectively. The tendon insertion unit was removed from the trochanter with an underlying small flake of bone using an osteotome.

---

[1] Steam sterilization has been shown to affect the oxide layer of titanium implants. Changes in Ti-oxide layer have been reported to affect cell behavior.

4.4.3.1 Visualization of the hip joint

An anterior capsulotomy exposed the head and neck of the femur (Fig. 4-24). The ligamentum teres was cut.

Figure 4-24 Exposure of the femoral head.

4.4.3.2 Joint Replacement

The hip was partially dislocated and a provisional femoral neck cut was made at the subcapital level with an oscillating saw. The femoral head was removed and the proximal end of the femur was retracted posteriorly to expose the acetabulum. The labrum and soft tissue within the acetabulum were removed by cautery. Any remaining soft tissue was curetted until the acetabular floor was well visualized.

Figure 4-25 Reaming the acteabulum.

Figure 4-26 Bleeding subchondral bone of the acetabular floor.

The acetabulum was reamed with hemispherical reamers (Fig.. 4-25) under copious irrigation to contour the acetabulum to fit the acetabular implant. The acetabulum was reamed sequentially with 25 mm and 27 mm reamers. The acetabulum was reamed in an anatomical position, with 45° of abduction and 15-20° of anteversion.

Figure 4-27 Acetabular cup seated in the anatomical position.

Reaming was stopped when the subchondral bone of the acetabular floor bled slightly and the acetabulum was hemispherical in shape (Fig. 4-26). Following reaming, the acetabulum was thoroughly irrigated and the 28 mm press fit acetabular implant was impacted into position (Fig. 4-27) with a 1 mm press fit. The implant was temporarily covered with a gauze during preparation of the femur to protect the component.

The femoral canal was broached through the piriformis fossa using a small tapered curette. The curette was inserted in line with the femoral canal to avoid varus/valgus misalignments. The femoral canal was not reamed but instead prepared with rasps similar to the implant shape. The rasps possessed sharp cutting surfaces that displaced encountered bone towards the endosteal cortex. Bone was not removed from the femur during preparation (Figs. 4.28 & 4.29) with this rasping method. The two undersized rasps were inserted in line with the femoral canal and maintained the anatomical anteversion (15 - 20°). The final rasp was 1 mm undersized with respect to the femoral implant to ensure a press fit. The 17 mm femoral head (Implex corp., Allendale New Jersey) was impacted on the femoral neck and the femoral implant was inserted in the same orientation as the rasps (Figs. 4.30 & 4.31). The femoral implant was firmly seated by impaction to a level that completely covered the grit blasted surface and/or restored the dog's preoperative leg length. (Figs. 4.32 & 4.33)

The joint space was thoroughly irrigated. The hip was reduced and tested for range of motion and stability.

Figure 4-28 Insertion of Rasp

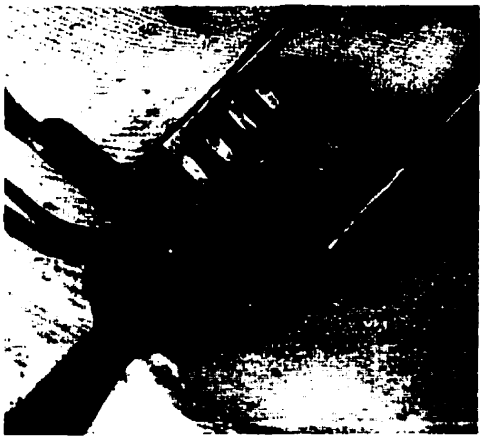

Figure 4-29 Preparation of femoral canal

Figure 4-30 Femoral implant with head prior to insertion.

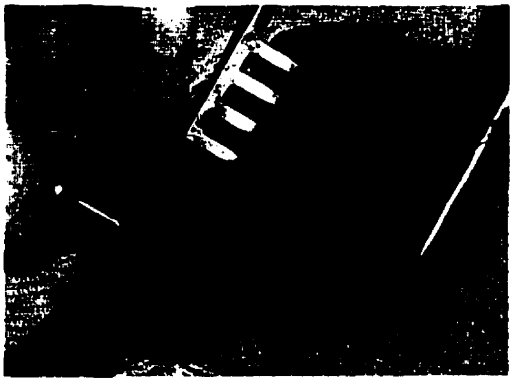

Figure 4-31 Insertion of femoral implant

Figure 4-32 Femoral implant seated in canal. A proximal fin is visible engaging cancellous and cortical bone (Bottom)

Figure 4-33 Reduced joint tested for mobility and stability.

4.4.3.3 Closure

Wounds were copiously irrigated and hemostasis achieved. The abductor muscle tendon unit was reattached to the trochanter through two drill holes using # 5 Tevdek (Ethicon, Sommerville, NJ) sutures. The gluteus maximus and vastus lateralis were re-approximated using 1-0 Vicryl (Ethicon, Sommerville, NJ). The tensor fascia lata was re-approximated with # 1 Vicryl in an interrupted fashion. The subcutaneous tissue was closed using interrupted 0 and 2-0 Vicryl and the skin was closed with resorbable sutures.

4.4.4 Post operative care

The animal was placed operated side up in a heated recovery room. An abduction pillow was placed between the legs and an inflatable support under the non-operated side. Following extubation, one gram of Cefazolin (Ancef; Keflex) was administered I.V. along with Temgesic I.V. [0.3 mg] (Bupronorphene, Reckitt and Coleman Pharmaceuticals inc., Richmond VA). To ensure animal comfort, temgesic was administered I.M. [0.3 mg t.i.d] for a minimum period of 48 hours. Dogs were maintained on p.o. Keflex (cephalexin, 500 mg b.i.d) for a period of 14 days following surgery. Dogs were fed a diet of canned and dry food and permitted to drink water ad libitum. Dogs were allowed unrestricted weight bearing activity and exercised daily. Weight bearing status was recorded.

Three months from the midpoint date of the surgeries the animals were radiographed (lateral and anterior-posterior) for assessment of implant stability, position and peri-implant bone.

4.5 HISTOLOGICAL ANALYSIS

4.5.1 Specimen and non-implanted control retrieval

The dogs were sacrificed by intravenous injection of Nembutal [1.8 g] followed by a lethal injection of KCl [1.5 g] (Astra Pharma inc., Missasuaga, Ont.). The femur and acetabulum were excised under non-sterile conditions and any surrounding soft tissue was removed.

To provide an example of the bone structure and density in the non-implanted femur, two pairs of non-implanted canine femora were obtained. Femora from dogs of similar size and weight to the study group were harvested and prepared for histological examination in the same manner as the implanted specimens.

High resolution x-ray images of the implant *in situ*, medial-lateral (L) and anterior-posterior (AP), were taken immediately after specimen retrieval. The images were captured on Kodak X-omat TL film (Eastman Kodak company, Rochester, NY 14650) in a Faxitron (Hewlett Packard, Boise Idaho) at 65 kVp for 35 seconds.

The specimens were placed in labeled jars of Formalin 10% v/v (American chemicals limited, Montreal QC)

4.5.2 Specimen preparation

4.5.2.1 Fixing and drying

Using a 3/32 drill bit, holes were drilled in the retrieved femora to facilitate the infusion of the various preparation fluids. Care was taken to avoid implant contact. The femora were stored sequentially in each of the following solutions for a minimum of 48 hours.

1. Buffered formalin 10 % solution vol./vol. for fixation.
2. 70 % solution v/v of ethanol (Commercial Alcohols Inc., Brampton, On.) and water for drying.
3. 95 % solution v/v of ethanol and water for drying.
4. 1:1 solution v/v of ether/acetone (JT Baker Inc. Jackson, TN) for degreasing and defatting.
5. Anhydrous ethanol for final drying.

In addition, magnetic stirring at each stage facilitated permeation of each fluid into the bone.

4.5.2.2 Embedding

Prior to embedding, all specimens were pre-soaked for a minimum of 48 hours in a solution of Polymethylmethacrylate (PMMA) (Aldrich Chemicals, Oakville, On.) inhibited with 10 ppm hyrdoquinone. The PMMA solution was activated with the addition of 3.5g of benzoyl peroxide (Aldrich Chemicals) per liter of PMMA monomer. The specimens in monomer were stored at 4 °C in a refrigerated environment and magnetically stirred.

All specimens were embedded in PMMA. The process of embedding yielded a sample that was encased in a hard, transparent plastic block. In this manner the specimens were well preserved and mechanically stable for a variety of analysis procedures.
The liquid monomer was prepared for polymerization as follows:

1.) The inhibited (10 ppm methyl hydroquinone) PMMA monomer was activated with the addition of 3.5g of benzoyl peroxide per liter of PMMA monomer.

2.) The activated monomer was heated at 55 ° C in a hot water bath for approximately six hours. During heating the monomer was stirred each 1/2 hour.

3.) When the consistency of the partially polymerized solution was similar to thin syrup and slightly yellow in color, the solution was removed from the hot water bath. Upon removal the solution was cooled under tap water and stored at 1 ° C.

Specimen embedding:

1.) Molds were fabricated from aluminum foil into which the implant and bone were placed. The partially polymerized PMMA (from polymerization step 3) was added to the mold until it completely covered the specimen.

2.) The specimens were then placed in a vacuum of 70 mm Hg for a minimum period of 12 hours (Fig. 4-34). During the initial stages of vacuum treatment the vacuum was interrupted regularly to force the polymer into the specimen and prevent the molds from overflowing.

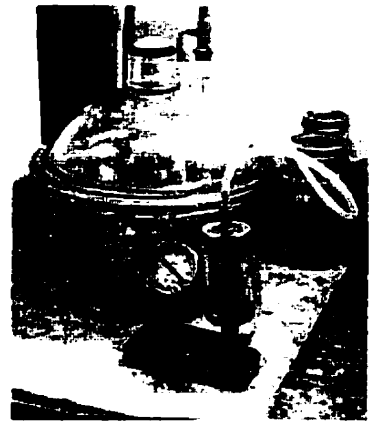

Figure 4-34 70 mm Hg vacuum enhanced PMMA infiltration

3.) The specimens in their molds were placed in sealed ziplock™ bags to cure for a period of 5 days or until the polymer had hardened. To maintain bone coverage, stock PMMA was added as necessary to compensate for losses due to evaporation and shrinkage.

4.) Once the specimens were hard and devoid of soft areas or liquid inclusions, they were placed in a heated chamber to ensure complete hardening. The embedded specimens were maintained at 35°C for 3 days. During the initial 12 hours, specimens were placed in the oven for one hour intervals then cooled for one hour.

4.5.2.3 Sectioning

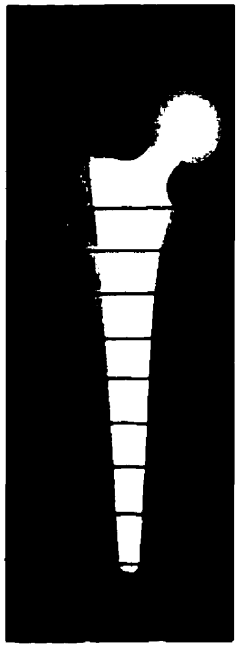

Figure 4-35 Section levels (9 x 2.0 mm slices at 10 mm centers).

Figure 4-36 Diamond wafering saw (left), blade & thin section (right).

Transverse serial sections were obtained using an Isomet 1000 variable speed diamond blade saw (Biomet, Markham, On.) (Fig.. 4-36). Each section was cut at 450 rpm with an applied weight of

150 grams. Radiographs of the specimens taken immediately after explantation served to locate the cutting region of interest. Lines were drawn on the PMMA block locating the position and angle of the implant for alignment in the cutting jig. Starting at the region just below the neck of the implant, cuts were made at 10 mm intervals. At each cm interval a 2.0 mm section was removed from the specimen yielding 9 thin sections per sample for analysis (Figure 4.35).

4.5.2.4 Transverse serial radiographs

After harvest and embedding, high resolution images of 2.0 mm thick transverse serial sections, centered at 10 mm intervals along the stem length were obtained. The transverse serial sections were positioned as they resided *in situ*, proximal to distal with the lateral edge of the implant in each section aligned. High resolution images were recorded on Kodak X-omat TL film in an HP Faxitron apparatus.

4.5.2.5 Polishing

All thin sections were polished to remove cutting artifacts on their surface prior to examination with the scanning electron microscope. Specimens were wet sanded on an Isomet Polimet 1 (Fig.. 4-37) table top grinder (Evanston, Il) in the following order:

Fig.ure 4-37 Rotary grinder/polisher

1. 360 grit*
2. 600 grit*
3. 800 grit*
4. 1000 grit*

*(Buehler, Lake Bluff, Il)

4.5.2.6 Cleaning

Immediately following polishing, sections were placed in anhydrous ethanol and ultrasonically cleaned for 6 minutes, polished face down. Specimens were left to air dry then stored and transported in lint-free paper.

4.6 BACKSCATTERED ELECTRON MICROSCOPY (BSEM)

Using the backscatter electron mode, a density-specific image of the top two to three microns of the implant-bone interface is obtained. When correctly attenuated, metal is viewed as white, bone as gray and all other tissue and dead space as black.

4.6.1 Specimen preparation

A coating of Au and Pd (Hummer IV sputtering system, Anatech ltd., Alexandria, VA) was applied to each transverse section to reduce charge concentration on the implant surface during electron microscopy. The specimens were coated for four (4) minutes in a vacuum environment (100 mm Hg), with the addition of 50 mm Hg of Ar. The voltage of the coating system was adjusted until the current flow between the anode and cathode averaged 13 milliamps.

4.6.2 Microscope parameters

Specimens were examined on a JEOL 840A Scanning Electron Microscope (JEOL, Peabody, MA) in compositional (backscatter) mode. Specimens were examined with an accelerating voltage of 15 kV at an average working distance of 48 mm. The probe current varied between 1×10^{-9} and 1×10^{-7} (Amps).

4.6.3 Photographs

Specimens were photographed using Polaroid type 55, ASA 50, 4 x 5 positive/negative instant sheet film (Polaroid, USA. PXW 1558) at a camera aperture of f-8. Specimens were usually photographed at a magnification of 13X. In cases where the entire specimen would not fit into the photographic frame, the image was photographed in two or four separate sections.

4.7 IMAGE ANALYSIS

4.7.1 Image preparation

Photographs were converted into digital format for analysis. Images were scanned without scaling on a Hewlett Packard Scanjet 4c/T image scanner (Hewlett Packard, Palo Alto, CA) at a resolution of 200 dpi and saved in the TIF format. Adobe Photoshop™ version 4.0 (Adobe Systems Inc., San Jose, CA) was used to create a composite image for specimens that could not be captured on one exposure.

4.7.2 Image Analysis

Complete digital Images were analyzed using the software package Matrox Inspector™ 2.1 for windows NT™, (Matrox Graphics Inc., Dorval, QC) running on a clone 200 MHz Intel Pentium pro platform with 64 Megabytes of RAM.

4.7.2.1 Calibration

The image analysis software was calibrated using the calibration bar of the scanned photograph.

4.7.2.2 Implant perimeter calculation

The perimeter of each implant was first smoothed with 5 iterations of the "averaging" filter to overcome a large and systematic source of error due to the inclusion of the irregularities of the implant surface in the perimeter calculation (Fig. 4.38-note differences in perimeter values below each image). The perimeter was then determined automatically by selection of the appropriate function.

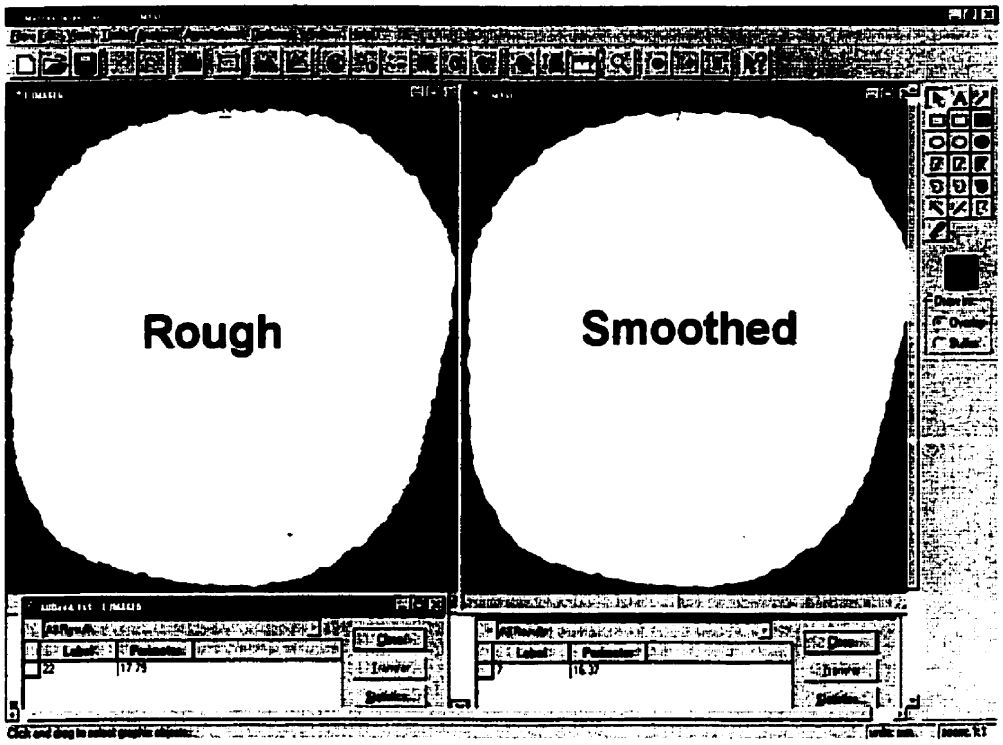

Figure 4-38 Smoothing of implant perimeter prior to quantification. Left image is unsmoothed right is smoothed. Differences of nearly 10 % in perimeter shown at bottom.

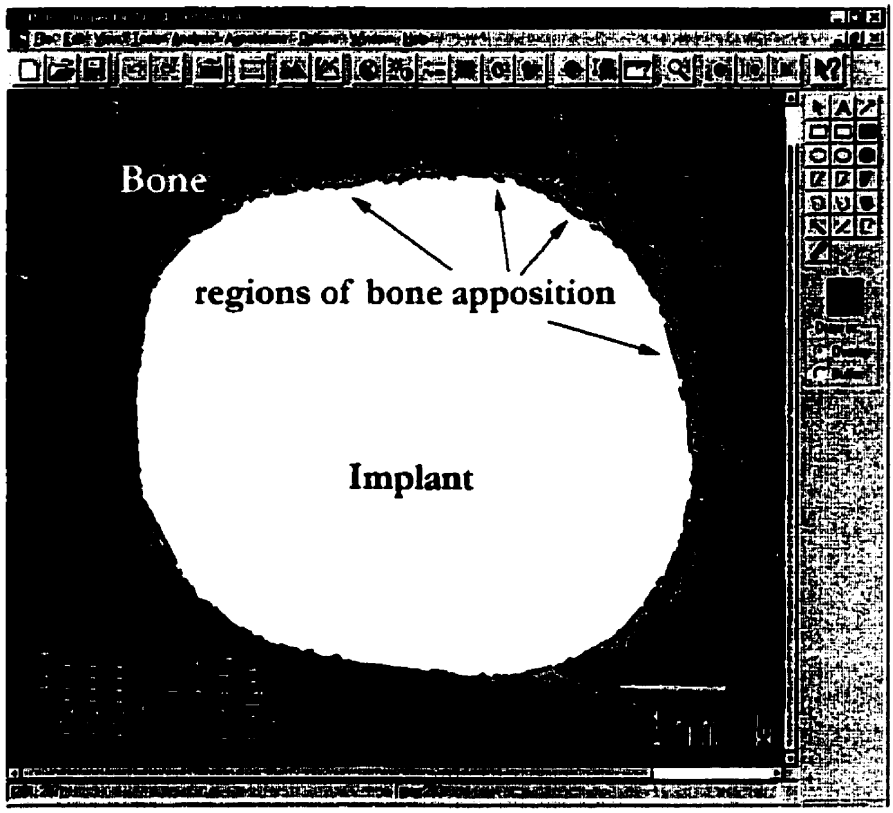

Figure 4-39 Measurement of typical regions of bone contact at implant surface (red) included in calculations of % bone apposition.

4.7.2.3 Length of bone apposition

The length of bone apposition to the implant surface was determined with the measurement tool (Fig. 4.39) and subject to the following criteria:

1. All osseous tissue contacting the implant surface was included.

2. Bone that did not directly contact the implant surface was included only when shrinkage of the PMMA could be ascertained. Shrinkage, indicated by a gap, was determined from secondary electron imaging (SEI) images of the area in question or during analysis (Fig. 4.40). If the irregularities of the bone edge closely matched that of the adjacent implant surface, shrinkage was determined to have occurred.

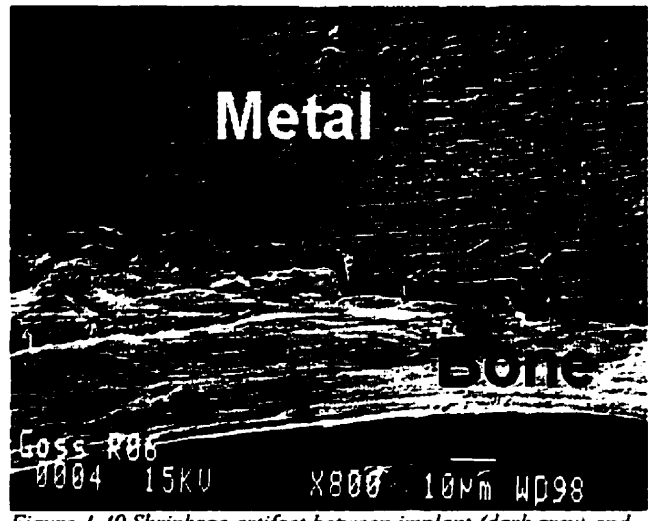

Figure 4-40 Shrinkage artifact between implant (dark grey) and bone(white). Bone mirrors implant surface. The shrinkage space is approximately 2-3mm wide.

4.7.2.4 Section aspect length

To determine the length of each aspect of the implant perimeter, the implant was bound by a four sided region of best fit and the length of each side was determined.

4.7.2.5 Calculation of bone apposition

The percentage of bone apposition to the implant perimeter of each transverse section was calculated as follows:

$$\text{\% BONE APPOSITION} = \frac{\Sigma \text{ BONE CONTACT LENGTH}}{\text{IMPLANT PERIMETER}} \times 100\%$$

4.8 DETERMINATION OF ERROR IN PERCENT APPOSITION DUE TO IMPLANT PERIOD OF RESIDENCY

In all animals, replacement surgeries were staged to permit full recovery before the subsequent operation. As a result of the staggered surgeries the duration each of a pair of implants resided in situ differed approximately three or four weeks. Implants were divided into two groups: in group 1, implants resided *in situ* for 5.5 months and in group 2 implants resided *in situ* for 6.5 months. The effect of implantation period on the percentage of bone apposition was determined. Data from analyzed sections were grouped according to implantation period and compared. A paired Student t-test was used to determine significance between the results.

4.9 DETERMINATION OF ERROR IN PERCENT APPOSITION MEASUREMENTS DUE TO SURFACE ROUGHNESS

In all samples a minor but systematic error existed due to the different measurement techniques used to quantify the implant section perimeter and length of bone apposition. Since the implant surface was rough and the digital software used for quantification had a high resolution, the measured perimeter included the changes in surface topography. However, all measurements of bone apposition follow a point-to-point method of measurement along the bone-implant interface (Fig. 4.41). As a result, the measurements of bone contact length are conservative and do not account for the greater actual contact arising from bone following the true surface topography. Effective

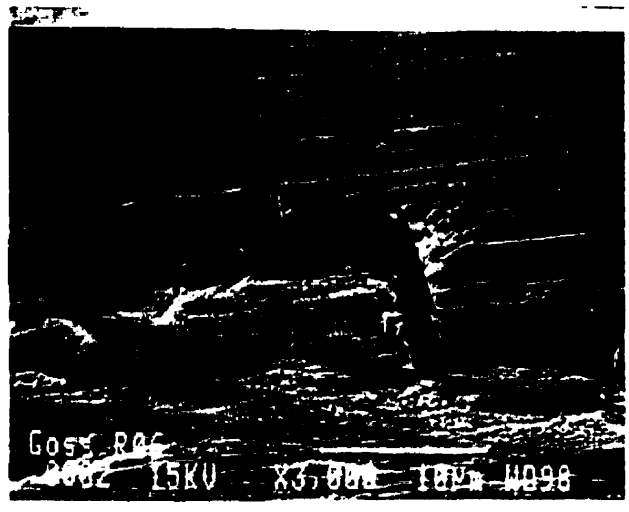

Figure 4-41 Differential measurements of implant perimeter and bone apposition length.

steps (table 4.3) were taken to smooth the perimeter of each implant (Fig. 4.38) prior to analysis although some residual effects remained.

Error was calculated based on the differences in measured perimeter resulting from the smoothing of the 16, 24 or 60 grit surfaces. It was determined that five iterative smoothing operations greatly expedited analysis compared with the 100 iterations needed to produce a completely smooth perimeter and yielded a relatively small error.

4.10 STATISTICAL ANALYSIS

Analysis of tissue response to different surface textures, serial section level, stem aspect and dogs was determined by one way analysis of variance (ANOVA), assuming unequal means and a confidence level of 95%. In addition, the Student t test was also performed where appropriate.

5.0 RESULTS

5.1 INTRA AND POST OPERATIVE COMPLICATIONS

A total of 28 stems, fourteen 60 grit, seven 24 grit and seven 16 grit, were implanted in fourteen dogs. Post operatively, all dogs regained nearly two-thirds of complete weight bearing on the implanted leg within the first week and had completely recovered full use of the operated limb by 3 weeks.

In three dogs one femur was fractured and in a fourth dog, both femurs were fractured during implant insertion. In three dogs, the fracture initiated anteriorly and extended approximately one cm distal to the osteotomized edge of the femoral neck. In the remaining dog a displaced fracture encompassing the proximal one and a half cm of the medial calcar region occurred. All fractures were stabilized with 20 gauge stainless medical steel cerclage wire. In addition, five dislocations required surgical revision in three 24 and two 16 grit implanted joints.

At the time of implant retrieval, in one dog there was severe discoloration (blackening) of the joint space. It was found that a loose head-neck taper had resulted in the generation of titanium wear debris from the neck. The animal presented no abnormalities in gait or indication of pain during the implantation period, however, high resolution x-rays revealed signs of peri-implant scalloping.

Three dogs were excluded from the study. Two dogs with a femoral fracture attributed to implant insertion failed to recover complete weight bearing at two months post op and were subsequently excluded. At four and a half months, one dog suffered a mid-femoral fracture and was excluded because of uneven weight bearing.

5.2 FINAL STUDY GROUP

After the exclusion of three dogs, the remaining study group included 22 stems, eleven 60 grit, four 24 grit and seven 16 grit, in eleven dogs. This represents the study group referred to in the subsequent portions of this thesis.

5.3 RADIOGRAPHIC RESULTS

5.3.1 Gruen Zones classification system

Radiographic areas in apposition to an implant are located by an identification system developed by Gruen et al as described in Figure 5.1. The implant is divided into thirds and the regions adjacent to the implant labeled as shown.

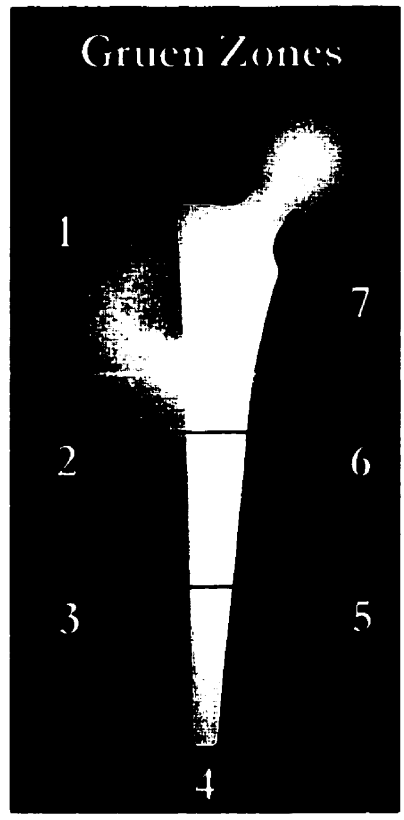

Figure 5-1 Gruen zone identification system

5.3.2 Medio-lateral and anterior-posterior radiographs

5.3.2.1 Three months post implantation

Twenty-two of 24 stems were judged to be stable radiographically at three months without signs of migration. Two stems developed a partial peri-implant radiolucency at the bone-implant interface. These two stems, however, revealed no signs of looseness or migration upon evaluation.

There was some variation in the positioning of the stems. Of the 22 stable stems at three months, fourteen stems were in 2-4 degrees of varus tilt and eight stems were in a neutral position. In the medio-lateral plane all stems were tight proximally, but the fit of the stem within the anterior-posterior plane of the femur varied from animal to animal. In two dogs there was a reasonably good fit as shown in Figure 5.11, unlike in the remainder where there was a fairly large disparity between the implant and endosteal dimensions. An extreme case is illustrated in Figure 5.10

At six months, all 22 stems were judged to be radiographically stable. In four of the 22 stems, a thin radiolucent line adjacent adjacent to the implant was visible in some radiographs (Fig. 5.2). Each of the implants was scrutinized for evidence of prosthetic migration but none was detected. In one femora the radiolucency extended the entire length of the stem; this was classified as stable fibrous fixation. The remaining three implants demonstrated incomplete radiolucencies in some regions.

Even with high resolution radiography, the peri-implant space was generally difficult to distinguish. In the lateral radiograph of Figure 5.2, the fibrous space can be distinguished but is difficult to detect in the AP radiograph of the

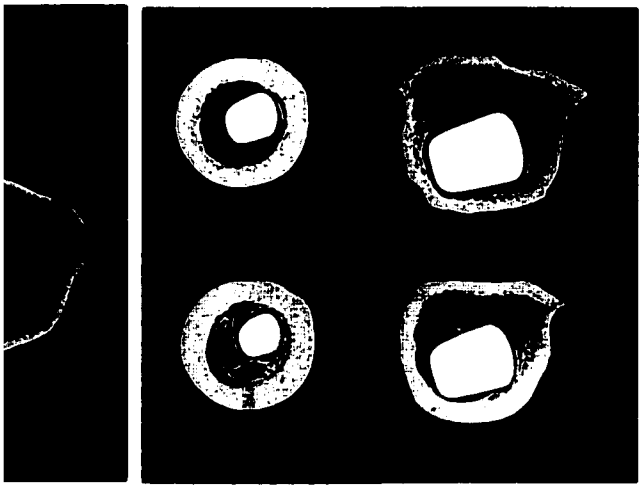

fi) and rtifact from

Figure 5-4 Mid and distal sections with periimplant radioluceny.

but only BSEM of the transverse serial sections enabled definitive characterization of the bone-implant interface. In one implanted femur where a uniform space between the implant and surrounding bone existed, the implant was encapsulated by a thin shell of cortical bone, (Figs. 5.3 and 5.4) indicative of stable fibrous fixation.[82]

Quantification of the peri-implant space was obtained from BSEM photographs of both proximal and distal sections of implants with complete or incomplete fibrous interfaces[1]. In some sections, a thin neocortex with radiating bony trabeculi was clearly visible (Fig. 5.5) in three of the 22 implants. In distal sections, the gap between the implant and bony shell averaged approximately one-third of a millimeter. Proximally, larger gaps were evident between the implant and surrounding bone in one femur suggesting greater relative motion at the proximal bone-implant interface and more rigid fixation distally (Fig. 5.6). However, these spaces may also have been a result of the burring used to seat the implant when the proximal femur was too narrow.

Figure 5-5 Stable distal section of 24 grit stem. Thin shell of cortical bone visible. Interposed fibrous tissue cannot be visualized with BSEM.

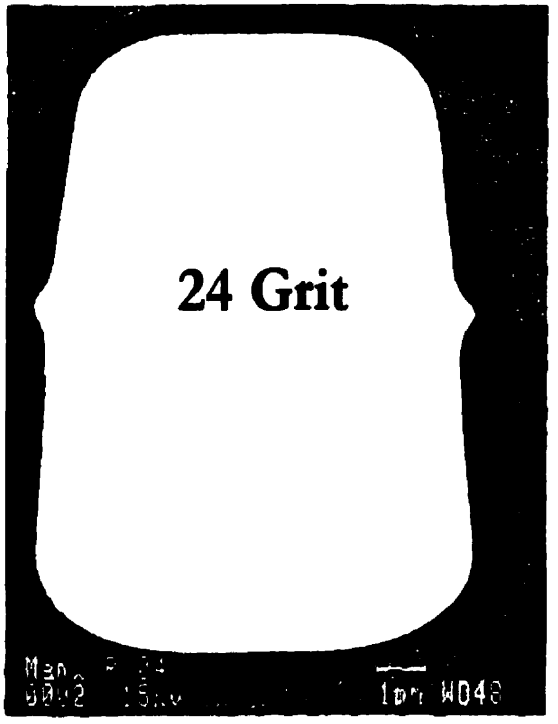

Figure 5-6 Proximal section of stable 24 grit stem. Gap indicative of fibrous fixation.

[1] Fibrous tissue appears black in BSE image.

At six months 21/22 stems were determined to be radiographically stable (Figs. 5.7-5.11 & 5.13) without complete peri-implant radiolucencies in Gruen zones 2 through 7. When compared with radiographs obtained at three months, no change in stem position was measured. In most specimens, the proximal implant fins (Figs. 5.7 & 5.8) appear to be engaged by both cancellous and cortical bone. However, a mismatch in fit between the implant and femur was clearly evident in lateral and anterior-posterior (AP) radiographs of all specimens. As a result, cortical contact was minimal along the remainder of stem length, generally occurring at the implant tip.

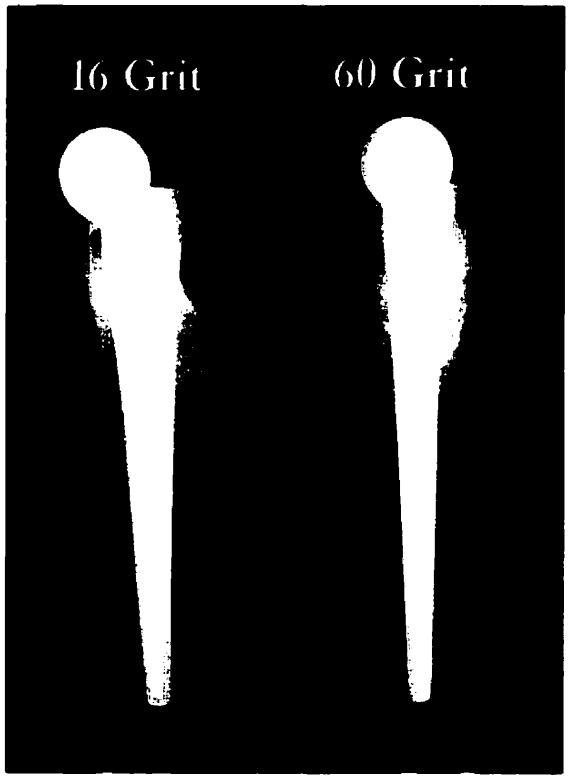

Figure 5-7 Matched 16 and 60 grit specimens. New bone formation is clearly visible at the distal end of the implant.

Figure 5-8 Matched 60 and 24 grit specimens. New bone formation is visible along the implant surface and within the medullary canal. Proximal fins (arrows) appear completely engaged by bone.

In some AP radiographs a slight radiolucency was visible adjacent to the shoulder of the implant in Gruen zone 1. A composite image (Fig. 5.12) of a non-implanted control

femur with a superimposed implant simulated the radiographic appearance of both the cortical and cancellous bone stock at the time of implantation. In the non-implanted femur with the superimposed implant, a similar space between the implant and femur is also present near the shoulder of the implant in Gruen zone 1, suggesting the space results from anatomical features (piriformis fossa).

New trabecular bone formed directly adjacent to the implant in the majority of medio-lateral (ML) and anterior-posterior (AP) radiographs. New bone formation was particularly notable in Gruen zones 3 through 5 where bone spanned large gaps (2-5 mm) connecting the endosteal cortex to the implant surface (Fig. 5.9). An enlargement of the distal region of the previously described non-implanted control (Fig. 5.10) provided a comparative image. A qualitative increase in both proximal and distal bone destiny was apparent when compared to the non-implanted control specimens. In addition, compared to Figure 5.12, there appears to be a slight reduction in cortical thickness in the proximal cortices of Figures 5.9-5.11. In some cases there was up to 3 mm of proximal medial resorption of bone in Gruen zone 7 (calcar) of cortical bone.

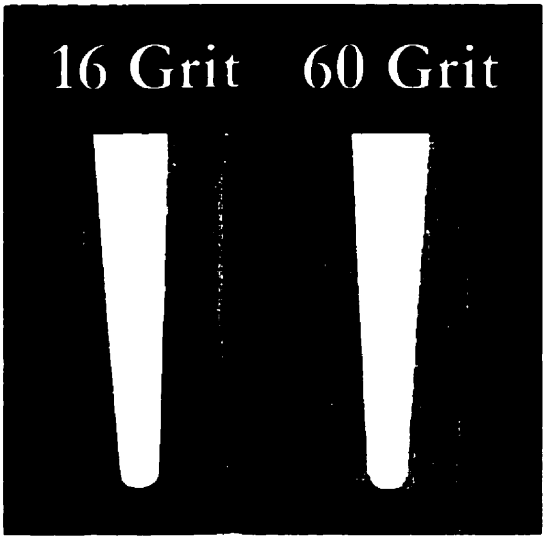

Figure 5-13 Distal third of paired 16 & 60 grit stems. New trabecular bone formation is clearly evident. Bar = 16.0 mm

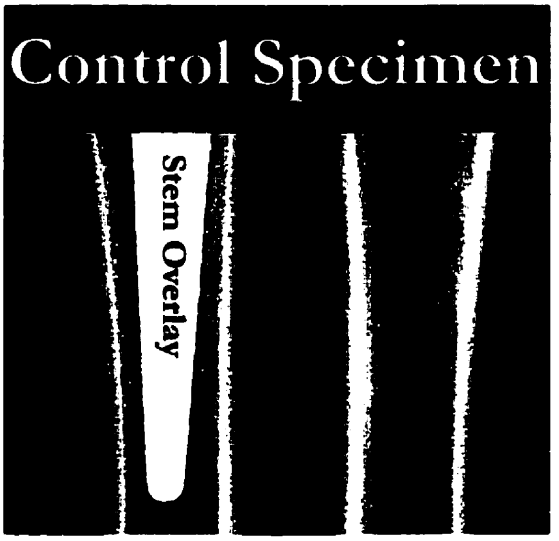

Figure 5-14 Non implanted femur & non implanted femur with digital overlay simulating immediate post-op appearance.

5.3.3 Transverse serial sections

Bone density, anatomical position and the appearance of the bone-implant interface were further examined by radiographing 2.0 mm thin sections removed at 10 mm intervals from the harvested femora . The thin sections were aligned to represent the implant orientation *in situ* .

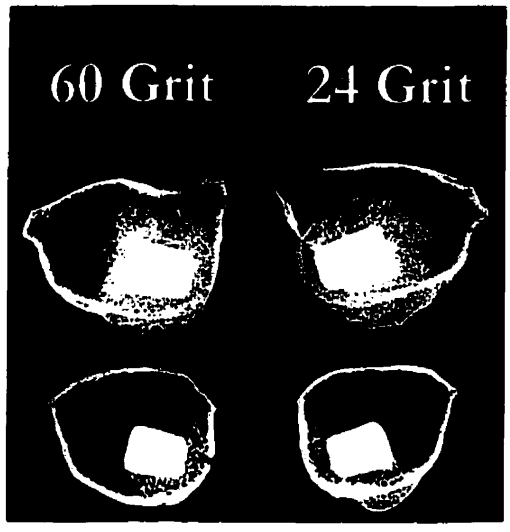

Figure 5-15 Paired proximal transverse sections. Notable Increase in trabecular bone density. New formation of periosteal bone. Bar=10 mm

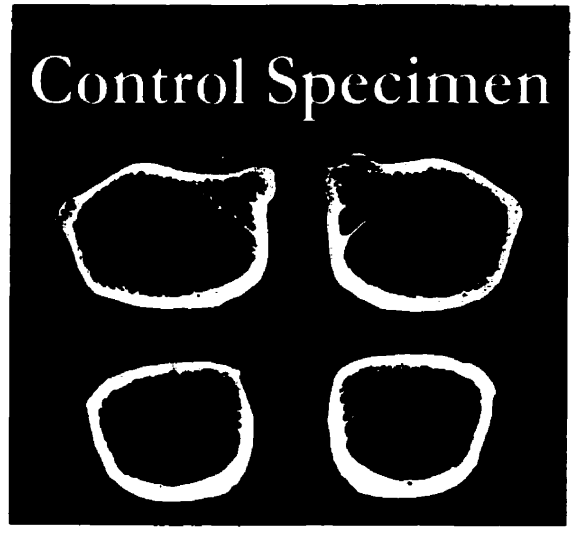

Figure 5-16 Matched transverse sections from non implanted femora.

Figure. 5.15 shows the osseous response typically observed in proximal sections. There was a notable increase in bone density in the area adjacent to the implant correlating to the increase in bone density observed in Lat. and AP radiographs. New trabecular bone enveloped the implant in 93% (156/168) of the section levels. This bone formation is clearly illustrated by comparing the implanted bone sections with sections from a non-implanted control femur (fig. 5.16). Twelve percent (20/168) of the thin transverse sections showed an osseous reaction at the periosteal surface. In most cases, this reaction was limited to the anterior or anteromedial aspect of the femur.

As observed in the AP and lateral radiographs, there was a significant difference in tissue response amongst implanted and matched non-implanted femora. The canine femur typically has little or no trabecular bone in the diaphyseal region. Comparing figures 5.17 & 5.18, the extent of new trabecular bone formation in implanted sections is clearly visible. In distal sections, trabecular bone spanned gaps up to 5 mm (fig. 5.17) linking the endosteal cortex and implant surface.

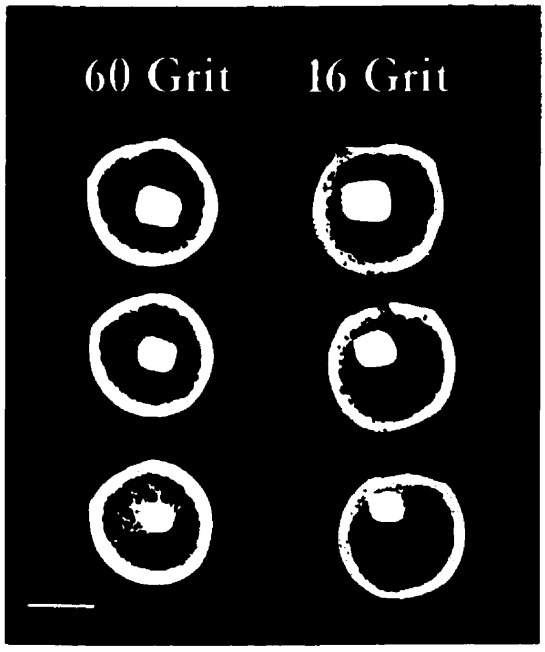

Figure 5-17 Transverse distal sections of 60 & 16 grit stems. Trabecular bone spans large gaps between implant and cortex. Bar = 10 mm

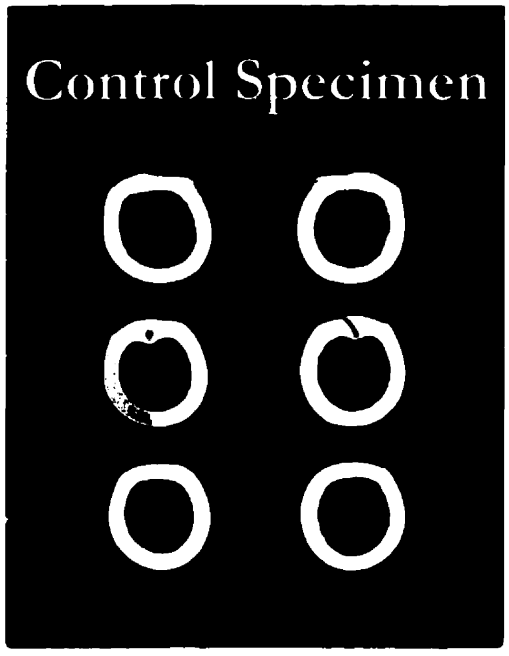

Figure 5-18 Matched transverse sections from non implanted specimen

Figures, 5.19-5.25 are paired sections from other dogs in the study, demonstrating the typical osseous response observed along the length of the implant. The most striking feature of these figures is the extent of new bone formation around osseointegrated implants when compared to paired sections from the non-implanted femora (fig. 5.26). In some of the most proximal sections of figures 5.19, 5.22, 5.23 & 5.25, the distal portion of the piriformis fossa can be seen, illustrating the anatomy of the canine femur potentially responsible for the apparent radiolucencies in Gruen zone 1 in figures 5.9, 5.10 & 5.11. In the 24 grit sections of figure 5.22, radiolucencies are apparent at the implant interface. A periosteal reaction is visible in some sections.

5.5 BACKSCATTERED ELECTRON MICROSCOPY OF THE BONE IMPLANT INTERFACE

In 93% (156/168) sections, there was substantial bone apposition along the implant perimeter. Bone contact occurred randomly in both short and long spans of apposition.

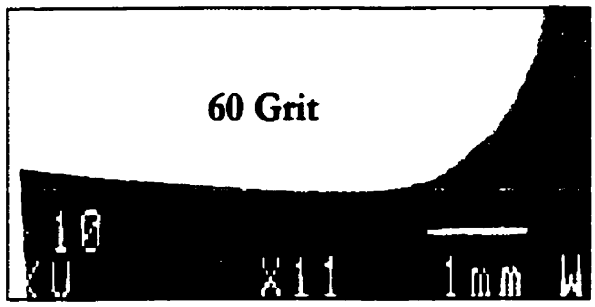

Figure 5-27 60 grit implant. New bone formation along implant surface away from trabecular contact point.

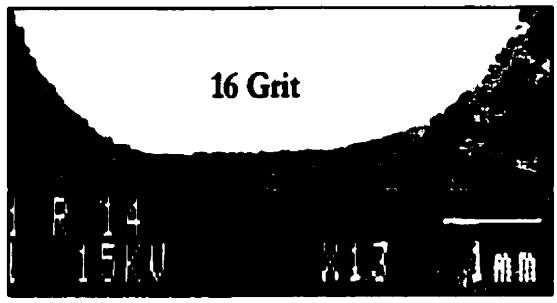

Figure 5-28 16 grit surface. New bone formation mainly at terminal end of trabeculae.

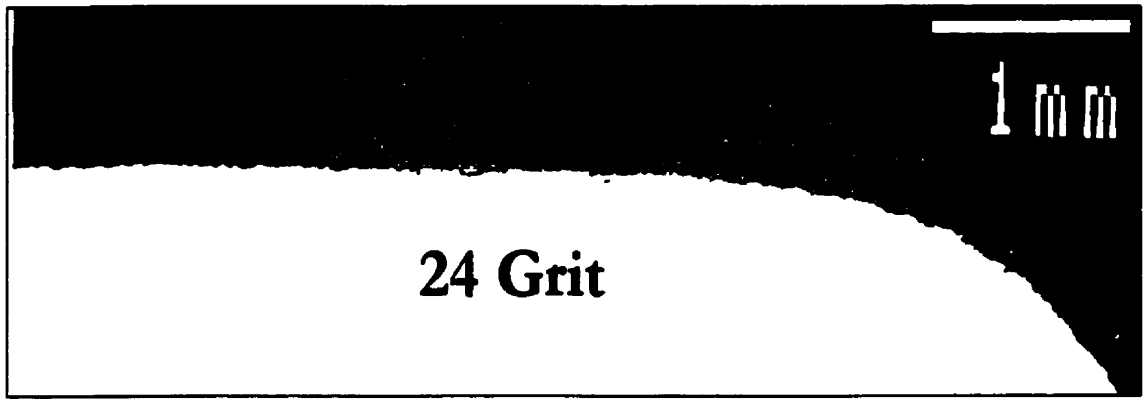

Figure 5-29 24 grit surface. New bone formation along implant surface clearly evident.

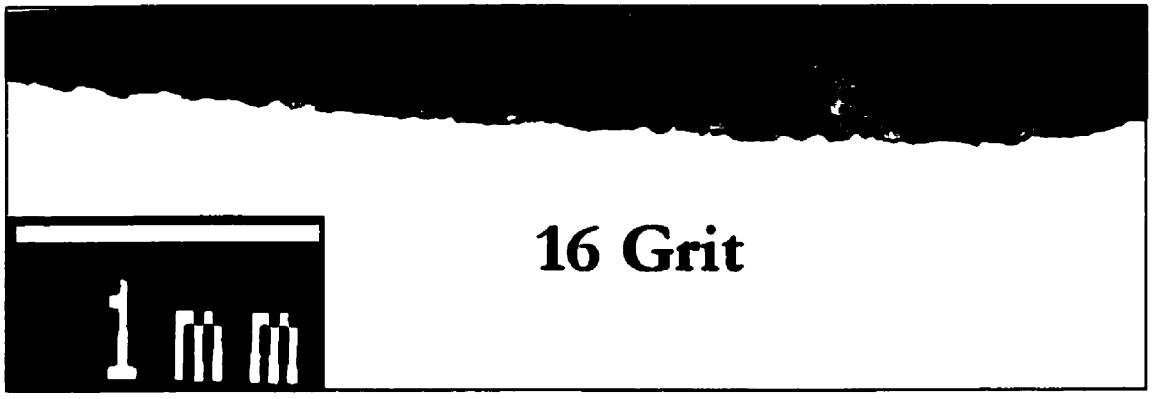

Figure 5-30 16 Grit surface. Less extensive bone formation along implant surface when compared to finer textures.

Frequently, new bone formed along the implant surface, spreading out from a point of trabecular contact (Fig. 5.27), thereby providing the impression of osteoconduction. This

osteoconductive effect was most often noted on the smoothest (60 & 24 grit) specimens (Fig. 5.27 & 5.29) while matched coarser (16 grit) specimens demonstrated shorter regions of contact (Figs. 5.28, 5.30 & 5.37) that terminated at the trabecular abutment.

Trabecular bone surrounding the implant had a mature, woven appearance with a high number of interconnected struts (Fig. 5.31 & 5.36). In distal sections new bone was often observed spanning large gaps between the endosteal cortex and the implant surface.

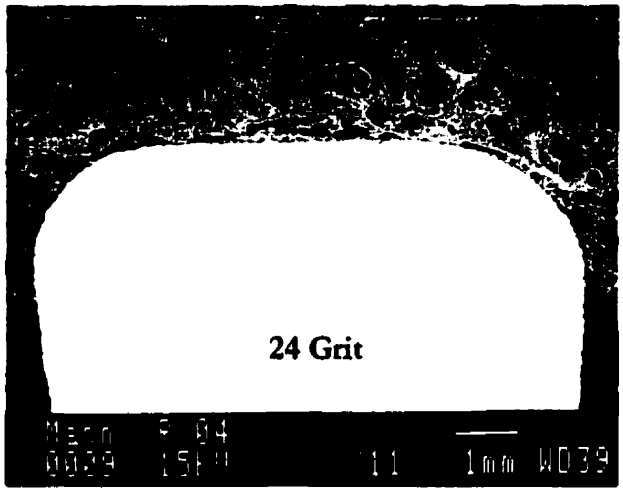

Figure 5-31 24 Grit stem. Dense interconnected trabecular bone and large extent of apposition.

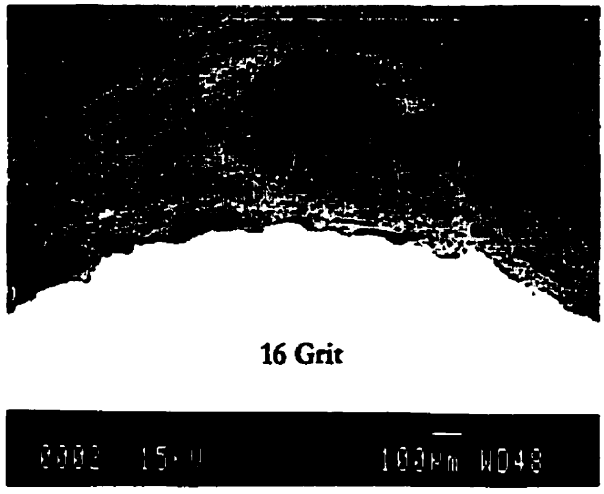

Figure 5-32 High power section from 16 grit stem. Note: load bearing lamellar structure of trabecular bone.

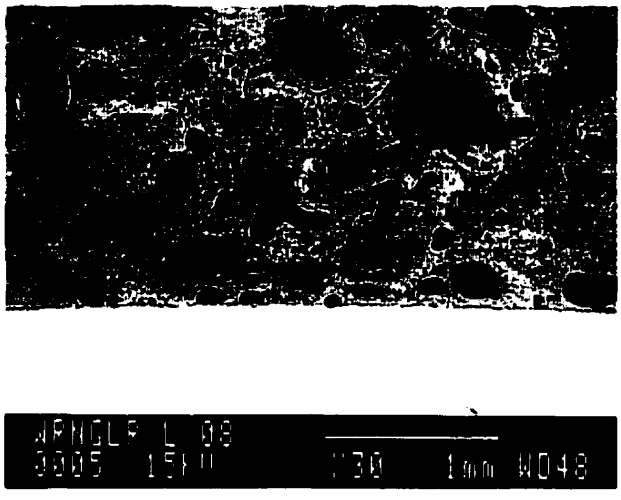

Figure 5-33 60 grit stem. Apposition of bone to implant surface.

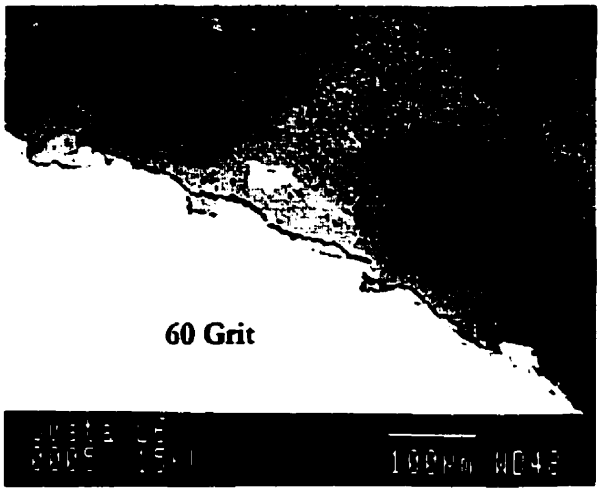

Figure 5-34 High power image of 60 grit surface. Microinterlock between bone and irregularities of implant surface. Gap and fractures are fixation artifacts.

Each

of the three surfaces demonstrated a positive osseous response with little apparent difference between different implant microtextures.

Figures 5.32-37 reveal the intimate contact between bone and the roughened implant surface. Bone adjacent to the perimeter of all implants showed microinterlock into the irregularities of the implant surface (Fig. 5.32, 5.34 - 5.37). Even the finest surface, the 60 grit surface, had sufficient roughness to develop mechanical interlock with surrounding bone (Fig. 5.34 & 5.35).

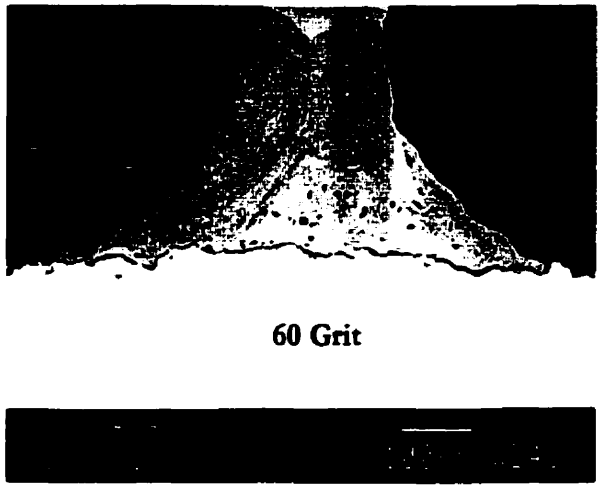

60 Grit

Figure 5-35 Trabecular abutment on 60 grit surface. Gap between bone and implant is a shrinkage artifact. Remodeled structure of trabeculae is visible.

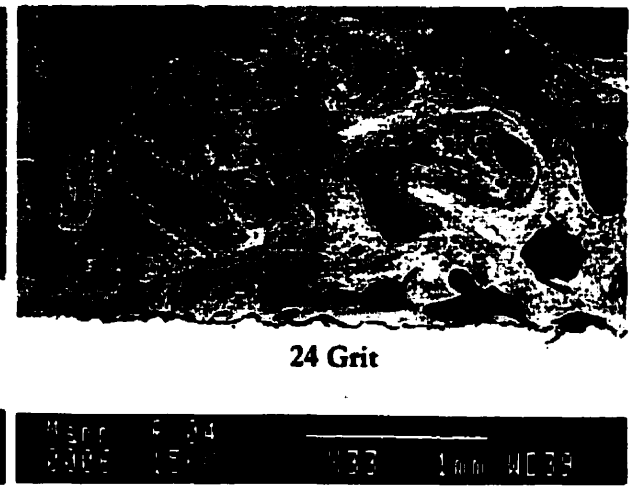

24 Grit

Figure 5-36 Extensive bone formation along 24 grit surface. Load bearing remodeled structure of trabecular bone is apparent. (Higher power image of figure 5.31)

Figure 5-37 Short spans of trabecular contact on 16 grit surface. Mechanical interlock of bone and close apposition to implant surface is apparent.

5.6 QUANTIFICATION OF BONE APPOSITION

Twenty one stems, eleven 60 grit, four 24 grit and six 16 grit with osseointegrated interfaces were used for the calculation of average bone apposition. Bone apposition was determined for all aspects of the implant (medial, lateral, anterior and posterior) as well as circumferentially. Average apposition for each surface finish was derived from the averages of individual sections (Fig. 5.38) as well as from the average apposition of each stem. The average bone apposition for the 168 sections ranged from 3.1% to 62.5%. Based on the averages of the thin sections, the bone apposition for the 60, 24 and 16 grit stems was 31.7% ± 14.1, 32.0% ± 14.0 and 27.9% ± 11.7, respectively. Based on the overall stem averages, the apposition for the 60, 24 and 16 grit stems was apposed by 31.7% ± 6.6, 32.0% ± 1.6 and 27.9% ± 3.0, respectively. For each of the three surfaces examined individually there was no significant difference in apposition (ANOVA, student's t-test, $p>0.05$) to the same implant surface amongst dogs, a finding which permitted pooling of the data and increased the statistical significance of the results ($n_{60\ grit}$= 88 sections). Comparisons were made between the paired sections of 60 grit implants and 24 grit implants and between the paired sections of the 60 and 16 grit implants. In addition, as there was no significant difference in the percentage of bone apposition to 60 grit implants amongst dogs, a direct comparison was made between the 16 and 24 grit surfaces. In all cases there was no significant difference in the percentage of the implant perimeter apposed by bone amongst the 60, 24 and 16 grit implant surfaces both amongst and within dogs (ANOVA, paired t-test, $p>0.05$).

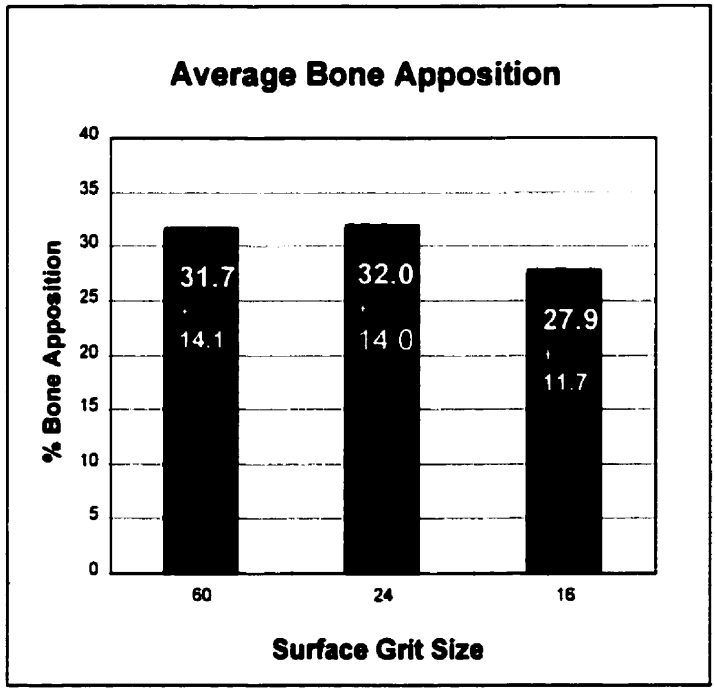

Figure 5-38 Osseous response to different surface treatments (sections used in calculation: n_{60}=88, n_{24}=32, n_{16}=48)

For all stems the average % surface covered by bone was 30.5 % (range 18.03 to 40.7 %).

Figures 5.39 & 5.40 are low power paired BSEM sections demonstrating the typical appearance of the average values of bone apposition. Implants appear to be nearly circumferentially apposed by bone, however, only bone in direct contact with the implant

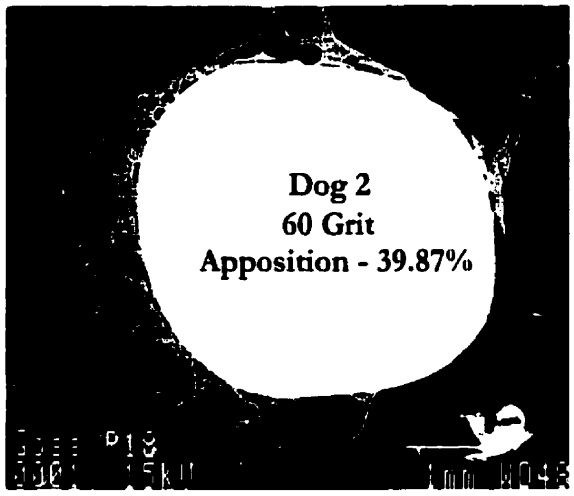

Figure 5-39 Dog #2. 60 grit stem. Bone apposition = 39.87%.

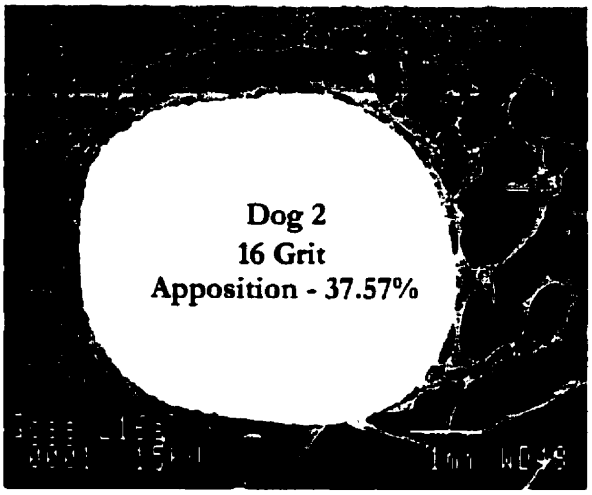

Figure 5-40 Dog #2. 16 Grit stem. Bone apposition = 37.57 %

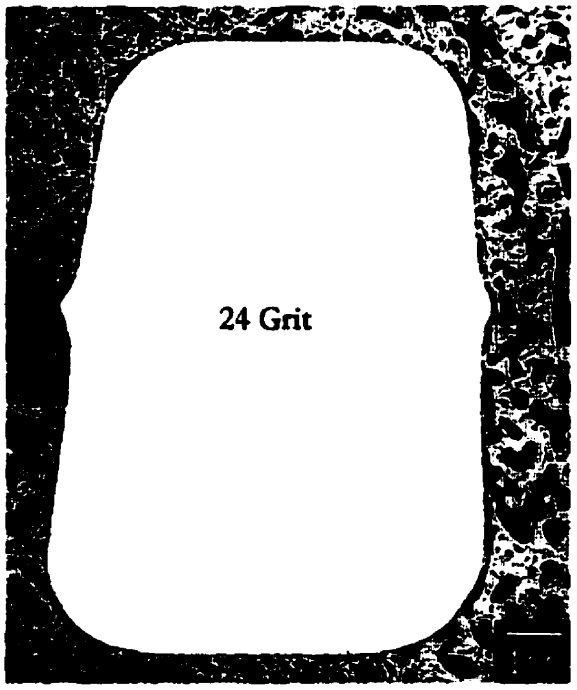

Figure 5-41 Proximal section of 24 grit stem. Bone apposition = 37.4 %

Figure 5-42 Proximal section of 16 grit stem. Bone apposition = 41.1 %

surface was included in the calculations. Bone apposition for all sections demostrating apposition ranged from 3.1 % to 62.5 %. Figures 5.41 & 5.42 demonstrate the appearance and greater amount of bone apposition observed in more proximal sections.

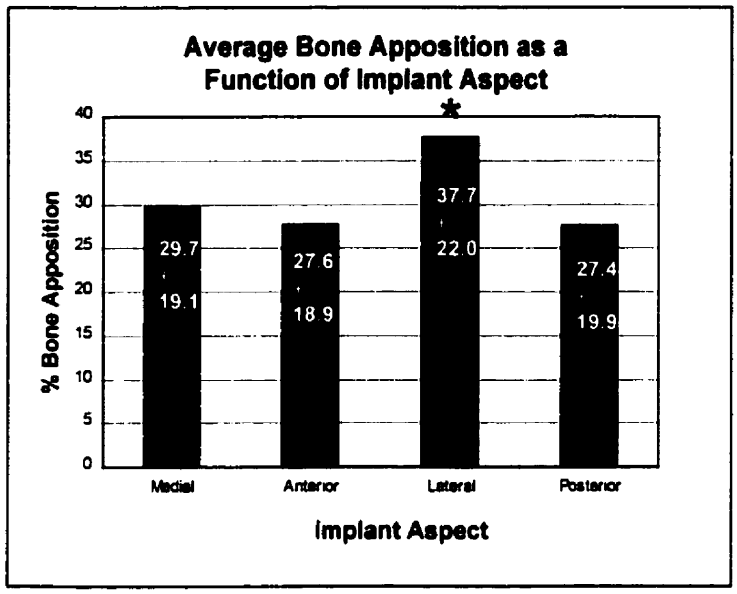

*Figure 5-43 Average apposition as a function of stem aspect. (n=144, * p= 0.005)*

Bone apposition was significantly greater at the lateral aspect of the stem surface (p=0.005, ANOVA) when compared to apposition at the medial, anterior and posterior aspects (Fig. 5.43).

Bone apposition (Table 5.1) was highest in the proximal regions of the stem (Fig. 5.44) and was significantly greater (*) at 30 mm compared with all other section levels (ANOVA p=0.004).

Table 5.1 Overall Apposition for stem aspect and section level

Section (mm)	Medial	Anterior	Lateral	Posterior	Average	std dev
20	31.77	22.22	22.80	19.74		13.98
30	40.09	32.63	42.36	39.30		16.01
40	26.97	30.16	56.23	31.82		12.35
50	25.28	26.39	35.58	26.71		11.06
60	29.09	29.78	33.36	21.47		15.15
70	24.99	27.07	30.37	23.71		10.87
80	29.10	25.08	38.05	29.78		12.47
90	31.92	28.05	44.52	28.41		13.59
Average					30.51	
std. dev.	19.10	18.92	22.04	19.90		

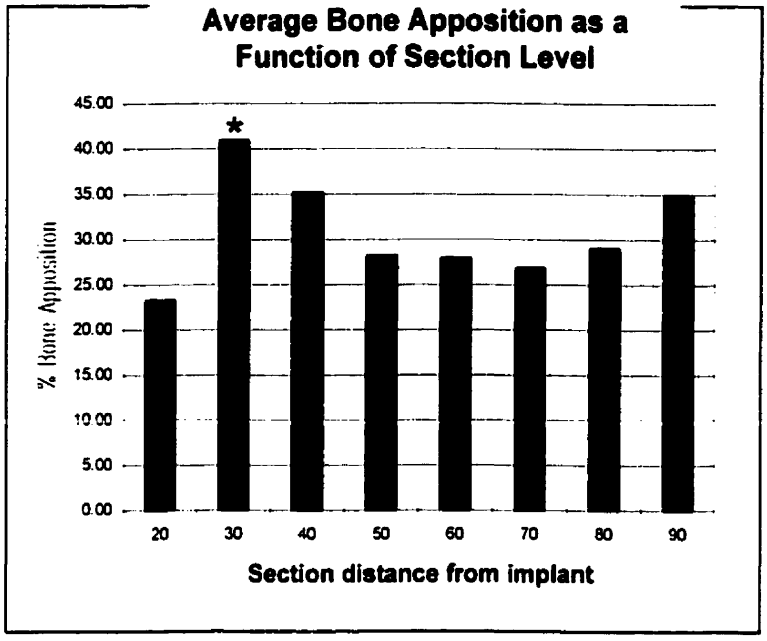

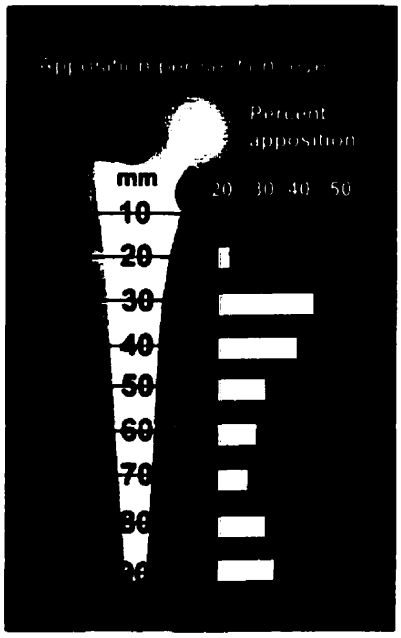

*Figure 5-44 (left) Bone apposition as a function of distance from the proximal end of the implant. Sections at 30 and 40 mm significantly different, * p=0.004 ($n_{section\ level}$ = 17) (right) Percent bone apposition shown in relation to stem section.*

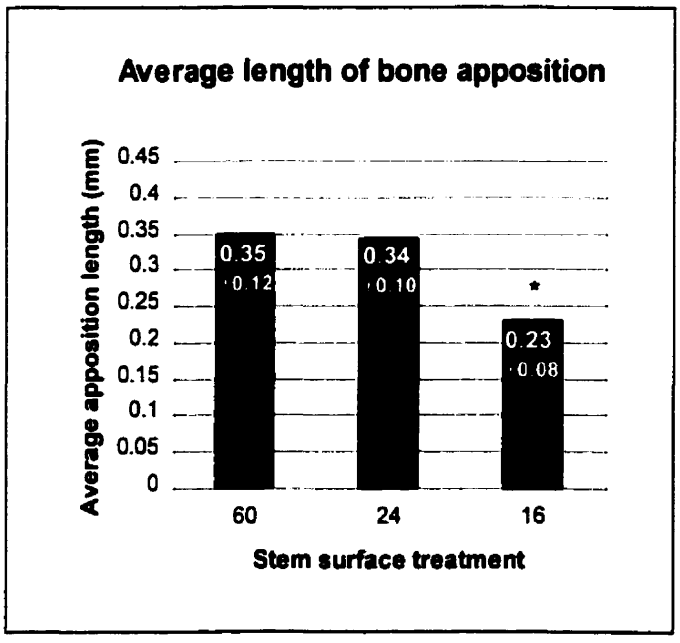

The average length of bone apposition was not significantly different between the 60 and 24 grit stems (Fig. 5.45). However, there was a significant difference in apposition length between both the 60 grit (0.349 mm) and 24 grit (0.344 mm) stems versus the 16 grit stems (0.231 mm). (Student t-test, p>0.02).

*Figure 5-45 Average bone contact length for each stem surface treatment. Significant difference between 60 or 24 grit and 16 grit stems (n_{60} ~ 6400, n_{24}~3200, n_{16} ~ 4200, * p= 0.02)*

5.7 CALCULATED ERROR IN BONE APPOSITION

The digital analysis software used was sensitive enough to include the implant surface roughness in the estimation of the length of the implant perimeter. The percentage error, resulting from the additive effect of surface roughness on the perimeter estimation, was determined. To reduce the unwanted effects of surface roughness on perimeter determination the image of the implant was smoothed 5 times using a digital filter. For each surface roughness a sample was selected and smoothed 5, 10, 20 or 100 times. The percentage error was determined as the percentage difference in the perimeter length between 5 and 100 smoothing operations (Table 5.2). The error increased with increasing surface roughness reaching a maximum of +3.2% for the 16 grit surface. .As the difference between 5 and 100 smoothing operations was slight, only five smoothing operations were performed to expedite analysis. The percentage error (maximum error), resulting from not smoothing the implant perimeter 100 times was added to the percent apposition of each section according to the implant surface treatment. All results were then recalculated with the error included and re-tested for statistical significance. There was no statistical difference between the results with and without the error compensation.

Table 5.2 Error in bone apposition incurred from method of analysis

SURFACE	UNSMOOTHED PERIMETER (mm)	SMOOTHED PERIMETER (mm)				MAXIMUM ERROR
		5x	10x	20 x	100 x	
60 grit	28.26	27.1	26.96	26.89	26.71	+1.4 %
24 grit	27.34	25.67	25.54	25.5	25.22	+1.8 %
16 grit	31.26	27.72	27.44	27.23	26.82	+3.2 %

5.8 EFFECT OF DIFFERING PERIODS OF IMPLANT RESIDENCY ON BONE APPOSITION

In each animal there was about a four week discrepancy between the first and second operations. Six 60 grit implants were in situ for 6.5 months and five for 5.5 months. No significant differences in bone apposition was found between the two time periods (fig 5.46).

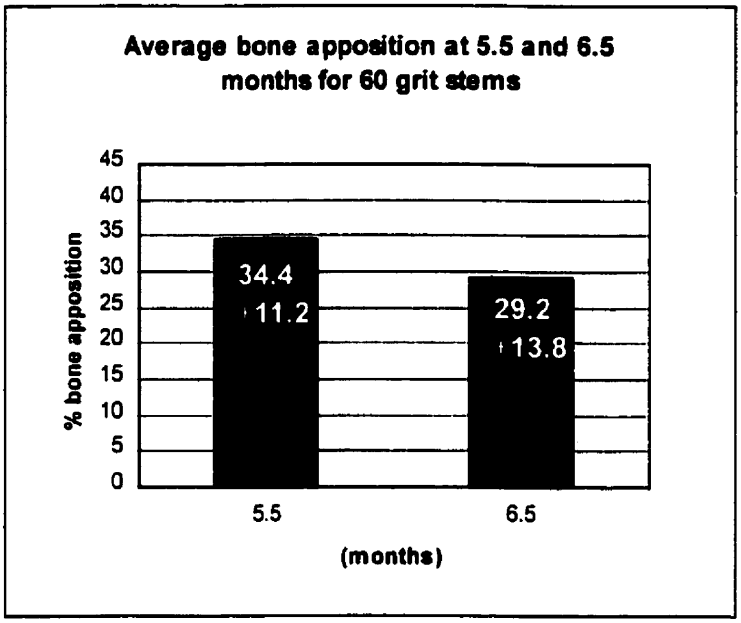

Figure 5-46 Bone apposition was not different between 5.5 and 6.5 months.

DISCUSSION

This study was conceived to provide new information about the osseous tissue response to load bearing implants with different grit blasted surfaces. Considering the mismatch in stem/femur shape and size, stem fixation was overall very good. All three types of grit blasted implants demonstrated consistently high amounts of bone apposition along all regions of the stem surface. There were no statistical differences amongst bone apposition with the 16, 24 and 60 grit surfaces, with an overall average of 30.5%.

Twenty-one of twenty-two stems were determined to possess osseointegrated interfaces despite the general stem/femur mismatch (Fig. 6.1). A tapered stem implanted within a very straight canal always results in a certain sizing mismatch. Although a range of stem/femur fit is achieved clinically, the fit is typically better than achieved in this canine study. An extreme case of fit is represented by the Zweymuller stem which is designed to fill both the metaphysis and the diaphysis (Fig. 6.1). This is in sharp contrast to the case of poorest fit obtained in the present canine study (Fig. 6.1).

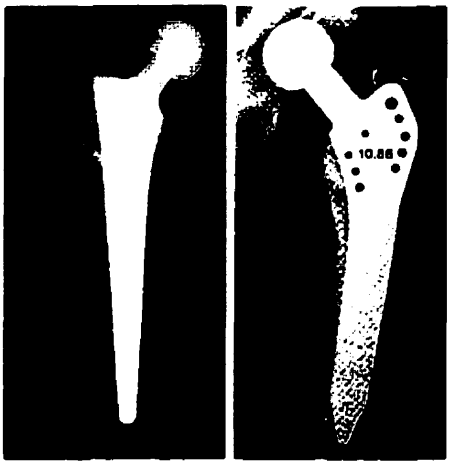

Figure 6-1 extreme case of poor fit in present canine study. (left) & Zweymuller prosthesis, an extreme case of good clinical fit (right)

The implant that developed a complete fibrous interface suggested that adequate initial implant stability was not achieved. With porous surfaces, implant motion greater than 40 μm relative to the porous implant-bone interface increases the likelihood of fibrous fixation.[83,84] It is possible that grit blasted implants are more susceptible to the effects of implant motion than porous coated implants. Sintered coatings typically possess pore spaces 100-400 μm in size[85]. The peak-to-peak spacing (S) of a grit blasted surface, measured as about 50 μm for the coarsest (16 grit) surface, is analogous to the pore size

of porous surfaces. If bone growth into the porous coating does not occupy the complete porous space, ingrown bone can tolerate some degree of motion before shearing trabecular struts.[91] However, the peak-to-peak spacing and lengths of trabecular abutment to the grit blasted surface are less than 40 μm. As a result, smaller amounts of relative motion at the bone-implant interface could interfere with osseous attachment (Fig. 6.2). There are no published data directly describing the relationship between motion and the tissue response to grit blasted surfaces.

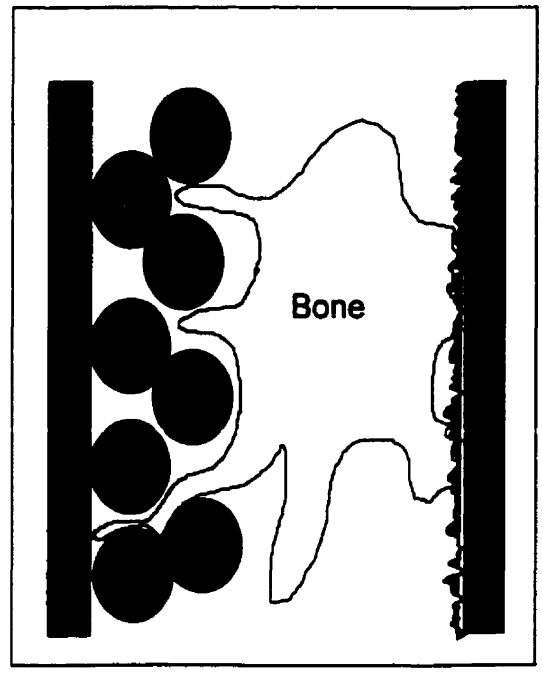

Figure 6-2 Comparison of relative size difference between porous and grit blasted surfaces

The absence of subsidence or migration and the parallel nature of the thin neocortex surrounding the implant without osseointegration was suggestive of stable fibrous fixation (Fig. 5.37). Although not directly quantified, stable fixation with a fibrous interface suggests that grit blasted surfaces support some degree of soft tissue attachment. During explantation, extraneous tissue removed from the proximal implant area often demonstrated a weak but notable adherence to the implant surface. Bobyn et al. have demonstrated that a tissue ingrown circumferential porous coating is necessary to restrict synovial fluid migration into the peri-implant space.[45] Whether or not soft tissue or osseous adhesion to grit blasted surfaces is sufficient and extensive enough to prevent particulate and synovial fluid migration into the periimplant space remains an important question concerning long term GB implant function.

Bone apposition varied somewhat along implant length. This variance was greatest in the most proximal sections (0 and 10 mm from the implant shoulder) which was attributed to the method of canal preparation or to implant insertion. In some cases, to prevent femoral fracture and permit proper seating of the rasp, additional rasping and/or bone removal with a high speed burr was necessary anteriorly and posteriorly. Fibrous tissue

formation in the most proximal regions may have resulted from either thermal damage to the adjacent bone or from excessive and unequal bone removal.

Bone apposition was greatest in the proximal regions of the stem, with a peak average of 41% at 30 mm from the implant shoulder (Fig. 5.44). This corresponded to the region of the femur with the highest density of trabecular bone as observed in the non-implanted control sections (Fig. 5.26). Bone densification from proximal load transfer may have contributed to the higher apposition in the metaphysis. Bone ongrowth declined in the mid-section of the implant to 28% at 70 mm and increased distally to 35% at 90 mm (Fig. 5.44) . This decline in bone apposition may be attributed to the poor fit between implant and femur caused by placing a tapered stem in a stovepipe canal. Radiographic evaluation revealed that the distance between the endosteum and implant was greatest around the 70 mm section levels. It is known that closeness of fit between implant and cortex is important to both the rate and extent of bone development.[86] As shown in Figures 5.9-5.12, with increasing distal location the implant-femur gap decreased and bone apposition increased. Additionally, 15 stems were implanted in varus resulting in the implant tip residing within a 2 mm proximity to cortical bone which most likely increased bone apposition in the most distal sections.

The extent of bone apposition reported in this study is in general agreement with published work using non-functional implant models. Buser et al.[60] reported bone apposition of 20-40% for a variety of grit blasted and acid etched specimens. Similarly, Wong et al.[22] at three months determined bone apposition on a range of surface R_a values to be approximately 30%. Intramedullary studies in rabbits with grit blasted implants of surface roughness comparable to the 60 grit sample examined in the present study have demonstrated similar findings. Both Goldberg et al.[21], and Feighan et al.[65] reported bone apposition of 30-35 % at three months. The results of this work do not correspond with those of Maistrelli et al.[20] who evaluated coarse grit blasted and HA coated implants in a 5 month canine model. Bone apposition to the grit blasted implants averaged 16% while the HA coated implants averaged 73%.

Other studies have shown that the extent of bone apposition is dependent upon surface roughness, however this finding may be valid only during the initial 3-4 weeks of

implantation. Feighan et al.[65] reported a significant difference in bone apposition at three weeks between surface R_a values of 4.2 and 5.9 μm. The 4.2 μm implants possessed nearly two fold-greater bone apposition than the 5.9 μm implants. However, at six and 12 weeks this difference was not significant. Wennerberg and Albrektsson et al.[66] reported significant differences in bone apposition between very fine grit blasted Ti_6Al_4V surfaces, (R_a = 1.11 μm and R_a = 2.5 μm) at four weeks. In a canine cancellous bone study, Wang et al [87] used a four-sided intramedullary implant with alternating HA (R_a = 12.55 μm) and grit blasted titanium (R_a = 3.56 μm) surfaces. New bone in the area adjacent to the implants reached a maximum at six weeks and changes were not significant thereafter. It would appear that the tissue response to textured implant surfaces can reach a steady state as early as 4 weeks. Furthermore, the present functional implant study indicated no significant difference in bone apposition between 5.5 and 6.5 months, suggesting that sufficient time existed for a mature tissue response.

In non-functional models with GB implants, new bone development generally reaches a steady state in substantially less time than typically required for a maximal response with porous implants. It is possible that this occurs simply because the process of bone apposition requires less total bone formation then bone ingrowth and hence takes less time. The shorter time may also reflect the stimulus for bone development that appears to be characteristic of grit blasted surfaces. Although it is important to characterize the short term osseous response to functional grit blasted implants, from a clinical perspective it is more helpful to understand the longer more steady-state osseous response. The results of this study emphasize the need to evaluate porous or textured surfaces in the context of long term load bearing models. Shorter term non-functional models may not provide a representative indication of the osseous response that occurs under more clinically relevant conditions.

It is unlikely that the absence of differences in bone apposition between the different surfaces was a result of the low sensitivity of the implant model due to the high potential for new bone formation in the canine. Many canine studies with HA coated implants have reported an appositional response significantly greater than 30-35%,[2,20,22,43,56,60,61,69,88] thus demonstrating a greater range of potential apposition than observed with grit blasted

implants. Differences in bone growth into beaded and fiber metal coatings have been detected as well (Table 2.2).[68]

One of the most striking findings in this study was the extent to which new bone spanned large gaps between the implant and endosteum and established osseointegration. This is exemplified by the sections illustrated in Figures 5.17, 5.18 (non implanted specimen) and 5.23. In many cases the distal half to third of the stem was completely distanced from the endosteal cortex and thus could not have participated in significant load transfer. Thus it is unlikely that the new bone formed for stress-related reasons. Preparation of the femoral canal by rasping may have enhanced the observed osseous response. Bone grafts, coral and particulate bone have been reported to stimulate new bone formation *in vivo*. The rasp used to prepare the femoral canal partially displaced bone towards the cortices and down the intramedullary canal. Therefore autograft bone particles were initially present and may have stimulated new bone formation. Another strong possibility is that the surface topography of the implants was a driving force for osseous formation and conduction as subsequently discussed.

Many studies have demonstrated that the topographical characteristics of the implant surface determine the type of apposed tissue formation. In addition, certain surface features may also control the direction and extent of new bone formation. Studies with a variety of cells have revealed that cell behavior and morphology can be manipulated by surface topography.[33,34,35,36,37,38,39,40,89] Fibroblast, nerve and epithelial cells became aligned on surfaces of varying roughness (Fig. 6.3). The coordination of cell migration along grooved surfaces may account for the differences in the length of bone apposition between the 16 and 24 or 16 and 60 grit surfaces. The topography of the 16 grit implant surface may have been sufficient to manipulate osteoblast migration and new bone formation.

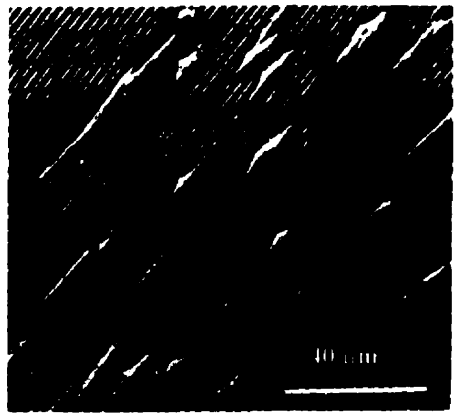

Figure 6-3 Nerve cells aligned on grooved substrata.(From Clark et al. [39])

peak height (R_z) and not peak spacing demonstrated significantly different amounts of bone apposition, further indicating that the relative change in topography affects osteoblast bone forming activity. Pertaining to the current study, a scaled evaluation of the osteoblast/implant relationship provides an appreciation of the significance of surface roughness to cellular size. In figures 6.4 and 6.5, representations of osteoblast cells are depicted to scale on actual profiles of the 16 and 60 grit surfaces.

Bearing in mind that the topographical change may induce a cellular response, it is helpful to consider the **average** peak to valley heights (R_z) of each implant used in the current study (Table 4.2). The R_z of the 60 and 24 grit surface is approximately the same as the diameter of an osteoblast cell (20 μm) while the R_z of the 16 grit surface is significantly larger (35 μm). From the frame of reference of the osteoblast, the 60 and 24 grit surfaces possesses a microtexture and the 16 grit surface possesses a macrotexture at the cell level (see page 13 for definitions).

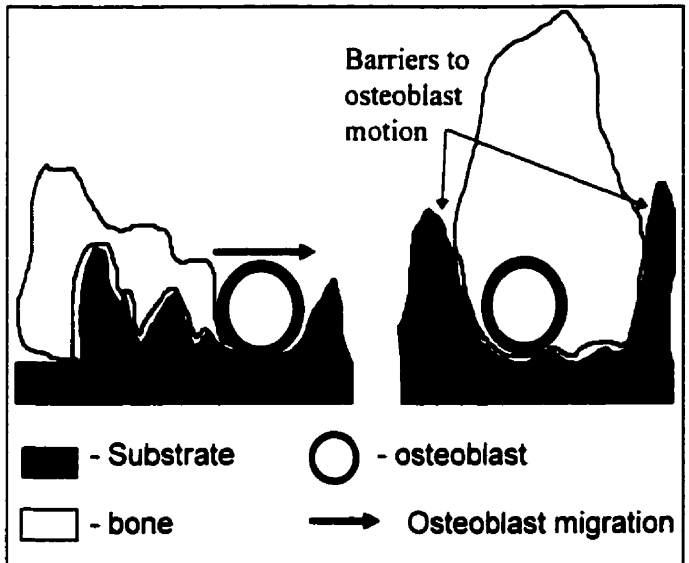

Figure 6-6 Possible depiction of osteoblast response on surafces of different Ra.(left) unhindered bone formation on 24 grit surface. (right) 16 grit surface limits osteobalst migration.

Perhaps microtexture controls tissue formation at the cellular level and macrotexture controls the extent and direction of new bone formation. Overall, bone formation showed no preference for any of the three surfaces, however, significantly different apposition lengths were measured. Since the substrate of each implant was identical, material factors can be discounted as contributing to the differences in apposition length. Images of each implant surface, resolved at the cellular level, reveal a notable microtexture (Figs. 4.14- 4.16) that may provide a suitable stimulus for bone formation. The high amount of bone apposition demonstrates the potential of the GB surfaces to trigger bone formation at the cellular level. Although not quantified, the secondary microtexture appears relatively

similar amongst all surfaces (Figs. 4.14- 4.16). If differences in bone apposition length are a function of surface structure then microtexture cannot be responsible and the differences in bone formation must arise from some other aspect of surface structure. As such, the gross surface structure, the macrotexture (Figs. 4.6, 4.8 & 4.10), may direct or limit bone formation once osseointegration has been initiated (Fig. 6.6). The observed bone formation implies that a suitable stimulus for new bone formation arises from either a chemical property of the grit blasted surface or from the microtexture superimposed upon the grit blasted surface. Sites of bone fracture represent regions of increased bone forming activity during repair, however the mechanism responsible for bone formation is not well understood. It was interesting to note that the fracture surface of the canine fracture specimen was strikingly similar to the grit blasted surfaces in Figures 4.17 & 4.14-4.16. This finding could be coincidental but could equally lend support to the theory that surface topography is a major factor responsible for both the osseous response at the site of a bone fracture and one the stimulatory effect of grit blasted surfaces. Further investigation into topographical properties of micro and macro textured surfaces may not only provide a control for the amount of bone apposed to implant surfaces but also the extent and direction of new bone formation.

While the connection between surface topography and fracture healing is theoretical, such a mechanism could account for new bone formation at both the fracture site and the grit blasted surface. In the adult fracture, cellular recruitment is both local and systemic. A specific surface structure provides a simple and effective means to locate the fracture site. Osteoblast stem cells, especially in the systemic circulation, cannot be "told" the precise location of the fracture site. As such, the fracture surfaces themselves must be recognized as a site for osteoblast activation and new bone formation. Chemotactic signaling may participate in new bone formation, but such signaling would be diffuse and only locate a general area; a specific "locator" is still a requisite. The contrast between the smooth surface of the endosteal cortex and the rough surface of the fracture is evident in Figure 4.18. In vitro studies have reported that smooth surfaces promote cell migration and generally do not stimulate osteoblast activity whereas rough surfaces increase osteoblast bone forming activity and decrease osteoblast migration. Such *in vitro* studies with grit blasted surfaces strongly suggest that the rough fracture surface would encourage bone forming osteoblast activity, while the smooth endosteal cortex

would promote cell migration, perhaps towards the fracture site. By virtue of their topography, grit blasted implants may effectively induce the local biology to integrate or "repair", the implant into surrounding bone.

It is difficult not to compare the osteogenesis and osteoconduction observed in the present study with similar observations reported in many studies with HA coated implants. It is generally accepted that HA coating on an implant acts as an osteoconductive agent that increases the amount of bone formation and apposition.[2] The mechanism for this increase is often discussed in the context of the HA chemistry, with calcium and phosphate being incorporated into new bone as osteoid calcifies. The surface roughness of HA coated devices has generally been overlooked as a contributing source of new bone formation. Interestingly, plasma sprayed HA surfaces generally possess a rough irregular topography with an RA that is similar to grit blasted surfaces (6-8 μm). It is therefore possible, if not likely, that the osseous response to HA coated implants is partially due to surface roughness, not just surface chemistry. Only one study has compared the effects of GB titanium and HA coated cylinders with nearly identical surface roughness. Carlsson et al.[57] compared grit blasted and HA coated implants in the human knee. This study was one of the first to compare grit blasted specimens and HA coated implants of similar surface roughness and peak spacing. It is notable that no significant difference in bone apposition was determined. Carlsson et al. concluded that the similarities in surface texture may have significantly influenced the results.

To predict the ability of a new surface for osseointegration to maintain fixation in the clinical environment, interface shear strength is often considered and evaluated. Wong et al.[20] reported that bone apposition to grit blasted surfaces (R_a=1.2-6.4 μm) correlates with interface shear strength. The fixation strength of grit blasted implants may arise solely from a mechanical interaction at the bone-textured surface interface. As surface roughness increases the volume available for bone ingrowth into the spaces created by grit blasting increases cubically ($V=\pi r^3$). Thus, rougher surfaces possess a greater available space for interdigitation of bone and therefore potentially can lead to greater mechanical interlock. Although the present study did not measure interface fixation

strength, it could be expected that the roughest (16 grit) surface would provide the greatest mechanical strength for any given amount of apposition. It should be recalled that the morphological presentation of bone at the implant surface differed between smooth (60 & 24 grit) and rough (16 grit) surfaces (Figs. 5.27-5.30). The smooth surfaces presented a thin covering of bone spanning large distances connected by a single or few trabeculae. The rough surfaces demonstrated shorter contact regions but a greater number of osseous contact points. As a result there was a greater number of trabecular struts present in close proximity to the 16 grit implant surface than either the 24 or 60 grit surface (it should be noted that in proximal regions of high trabecular density morphological differences could not be determined). Whether or not the differences in pattern of bone apposition would influence interface shear strength is difficult to speculate upon.

An additional issue regarding surface roughness concerns the strength of the implant substrate. It is well known that surface modifications induced by porous coating reduce the fatigue strength of titanium because of its notch sensitivity[12,91]. Similar sensitivity to surface notches would exist for corundum blasted implants as well. Investigations into the fatigue properties of grit blasted titanium alloy would yield valuable information pertinent to the selection of the optimum surface texture.

In the final analysis there is the question about whether an optimum corundum blasted surface exists for functional load bearing implants. From a bone apposition standpoint, all three surfaces were essentially equally effective for osseointegration. From a mechanical standpoint, if the coarseness of the 16 grit surface excessively reduced the fatigue properties of the titanium implant (by notch sensitivity) then the 60 and 24 grit surfaces would be preferred options. Of these two, from an interface strength standpoint the 24 grit surface might be preferred because of the increased micro-mechanical interlock and fixation strength afforded by bone apposition. Further fundamental studies of the type described in this thesis, in conjunction with the continued clinical evaluation of grit blasted devices coupled with autopsy retrieval analyses, will provide more definite answers to these questions.

The findings of this study clearly indicate that rough irregular titanium surfaces with R_a of 2.8 to 6.7 μm created by corundum blasting both encourage and support stable and intimate interfaces with osseous tissue. The functional hip implants with grit blasted surfaces demonstrated consistent bone apposition averaging 30.5 over the stem length. The apposition in combination with stem geometry were sufficient to withstand interface forces in a long term *in vivo* load bearing model.

1. No significant difference in the extent of bone apposition was determined amongst 60, 24 and 16 grit femoral implants with average surface roughnesses of 2.8±0.26 μm, 4.2±0.25 μm and 6.7±0.56 μm respectively. The 60, 24 and 16 grit stems were apposed by 31.7% ±14.1, 32.0% ±14.0% and 27.9 %±11.7 of bone, respectively.

2. A significant difference in bone apposition contact length was determined between the 16 and 24 grit surfaces and between the 16 and 60 grit surfaces. Furthermore, it was determined that the 24 and 60 grit surfaces demonstrated osteoconductive properties. These two findings indicate that the morphology of trabecular bone was markedly different at the bone-implant interface and that the roughest surface (16 grit) possessed significantly more trabeculae in contact with the implant surface.

3. In the distal femur, extensive new heterotropic bone formation occurred within the intramedullary canal in close apposition to the implants, strongly suggesting that surface roughness stimulates an osseous response.

4. No change in bone apposition was determined between 5.5 and 6.5 months for the 60 grit stems indicating a relatively mature osseous tissue response and the suitability of the study protocol.

The results of this study support the continued investigation of textured surfaces for implant fixation by the ongrowth of bone. Several unanswered questions remain that may greatly increase the understanding of the osseous reaction to textured interfaces. Procurement of such answers has the potential to improve the function and longevity of noncemented reconstructive devices for clinical use. This study has suggested a number of future topics for further research.

1. To determine the surface roughness at which point the fatigue properties of textured titanium alloy implants are critically reduced.
2. To determine the acceptable limit of micromotion with corundum blasted surfaces of varying topography.
3. To investigate the properties of textured surfaces that modulate osteoconduction.
4. To determine the surface topography that optimizes both the rate of new bone formation and the interface fixation strength.
5. To investigate the osseous response to grit blasted implants under pathological conditions and in older patients.
6. To investigate the potential efficacy of grit blasted surfaces in conjunction with macro textured surfaces for enhancing the extent of osseointegration and reduce the time period of new bone formation.
7. To determine the effects of varying surface topography of tapered stems on long term bone remodeling.
8. To determine the effects of the extent of surface roughness on tapered stems on long term bone remodeling.
9. To determine the optimal implant-femur fit for successful long term results.

[1] Charnley J, Low Friction Arthroplasty of the hip. Theory and Practice, New York: Springer-Verlag, 1979

[2] Søballe K, "Hydroxyapatite ceramic coating for bone implant fixation", Acta orth. scand. suppl., **64**, No. 235 pp 1-57, 1993

[3] Cameron H, in Bone Implant Interface, Toronto: Mosby, pp.201, 1994

[4] Bragdon CR, Burke D, Lowenstein JD, O'Connor DO, Ramamurti B, Jasty M, Harris WH, "Differences in stiffness of the interface between a cementless porous implant and cancellous bone in vivo in dogs due to varying amount of implant motion", J. Arthroplasty, **11** (8) pp.945-951, 1996

[5] Bobyn JD, "The Susceptibility of Smooth Implant Surfaces to Periimplant Fibrosis and Migration of Polyethylene Wear Debris", Clinical Orthopaedics and Related Research, **311**, pp. 21-39, 1995

[6] Brown CC, McGlaughlin RE, Balian G, "Intramedullary bone repair and ingrowth into porous coated implants in the adult chicken: a histologic and biochemical analysis of collagens", J. Orthopaedic Research, **7** pp. 316-325, 1989

[7] Bobyn JD, Determination of the Criteria for the Design and Application of Porous Coated Implants, PhD Thesis, University of Toronto, 1980

[8] Bobyn JD, The Strength of Fixation of Porous Metal Implants by the Ingrowth of Bone, Master's Thesis, McGill University, 1977

[9] TH Mallory, WC Head, AV Lombardi, RH Emerson, RW Eberle, MB Mitchell, "Clinical and radiographic Outcome of a Cementless, Titanium, Plasma Spray-Coated Total Hip Arthroplasty Femoral Component", J. of Arthroplasty, **11** (6) pp. 653-660.

[10] Metals Handbook (desk edition), eds Boyer HE, Gall TL, Metals Park Ohio: American Society for Metals, 1995.

[11] Bobyn JD, Glassman JD, Krygier, JJ, Dujovne AR, Brooks CE, "Microknurled surfaces for implant attachment by bone Ingrowth: Development and Evaluation in Canine Studies", Trans - Fourth world Biomaterials Congress, Berlin, Germany 1992.

[12] Bourassa L, "Improving The Fatigue Strength of Ti-6Al-4V by Surface Thermomechanical Processing" Master's Thesis, McGill University, 1994.

[13] Matsuda T, Nakayama Y, "Surface microarchitectural design in biomedical applications: In vitro transmural endothelialization on microporous segmented polyurethane films fabricated using an excimer laser", J. Biomedical Materials Research, **31**, pp. 235-242, 1996

[14] Woolson ST, Maloney WJ, Milbauer JP, Bobyn JD, Yue S, "Fatigue fractures of modern forged Cobalt Chrome alloy stem", Trans Amer. Acad. Orth. Surg., 64th meeting, SF CA, 1997

[15] MC Melican, AR Ponnambalam , MC Zimmerman , M Dhillon, D Treacy, A Curodeau, "Three dimensional Printing: An alternative to Sintered Beads for Orthopaedic Implants", Trans - Orthopaedic Research Society, pp 757, San Francisco CA, USA, 1997

[16] Legros and Craig,. Strategies to affect bone remodeling. Journal of Bone and Mineral Research 1993; **8**: supl 2, 1993

[17] Rothman RH, Hozack WJ, Ranwart A, Moriarty L, "Hydroxyapatite-coated femoral stems" J. Bone and Joint Surgery 78A **3** p 319, 1996

[18] Wheeler S, "Eight year clinical retrospective study of titanium plasma-sprayed and hydroxyapatite coated cylinder implants" International JOMI, vol.11 **3**, pp. 340-350, 1996

[19] Berndt CC, Haddad GN, Gross KA, "Thermal spraying for bioceramic application" in Bioceramics ed. G Heimke, Proceedings of the 2nd International symposium of ceramics in medicine, **2**, pp. 201, Heidelberg, 1989

[20] Maistrelli GL, Mahomed N, Fornasier V, Antonelli L, Li Y, Binnington A. Functional Osseointegration of Hydroxyapatite-coated Implants in a Weight-bearing Canine Model. J. of Arthroplasty, **8** pp. 549-553, 1993

[21] Goldberg VM, Stevenson S, Feighan J, Davy D, "Biology of Grit-Blasted Titanium Alloy Implants", Clinical Orthopedics and Related Research, 319 pp.122, 1995

[22] Wong M, Eulenberger SR, Hunziker, "Effect of surface topology on the osseointegration of implant materials in trabecular bone" J. Biomedical Materials Research, **29** pp. 1567-1575, 1995

[23] Kasemo B, "Biocompatibility of titanium implants: Surface science aspects", J of Prosthetic Dentistry, **48** (6), pp. 832-837, 1983

[24] J.Lausmaa, L.Mattson, U. Rolander and B Kasemo, "Chemical composition and morphology of titanium surface oxides", Mater. Res. Soc. Symp. Proc., **55** pp.351-359, 1986

[25] Saito T., Albelda SM, Brighton CT. Identification of Integrin Receptors on Cultured Human Bone Cells. J. Orthopaedic Research **12** pp. 384-394, 1994

[26] Hansson HA, Albrektsson T, Branemark P-I, "Structural aspects of the interface between tissue and titanium implants", The J Prosthetic Dentistry, **50** (1) pp. 108-113, 1983

[27] Kasemo B, and Lausmaa, "Surface Science Aspects of Biocompatability", vol. 1, CRC Press, Boca Raton, FL, pp. 159-181, 1981

[28] Cannas M., Denicolai F, Webb LX, Gristina AG. "Bioimplant Surfaces: Binding of Fibronectin and Fibroblast Adhesion", J. Orthopaedic Research, **6** pp. 58-62, 1988

[29] Könönen M, Hormia M, Kivilahti J, Hautaniemi J. Thesleff I, "Effect of surface processing on the attachment, orientation, and proliferation of human gingival fibroblasts on titanium", J. Biomedical Materials Research, **26** pp. 1325-1341, 1992

[30] Puleo DA, Bizios R., "Formation of focal contacts by osteoblasts cultured on orthopaedic biomaterials", J. of Biomedical Materials Research, **26** pp. 291-301, 1992

[31] Hearly KE, Ducheyne P, "Hydration and preferential molecular adsorption on titanium *in vitro*", Biomaterials, **13** pp.553-561, 1992

[32] Kitsugi T, Nakamura T, Oka M, Goto T, Shibuya T, Kokubo T, Miyaji S, "Bone bonding beahvior of titanium and its alloys when coated with titanium oxide (TiO_2) and titanium silicate (Ti_5Si_3)", J. Biomedical Materials Research, **32** pp. 149-156, 1996

[33] S.R. Taylor and D.f. Gibbons, "Effect of surface texture on the soft tissue resposne to polymer implants", J. Biomedical Materials Research, **17** pp. 205-227, 1983

[34] T. Inoue, J.E. Cox, R.M. Pilliar, and A.H. Melcher, "Effect of the surface geometry of smooth and porous- coated titanium alloy on the orientation of fibroblasts in vitro", J. of Biomedical Materials Research, **21** pp. 107-126, 1987

[35] D.M. Brunette, "The effects of implant surface topography on the behavior of cells", Int. J. of Oral and Maxiofacialary Implants, **3** pp. 231.246, 1988

[36] Michaels CM, Keller JC, Stanford CM, Solursh M, "In vitro cell attachment of osteoblast like cells to titanium", J. Dental Research, **68** (special issue) pp. 276, 1989

[37] Schwartz Z, Boyan BD, "Underlying mechanisms at the bone-biomaterial interface", J. of Cellular Biochemistry, **56** (3) pp. 340-347, 1994

[38] Keller JC, Stanford CM, Wightman JP, Draughn RA, "Characterizations of titanium implant surfaces. III", J. Biomedical and Materials Research, **28** pp. 939-946, 1994

[39] Clark P, Connolly P, Curtis ASG, Dow AJT, Wilkinson CDW, "Topographical control of cell behavior I. Simple step cues.", Development, **99** pp.439-448, 1987

[40] Chehroudi B, Gould TRL, Brunette DM, "Titanium-coated micromachined grooves of different dimensions affect epithelial cells and connective tissue cells differently *in vivo*", J. of Biomedical Materials Research, **24**, 1230-1219, 1990

[41] Predecki P, Stephan EJ, Auslaender BA, "Kinetics of bone ingrowth into cylindrical channels in aluminum oxide and titanium", J. Biomedical Materials Research, **6** pp. 375-400, 1971

[42] Stanford CM, Keller JC, Solursh M, "Bone cell expression on Titanium surfaces Is altered by sterilization treatments", J. of Dental Research, **73**(5), 1061-1071, 1994

[43] Lind M, Overgaard S, Soballe K, Nguyen T, Ongpipattanakul B, Bunger C. "Transforming Growth Factor-ß1 Enahnces Bone Healiing to Unloaded Tricalcium Phospahte Coated Implants: An Experimental Study in Dogs", J. of Orthopaedic Research, **14** pp. 343-350, 1996

[44] Yasko AW, Lane JM, Fellinger EJ, Rosen V, Wozney JM, Wand EA, "The healing of segemental bone defects, induced by recombinant human bone morphogenic protein (rhBMP-2). A radiographic, histological, and biomechanical study in rats", JBJS, **74**(7), pp. 659-70, 1992

[45] Bowers KT, Keller JC, Randolph BA, Wick DG, Michaels CM, "Optimization of Surface Morphology for enhanced Osteoblast Response in Vitro" Int. J. Oral & Maxiofacial Implants, **7** pp. 302-310, 1992

[46] Martin JY, Schwartz Z, Hummert TW, Schraub DM, Simpson J, Lankford Jr. J, Dean DD, Cochran DL, Boyan BD. "Effect of titanium surface roughness on proliferation, differentiation, and protein synthesis of human osteoblast-like cells" (MG63). J. Biomedical Materials Research, **29** pp. 389-401, 1995

[47] Thompson GJ, Puleo DA, "Effects of Sublethal Metal Ion Concentrations on Osteogenic Cells Derived from Bone Marrow Stromal Cells"

[48] Ramsay, WS, Hertl W, Nowlan ED, Binkowski NJ, "Surface treatments and cell attchment", In Vitro, **20** pp. 802-808, 1984

[49] Kieswetter K, Schwartz Z, Hummert TW, Cochran DL, Simpson J, Dean DD, Boyan BD, "Surface roughness modulates the local production of growth factors and cytokines by osteoblast-like MG-63 cells" J. Biomedical Materials Research, **32** pp. 55-63, 1996

[50] Stanford CM, Keller JC, Solursh M, "Bone cell expression in titanium surfaces is altered by sterilization treatments", J. Dental Research, **73**(5) pp.1061-1071, 1994

[51] Ninoyima JT, Struve JA, Abel, SM,Shetty RH, Lin SD, "Orthopedic implant surfaces induce gene expression and protein synthesis for mediators of bone resorption" 43rd Trans. ORS, pp. 737, 1997

[52] Schwartz Z, Martin JY, Dean DD, Simpson J, Cochran DL, Boyan BD, "Effect of titanium surface roughness on chondrocyte proliferation, matrix production and differentiation depends on the state of cell maturation", J. Biomedical Materials Research, **30** pp.145-155, 1996

[53] Tencer AF, Holmes RE, Johnson KD, "Osteocompatability Assessment", in Hand Book of Biomaterials Evaluation, von Recum, AF editor, Toronto: Macmillan Publishing, pp. 321-338, 1986

[54] Eitel F, Klapp F, Jacobsen W, Schweiberer L, "Bone regeneration in animals and in man. A contribution to understanding the relative value of animal experiments to human pathophysiology.", Archives of Orthopaedic Trauma Surgery, **99** pp. 59-64, 1981

[55] Sumner DR, Bryan JM, Urban RM, Kuszak JR, :Measuring the volume fraction of bone ingrowth a comparison of three techniques", J. of Orthopaedic Research, **8** pp. 448, 1990

[56] Thomas KA, Cook SD, "An evaluation of variables influencing imlant fixation by direct bone apposition", J. Biomedical Materials Research, **19** pp.875-901, 1985

[57] Carlsson L, Regnér L, Johansson C, Gottlander M, Herberts P, "Bone Response to Hydroxyapatite-Coated and Commercially Pure Titanium Implants in the Human Arthritic Knee", J. Orthopaedic Research, **12** pp. 274-285, 1994

[58] Chappard D, Grizon F, Brechet I, Basle MF, Rebel A, "Evolution of the bone-titanium interface on implants coated/noncoated with xenogenic bone particles: Quantitative microscopic analysis", J. Biomedical Materials Research, **32** pp.175-180, 1996

[59] Larsson C, Thomsen P, Aronsson BO, Rodahl M, Laussmaa J, Kasemo B, Ericson LE, "Bone response to surface-modified titanium implants: studies on the early tissue response to machined and electropolished implants with different oxide thicknessess.", Biomeaterials, **17**(6) pp. 605-616, 1996

[60] Buser D, Schenk RK, Steinemann S, Fiorellini JP, Fox CH, Stich H, "Influence of surface characteristics on bone integration of titanium implants. A histomorphometric study in miniature pigs", J. Biomedical Materials Research, **25** pp. 889-902, 1991

[61] Gotfredsen K, Wennerberg A, Johansson C, Teil Skovgaard L, Hjorting-Hansen E. "Anchorage of TiO_2 blasted, HA coated, and machined implants: An experimental study with rabbits", J. Biomedical Materials Research, **29** pp. 1223-1231, 1995

[62] Friedman RJ, Yuehuei HA, Ming J, Draughn RA, Bauer TW. "Influence of biomaterial Surface Texture on Bone Ingrowth in the Rabbit Femur", J. Orthopaedic Research, **14** (3) pp. 455-464, 1996

[63] Luckey HA, Lamprecht EG, Walt MJ, "Bone apposition to plasma-sprayed cobalt-chromium alloy", J. Biomedical Materials Research, **26** pp.557-575, 1992

[64] Saha S, Albright JA, Keating ME, Raghunath PM, "A Biomechanical and Histological Examination of Different Surface Treatments of Titanium Implants for Total Joint Replacement" in Quantitative Characterization and Performance of Porous Implants for Hard Tissue Applications, JE Lemons, editor, ASTM: West Hanover MA, 1987

[65] Feighan JE, Goldberg VM, Davy D, Parr J, Stevenson S, "The influence of Surface-Blasting in the incorporation of Titanium-Alloy Implants in a Rabbit Intramedulary Model" Journal of Bone and Joint Surgery, **77-A** (9) pp.1380-1395, 1995

[66] Wennerberg A, Albretktsson T, Johanasson C, Andersson B, "Experimental study of turned and grit-blasted screw shaped implants with special emphasis of blasting material and surface topography", International J. Oral and Maxillofacial Implants, **11**(1) pp. 38-45, 1996

[67] Sumner DR, Gallante JO, "Determinants of Stress Shielding", Clinical Orthopaedics and Related Research, number 274, pp. 202-212, 1992

[68] Sumner DR, Turner TM, Urban RM, Gallante JO, "Remodeling and ingrowth of bone at two years in a canine cementless total hip arthroplasty model", J. Bone an Joint Surgery, **74-A** pp. 239-248, 1992

[69] Geesink RGT, De Groot K, Klein K, "Chemical Implant fixation using hyroxyl-apatite coatings", Clinical Orthopaedics and Related Research, **235**, pp. 147-170, 1987

[70] McCutchen JW, Collier JP, Mayor MB, "Osseointegration of titanium implants in total hip arthrolasty", Clinical Orthopaedics and Related Research, **261** pp. 114- 125,1990

[71] Lintner F, Zweymuller K, Brand G, "Tissue reations to titanium endoprosthesis. Autoposy studies in four cases .", J. Arthroplasty, **1**, pp. 183-195, 1986

[72] Weill D, "The Cementless CLW System" in Endoprosthetics, E.W Morsher editor., New York: Springer , 1995 pp. 297-308

[73] Wagner H, Wagner M, "Conical Stem Fixation for Cementless Hip Prosthesis for Primary Implantation and Revision" in Endoprosthetics, E.W Morsher editor., New York: Springer , 1995 pp. 258-267

[74] Zweymuller K, Litner FK, Semlitsch MF, "Biologic Fixation of a Press-Fit Titanium Hip Joint Endoprosthesis" Clinical Orthopaedics and Related Research, **235**, pp. 195-206, 1988

[75] Zweymuller K, "A Cementless titanium hip endoprosthesis system based on press-fit fixation: basic research and clinical results", in Instructional course Lectures , vol. 24, American Academy of Orthopaedic Surgeons pp. 203-225

[76] Zweymuller K, Litner F, Bohm G, "The Development of a Cementless Hip Endoprosthesis" in Endoprosthetics, E.W Morsher editor., New York: Springer , 1995 pp. 309-325

[77] Delaunay CP, Kapandji AI, "Primary total hip Arthroplasty using the Zweymuller First Generation Prosthesis" J. Arthroplasty, **11** (6), pp. 643-652, 1996

[78] Huo MH, Martin RP, Zatroski LE, Keggi KJ, "Total Hip Arthroplasty Using the Zweymuller Stem Implanted Without Cement" J. Arthroplasty, **10** (6) pp. 793-799, 1995

[79] Robinson RP, Deysine GR, Green TM, "Uncemented Total Hip Srthoplasty Using the CLS Stem: A Titanium Alloy Implant With a Corundum Blast Finish", J. Arthroplasty **11** (3) pp. 286-292, 1996

[80] Blaha DJ, Grappiolo G, Gruen TA, Spotorno L "Five to eight-year follow-up of a cementless, press fit non bone ingrowth total hip stem", Trans AAOS, San Francisco CA, pp.76, 1993

[81] Spotorno L, Romagnoli S, Ivaldo N, Grappiolo G, Bibbiani E, Blaha, DJ, Guen, TA. "The CLS system Theoretical Concepts and Results" Acta Orthopaedica Belgica, **59** - suppl 1, pp. 144-148, 1993

[82] Engh CA, Bobyn JD, Glassman AH, "Porous coated hip replacement: The factors governing bone ingrowth, stress shielding and clinical results." J. of Bone and Joint Surgery, **69B** pp. 45-55, 1987

[83] Pilliar RM, Lee JM, Maniatopolous C, "Observations on the effect of movements on bone ingrowth into porous-surfaced implants" Clinical Orthopaedics and Related Research, 208, pp. 108-113.

[84] Jasty M, Bragdon C, Burke D, O'Connor D, Lowenstein J, Harris, W, "*In Vivo* Skeletal Responses to Porous-Surfaces Implants subjected to Small Induced Motions", J. of Bone and Joint Surgery, **79-A**, pp. 707-714, 1997

[85] Bobyn JD, Pilliar RM, Cameron HU, Weatherly GC, "Osteogenic phenomena across endosteal bone-implant spaces with porous surfaced intramedullary implants." Acta Orthop. Scand. **52** pp. 145-153, 1981

[86] Wang BC, Chang E, Yang CY, "A histomorphometric study on osteoconduction and osseointegration of titanium alloy with and without plasma-sprayed hydroxyapatite coating using backscattered electron images", J of Materials Science: Materials in Medicine, **4** pp.394-403, 1993

[87] Parr GR, Steflik DE, Sisk AL, "Histomorphometric and histologic observations of bone healing around immediate implants in dogs", International Journal of Oral and Maxiofacillary Implants, **8** (5), pp. 534-540,1993.

[88] Curtis ASG, Clark P, "The effects of topographical and mechanical properties of materials on cell behavior", Critical Reviews in Biocompatibility, **5**(4), pp. 343-362, 1990

[89] Clark P, Connolly P, Curtis ASG, Dow JAT, Wilkinson CD, "Topographical control of cell behavior: multiple grooved substrata", Development, **108**(4) pp. 635-644, 1990

[90] Pilliar RM, Lee JM, Maniatopolous C, "Observations on the effect of movements on bone ingrowth into porous-surfaced implants" Clinical Orthopaedics and Related Research, **208**, pp. 108-113.

[91] Jasty M, Bragdon C, Burke D, O'Connor D, Lowenstein J, Harris, W, "*In Vivo* Skeletal Responses to Porous-Surfaces Implants subjected to Small Induced Motions", J. of Bone and Joint Surgery, **79-A**, pp. 707-714, 1997

[92] Bobyn JD, Pilliar RM, Cameron HU, Weatherly GC, "The optimum pore size for the fixation of porous surfaced metal implants by the ingrowth of bone.", Clinical Orthopaedics and Related Research, **150** pp. 263-270, 1980

[93] Bobyn JD, Pilliar RM, Cameron HU, Weatherly GC, "Osteogenic phenomena across endosteal bone-implant spaces with porous surfaced intramedullary implants." Acta Orthop. Scand. **52** pp. 145-153, 1981

[94] Wang BC, Chang E, Yang CY, "A histomorphometric study on osteoconduction and osseointegration of titanium alloy with and without plasma-sprayed hydroxyapatite coating using backscattered electron images", J of Materials Science: Materials in Medicine, **4** pp.394-403, 1993

[95] Parr GR, Steflik DE, Sisk AL, "Histomorphometric and histologic observations of bone healing around immediate implants in dogs", International Journal of Oral and Maxiofacillary Implants, **8** (5), pp. 534-540,1993.

[96] Curtis ASG, Clark P, "The effects of topographical and mechanical properties of materials on cell behavior", Critical Reviews in Biocompatibility, **5**(4), pp. 343-362, 1990

[97] Clark P, Connolly P, Curtis ASG, Dow JAT, Wilkinson CD, "Topographical control of cell behavior: multiple grooved substrata", Development, **108**(4) pp. 635-644, 1990

[98] Yue S, Pilliar RM, Weatherly GC, "The fatigue strength of porous coated Ti-6%Al-4%V implant alloy", J. of Biomedical Materials Research, **18** pp. 1043-1058, 1984

[99] Groessner-Schreiber B, Tuan RS, "Enhanced extracellural matric production and mineralization by osteoblasts cultured on titanium surfaces in vitro", J. of Cell Science, **101**, pp. 209-217, 1992

[100] Hosip-Flor S, Lester KD, "Human postmortem retreival of total hip arthroplasty", J. of Arthroplasty, **12**, pp. 562-567, 1997